DEPOSITIONAL CONTROLS AND STRATIGRAPHIC ARCHITECTURE OF A MIXED CARBONATE-SILICICLASTIC DEPOSITIONAL SYSTEM IN THE MISSISSIPPIAN (LOWER CARBONIFEROUS) OF THE SOUTHERN MIDCONTINENT, OKLAHOMA, USA

By

JAMAR BYNUM

Bachelor of Science in Earth & Planetary Sciences
University of New Mexico
Albuquerque, NM
2007

Master of Science in Geology
Oklahoma State University
Stillwater, OK
2010

Submitted to the Faculty of the
Graduate College of the
Oklahoma State University
in partial fulfillment of
the requirements for
the Degree of
DOCTOR OF PHILOSOPHY
December, 2022

DEPOSITIONAL CONTROLS AND STRATIGRAPHIC ARCHITECTURE OF A MIXED CARBONATE-SILICLASTIC DEPOSITIONAL SYSTEM IN THE MISSISSIPPIAN (LOWER CARBONIFEROUS) OF THE SOUTHERN MIDCONTINENT, OKLAHOMA, USA

Dissertation Approved:

Dr. Jack Pashin

Dissertation Adviser

Dr. Jim Puckette

Dr. Michael Grammer

Dr. Runar Nygaard

Dr. Bill Coffey

ACKNOWLEDGEMENTS

I would like to thank Devon Energy for allowing access to their extensive core data sets for this study, along with the Oklahoma Geological Survey staff at the Oklahoma Petroleum Information Center, who facilitated numerous core preparation and sample requests. Would also like to thank all of the influential geologists during my career for their support and encouragement. I would also like to dedicate my Midcontinent Mississippian research to the late Dr. Boardman who was with me from the start of my PhD goals. Thank you to Dr. Cory Godwin for the collaboration and meaningful discussions on biostratigraphic outcrop studies and their relationship to the Anadarko Basin subsurface, and to my dissertation committee for their constructive comments that greatly improved this dissertation work. Finally, would like to thank my husband Conn Wethington for all his support and late-night geologic brainstorming sessions that helped me get to the finish line.

Acknowledgements reflect the views of the author and are not endorsed by committee members or Oklahoma State University.

Name: JAMAR BYNUM

Date of Degree: DECEMBER, 2022

Title of Study: DEPOSITIONAL CONTROLS AND STRATIGRAPHIC ARCHITECTURE OF A MIXED CARBONATE-SILICICLASTIC DEPOSITIONAL SYSTEM IN THE MISSISSPPIAN (LOWER CARBONIFEROUS) OF THE SOUTHERN MIDCONTINENT, OKLAHOMA, USA

Major Field: GEOLOGY

Abstract: The Anadarko Basin of the North American Midcontinent has been explored by the hydrocarbon industry for decades, and recent efforts have created an opportunity to analyze robust modern geologic datasets for investigating the depositional controls and stratigraphic architecture of Mississippian (Lower Carboniferous) reservoirs in the region. Core-based facies analysis coupled with the integration of geophysical well logs and previous biostratigraphic studies are the fundamental building blocks for investigating the evolution of a carbonate depositional system to a mixed carbonate-siliciclastic system. Initial deposition in the region was characterized by marine transgression and followed by a period of stabilization, with aggradation of the carbonate system on the Burlington shelf and coeval deposition of biostromal sponge gardens and outer ramp facies in the study area. This event was followed by progradation of the carbonate system, establishing the Meramecian (Viséan) Boardman ramp margin in north-central Oklahoma, where thick successions of carbonate shoal and proximal storm deposits accumulated. The final depositional episode was characterized by an abrupt transition from carbonate to siliciclastic deposition, in which thick successions of Chesterian (Viséan-Serpukhovian) siliciclastics prograded from the Boardman ramp margin into the Anadarko Basin. As a result of this depositional evolution the reservoir architecture changes across the Anadarko Basin as progradational proximal carbonate facies transition to storm dominated ramp margin conditions, and finally to the more prolific unconventionally targeted siliciclastic siltstone and mudstone facies of the outer ramp. The vertical and lateral facies distributions were investigated further within the STACK play. Statistical analysis on facies logs indicates a highly layered rhythmic succession, where thickness frequency distributions and Markov chain analysis indicate the lithologic transitions were stochastically regulated with no apparent lithologic cyclicity. Overall, the Mississippian contains two progradational parasequence sets separated by a disconformity associated with the inception of the Ouachita Orogeny. While the onset of transition from a greenhouse to icehouse climatic regime was underway, far-field tectonic effects provided the predominant controls on deposition.

TABLE OF CONTENTS

Chapter Page

LIST OF TABLES

Table Page

LIST OF FIGURES

Figure Page

Figure Page

CHAPTER I

INTRODUCTION

The Anadarko Basin provides a unique opportunity to analyze a significant portion of continuous section within the Mississippian (Lower Carboniferous) and integrate it with the extensive outcrop work conducted regionally. Initial subsurface investigation began with focused core studies for the hydrocarbon industry to understand the geologic controls on production within these Mississippian reservoirs. Multiple cores were acquired and integration allowed for a broader focus on the depositional architecture and how the subsurface strata of the Anadarko Basin are stratigraphically related to the outcrop belt in SE Kansas, SW Missouri, NE Oklahoma, and NW Arkansas. This regional scale integration of data and interpretation of depositional systems provided the building blocks for investigating architecture and facies distributions influencing hydrocarbon production and where other potential productive fairways may reside.

This dissertation compiles three papers that clarify different aspects of Mississippian sedimentation in the Anadarko Basin. The first paper (Chapter 2), which has been published in the journal, Facies (Bynum et al., 2022), describes the depositional and stratigraphic architecture of the Mississippian System in the Anadarko Basin. The second paper (Chapter 3) focuses on facies heterogeneity and lithologic ordering in Mississippian strata and includes statistical analyses that test the hypothesis that stochastic processes were a critical factor regulating sedimentation. The final paper (Chapter 4) considers the mix of tectonic and eustatic events that are recorded in the Mississippian section.

CHAPTER II

DEPOSITIONAL AND STRATIGRAPHIC ARCHITECTURE OF A MIXED CARBONATE-SILICICLASTIC DEPOSITIONAL SYSTEM IN THE MISSISSIPPIAN (LOWER CARBONIFEROUS) OF THE SOUTHERN MIDCONTINENT, OKLAHOMA, USA.

Introduction

Geologic investigations of the Anadarko Basin have been conducted for decades, and recent efforts have advanced our understanding of the Mississippian (Lower Carboniferous) strata across the US Midcontinent (Boardman et al. 2013; Grammer et al. 2020; Hanford 1995; Smith 2000; Mazzulo et al. 2020), while recent unconventional reservoir development has provided the opportunity to integrate modern geologic datasets to improve the geologic understanding of Mississippian strata in the subsurface. Extensive work on the Mississippian outcrop belt in southwest Missouri, northwest Arkansas, and northeast Oklahoma has provided key insights into the depositional processes and stratigraphic framework for the region. The development of a complex stratigraphic nomenclature across the outcrop belt and lack of biostratigraphic analysis in the subsurface have made regional stratigraphic correlations difficult. Detailed stratigraphic and sedimentologic analyses based on cores in the Anadarko Basin in this study have been integrated with geophysical well logs and biostratigraphic analysis for characterizing the depositional and stratigraphic architecture of Mississippian strata in the Anadarko Basin (Fig. 1).

This workflow was developed to identify the critical depositional controls that affect reservoir performance in a region where carbonate depositional systems were succeeded by mixed carbonate-siliciclastic systems.

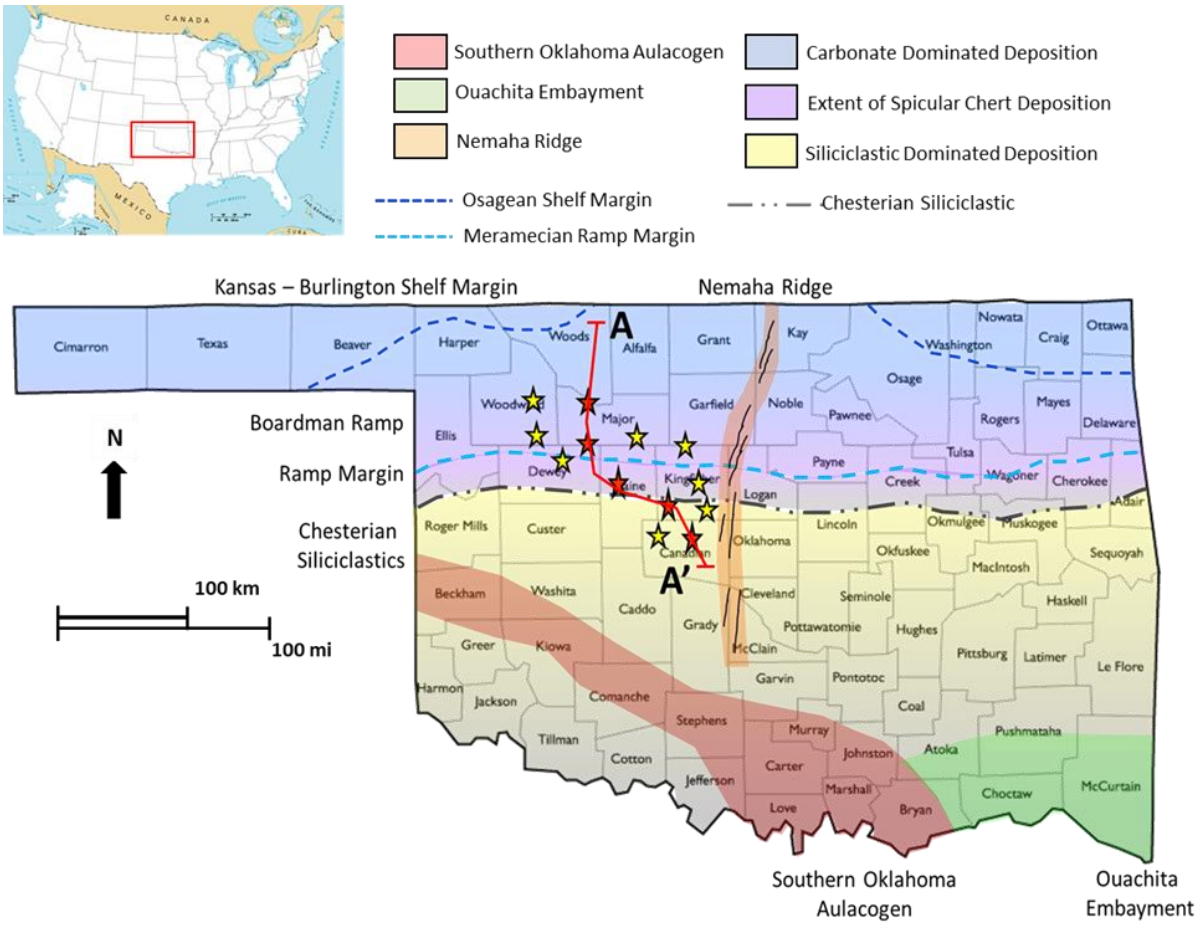

Figure 1. Location map of Oklahoma within the continental United States (red box), and showing the relationship between the study area and Mississippian palaeogeographic features. The Boardman ramp margin represents the progradational extent of shallow marine carbonate deposition during the Late Mississippian (light blue dashed line) from the Early Mississippian Burlington shelf (dark blue dashed line). Late Mississippian siliciclastic strata predominate in distal mid ramp to outer ramp environments (gray dash-dot line). Yellow stars indicate locations of the cores evaluated for this study, and red stars indicate cores displayed in cross section (Fig. 2).

Geologic Background

The Anadarko Basin is the deepest Phanerozoic sedimentary basin in the North American craton (Perry 1989). The basin is asymmetric and structurally deepest along the southwestern margin adjacent to the Wichita and Amarillo uplifts, where the basin contains more than 12 km (~40,000 ft) of sediment ranging in age from Cambrian to Permian (Perry 1989). This basin is 160 km (100 mi) wide along a regional northwest strike and 480 km (300 mi) long along the south-southwest dip direction (Higley 2014). The basin is bounded on the east by the Nemaha Uplift, on the southeast by the Arbuckle Uplift and Ardmore Basin, on the southwest by the Wichita and Amarillo Uplifts, and to the west by the Cimarron Arch (Johnson 1988). The northern part of the basin includes the so-called Anadarko shelf, where basement is less than 1 km deep (~3,000 ft) (Ball 1991).

During the Late Devonian through Early Carboniferous, the Anadarko Basin was located on the western intracontinental margin of the Laurussian Plate between 10 and 20°S. This location produced nutrient-rich upwelling currents that originated from the Ouachita Embayment (Gutschick 1983). This upwelling resulted in high organic productivity, including siliceous plankton blooms (i.e., radiolarians) and siliceous bottom fauna (sponges). However, as the Gondwanan and Laurussian plates continued to collide through the Late Mississippian to Pennsylvanian (Middle to Late Carboniferous), the closing of the Rheic Ocean cut off the strong upwelling zones to create the more isolated Midcontinent Sea (Algeo 2008) leading to a drastic decrease in biogenic silica production. The Late Mississippian (middle Carboniferous) marks the transition to an icehouse world as Pangaea formed and glaciation drove high-frequency sea-level change in the Milankovitch band (Crowley 1993; Fielding 2007; Frakes 1992; Saunders 1986; Smith 2000).

Thick carbonate successions of the Mississippian were deposited across North America in the Appalachian, Black Warrior, Illinois, Eastern Interior, Michigan, Arkoma, Anadarko, Williston, and Permian Basins (Ettensohn et al. 2004; Grammer et al. 2018, 2020; Pashin 1994; Pashin et al. 2009; Silberling 1995; Smith 2000; 2019). The composition of the carbonate bank that developed on the western Laurussian craton during the Mississippian changed abruptly in response to orogenic events, which increased the input of siliciclastic sediment (Ettensohn et al. 2019; Sandberg 1982). The Neo-Acadian and Alleghanian synorogenic clastic wedges contain mosaics of open marine, marginal marine, and terrestrial facies that built out from the eastern highlands onto parts of the stable craton (Ettensohn 2004; Friedman 1988; Meckel 1970; Pashin et al. 2009). Similar thick clastic successions, such as the Humbug Delta, prograded cratonward from the west, and were sourced by the Antler and Ancestral Rocky Mountain highlands (Sandberg 1982). In proximity to the study area, the Mississippian Batesville and Wedington deltaic complexes were apparently sourced from the northern Appalachians and prograded onto the Arkoma shelf (Hanford 1988; 1995). Sediment was transported along fluvial axes through the Michigan and Illinois Basins and was ultimately deposited in the Arkoma and Black Warrior Basins via the Mississippi Valley Graben (Craddock 2013; Hanford 1995; Pashin et al. 2009; Xie et al. 2016).

Methods and Data Sets

The data used in this study come from subsurface cores and geophysical well logs taken from a transect across the Anadarko Basin and Anadarko shelf (Fig. 1). Core plug samples were extracted for X-ray diffraction (XRD), total organic carbon (TOC), porosity, permeability, and thin-section analysis. Descriptive work was performed on clean polished slabs and butt slabs of the cores for recording lithology, sedimentary features, and ichnological indicators. Framework mineralogy and grain size were analyzed in XRD and thin section using the standard Udden-

Wentworth grain-size scale. The intensity of bioturbation was characterized using the ichnofabric index of MacEachern and Bann (2008).

Thin sections were analyzed under a petrographic microscope to identify sedimentary structures, rock texture, fabric, mineralogy, fossils, and pore types. Thin sections were impregnated with UV-epifluorescence dye to aid micro-pore identification under UV light. Thin sections were stained on half of the slide with Alizarian Red S and potassium ferricyanide to aid in distinguishing calcite, ferroan calcite, ferroan dolomite, and feldspar. The Folk classification scheme was used for siliciclastic rock types (Folk 1980), the Dunham classification scheme was used on carbonate rock types (Dunham 1962), and the Choquette and Pray scheme was used to classify pore types (Choquette and Pray 1970).

Facies analysis was performed for each core described in the project area, and are distinguishable from one another by their spatial relationships and internal characteristics. This analysis provides the fundamental building blocks for interpreting the Mississippian sedimentary succession (Noel 2010). Facies are defined by their composition, lithology, sedimentary structures, and ichnology in order to provide insight into the genetic relationships between the sedimentary succession and depositional environment.

Digital facies logs were generated for each core described in the project area and are defined by the facies scheme that was developed. Each facies is designated by a specific number and assigned to the corresponding depth at which it was observed within core at 15cm (~0.5 ft) intervals. The facies logs were then calibrated to core spectral gamma logs for integrating the facies logs with geophysical log signatures. These facies logs were then analyzed using JewelSuite subsurface modeling software to make regional correlations and statistical analysis of facies distributions. This provides insight into the lateral and vertical distributions of the facies,

and are the building blocks for constructing the regional depositional and stratigraphic architecture.

The three chronostratigraphic stages within the Mississippian represented in the study area as denoted by the International Commission on Stratigraphy are the Tournaisian (346.7-358.9 Ma), Viséan (330.9-346.7 Ma), and Serpukhovian (323.2-330.9 Ma). These stages are defined globally by a combination of relative and absolute age-dating methods. North American stages, however, are more commonly used in the Midcontinent USA and referenced in this study for the Mississippian and these include the Kinderhookian, Osagean, Meramecian, and Chesterian. Although the North American stages rely on provincial palaeontological data and their boundaries do not align with those of the international stages, the relationship between the two sets of stages can be assessed through various palaeontological methods, including conodont biostratigraphic data (Godwin, 2020). Thus, these stratigraphic intervals were integrated and correlated within the project area utilizing conodont biostratigraphic studies on outcrop and core for establishing the stratigraphic architecture of Mississippian strata within the subsurface of the Anadarko Basin (Boardman 2000; Godwin 2020; Hunt 2016; Miller 2020; Stuckey 2020).

Results

Results from this project were produced through integration of geologic datasets provided from core and geophysical well log analyses for the purposes of establishing the depositional and stratigraphic architecture of the Mississippian system in the Oklahoma portion of the Southern Midcontinent.

Facies Analysis

Carbonate and siliciclastic facies associations were identified within the project area, and they are defined by their genetic relationship in regards to composition, depositional processes, and distribution geometries (Table 1). The Mississippian succession in the project area is defined as a mixed carbonate and siliciclastic ramp system based on the following facies analysis. Integration of the facies analysis performed on core and geophysical well logs will provide key insights into the depositional and stratigraphic architecture by investigating the temporal changes of the lateral and vertical facies distributions.

Depositional Environment	Lithofacies	Sed Structures/Ichnology	Notes
Inner - Ramp	Grainstones	Cross-Laminated to Laminated	Constituents - crinoids, bryozoan, brachiopods, ooids, peloids,
Carbonate Shoal Banks	Packstones	Massive	Pore Types - Intraparticle, moldic, fracture
Tidal Inlets		Bioturbated, Indices 1-3	Sedimentation affected by fair weather wave base and longshore currents
		Skolithos Ichnofacies	
Mid - Ramp (Proximal)	Sandy Packstones	Cross-Laminated to Laminated	Constituents - microbioclastic debris (crinoids, bryozoan, brachiopods), peloids,
Subtidal Carbonate Sand Sheets	Wackestones	Biogenic Structure	quartz, feldspars, carbonate mud, clays
Carbonate/Silicidastic Current Mixing		Bioturbated, Indices 3-5	Pore Types - Intraparticle, moldic, fracture
		Skolithos to Proximal *Cruiziana* Ichnofacies	Below fair weather wave base, sedimentation affected by carbonate bank shedding
Mid - Ramp (Distal)	Sponge Gardens	Laminated to Hummocky Cross-Laminated	Constituents - microbioclastic debris (crinoids, bryozoan, brachiopods), peloids,
Carbonate/Silicidastic Current Mixing	Wackestones	Massive	quartz, feldspars, carbonate mud, clays
Storm Sand Sheets	Silty Packstones	Bioturbated, Indices 3-6	Pore Types - Intraparticle, moldic, fracture, partial dissolution (feldspars)
Turbidite Channels	Calcareous Siltstones	*Cruiziana* to Proximal *Zoophycos* Ichnofacies	Below fair weather wave base, sedimentation affected by storm wave base
Bottom Current Reworking			
Outer - Ramp	Wackestones	Laminated	Constituents - quartz, feldspars, clays, benthic foraminifera, conodonts,
Bottom Current Reworking	Spiculitic Chert	Massive	amorphis organic matter, microbioclastic debris (crinoids, brachiopods)
Turbidite Channels	Silty Packstones	Bioturbated, Indices 1-3	Pore Types - Interparticle, partial dissolution (feldspars), intraparticle
Debrite/Turbidite Fans	Calcareous Siltstones	*Zoophycos* Ichnofacies	Below storm wave base, sedimentation affected by debris flows, turbidity & bottom currents
Upper Shoreface, Distal Inner-Ramp	Arkosic Sandstones	Cross-Laminated to Laminated	Constituents - medium to fine grained sand sized quartz & feldspars, large mica flakes,
Longshore Current Sand Bars & Sheets	Calcareous Sandstones	Massive	varying amounts of clay, microbioclastic debris (crinoids, brachiopods)
Delta Front Sand & Silt Bodies		Bioturbated, Indices 1-3	Pore Types - Interparticle, partial dissolution (feldspars), intraparticle
Reworked Carbonate Shoal Banks		*Skolithos* Ichnofacies	Sedimentation affected by fair weather wave base and longshore currents
Lower Shoreface, Mid - Ramp	Calcareous Sandstones	Laminated to Hummocky Cross-Laminated	Constituents - very fine sand to silt sized quartz & feldspars, large mica flakes,
Reworked Carbonate Shoal Banks	Sandy Packstones	Massive	varying amounts of clay, microbioclastic debris (crinoids, brachiopods)
Prodelta Silt & Mud Sheets	Calcareous Siltstones	Bioturbated, Indices 3-6	Pore Types - Interparticle, partial dissolution (feldspars), intraparticle
Storm Sand Sheets	Siltstones	*Cruiziana* Ichnofacies & Transported *Skolithos*	Below fair weather wave base, sedimentation affected by storm wave base
Turbidite Channels			
Offshore, Outer - Ramp	Calcareous Siltstones	Laminated	Constituents - quartz, feldspars, clays, benthic foraminifera, conodonts,
Bottom Current Reworking	Siltstones	Massive	amorphis organic matter, microbioclastic debris (crinoids, brachiopods)
Turbidite Channels	Organic Mudstones	Bioturbated, Indices 1-3	Pore Types - Interparticle, partial dissolution (feldspars)
Debrite/Turbidite Fans		*Zoophycos* Ichnofacies & Transported Cruiziana	Below storm wave base, sedimentation affected by debris flows, turbidity & bottom currents
Unknown Depositional Environment	Glauconitic Sandstones	Laminated	Constituents - phosphate nodules, quartz, feldspars, clays, conodonts,
Transgressive Sands	Phosphatic Sandstones	Bioturbated, Indices 5-6	microbioclastic debris (crinoids, brachiopods), pyrite, Fe-Dolomite
Condensed Sections		Glossifungites Ichnofacies	Pore Types - Intraparticle, interparticle, partial dissolution (feldspars)

Table 1. Summary of facies definitions and depositional environments based on relationships between lithofacies, sedimentary structures, ichnofacies, composition, and pore types observed in core.

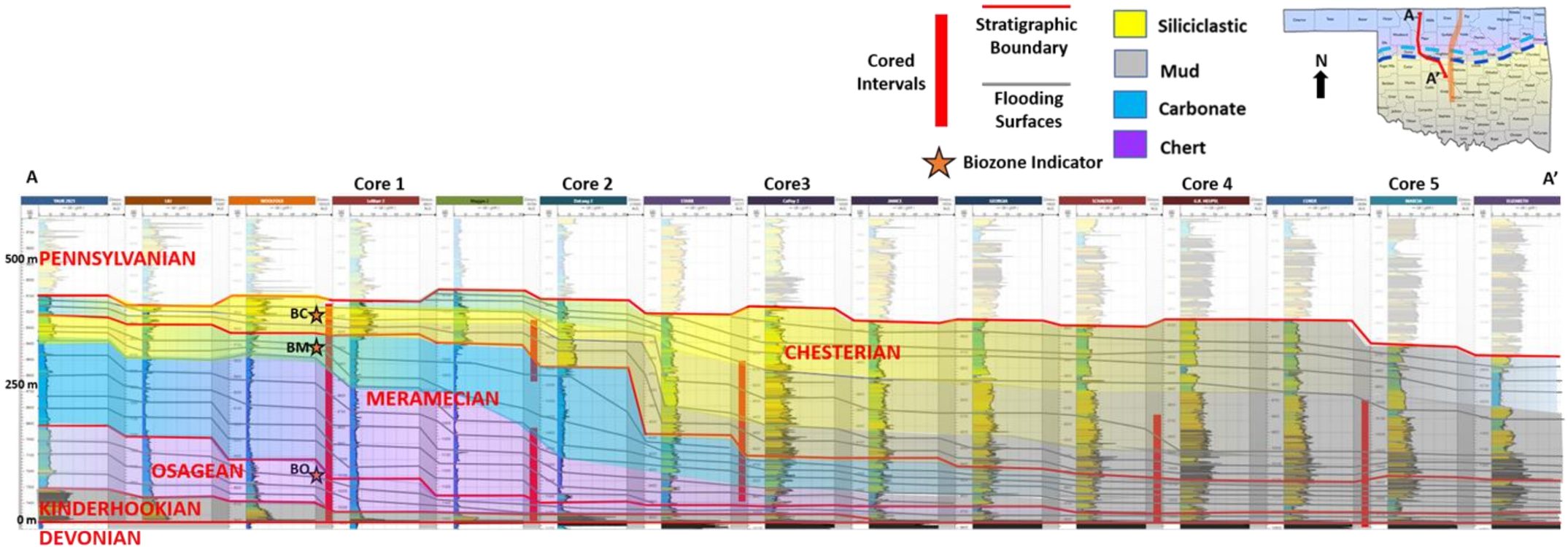

Figure 2. Cross section showing facies relationships and stratal geometry in the Mississippian section. Depositional packages to the north are dominated by carbonate shoals on the Boardman ramp crest and are composed of grainstone and packstone facies represented by the distribution of blue, while transitioning down dip to the biostromal sponge facies at the ramp crest toe of slope represented by the distribution of purple. Depositional packages to the south are dominated by the distal storm and outer ramp deposits composed of calcareous sandstone, siltstone, and mudstone facies represented by the distribution of yellow and gray. Biostratigraphic age constraints were analyzed in Core 1 (Stukey, 2020), and conodont zonations are represented by the orange stars. BO represents the top of the Osagean biozone, BM represents the top of the Meramecian biozone, and BC represents Chesterian biozone deposition. These zonations are marked by significant stratigraphic surfaces identified in core, and they are correlated regionally to define the Meramecian Boardman ramp crest margin. Chesterian siliciclastic units thicken off the Boardman margin and comprise the majority of the Mississippian succession in the Anadarko Basin. Though not cored within the project area, low gamma ray signatures within the upper Chesterian strata suggest the return of carbonate content and potential regional relationship as Pitkin Limestone equivalent.

Carbonate Facies

Five lithofacies were identified within the Mississippian carbonate section: the grainstone, packstone, wackestone, biostromal sponge, and spicular chert lithofacies. These lithofacies dominate deposition within the Kinderhookian-Meramecian (Tournaisian-middle Viséan) section and decrease in occurrence upward into the Chesterian (upper Viséan-Serpukhovian) section (Fig. 2). Facies associations were established to group key lithofacies in order to understand their occurrence in a broader depositional context (Table 1).

Grainstone-Packstone Facies

The grainstone-packstone facies consists of light gray to brownish gray grainstone and packstone with the most porous beds containing hydrocarbon stain. Individual beds have sharp bases and tops, are thick bedded, 10 to 30 cm (~0.25 to 1ft) thick, and are cross-laminated to planar-laminated. Bioturbation is rare and constitutes isolated vertical burrows. Calcareous fossil fragments consist of very coarse-sand sized crinoids, brachiopods, and bryozoans (Fig. 3). Peloids and ooids were observed along with abundant interparticle calcite cement. Moldic and intraparticle porosity within carbonate fossil debris and peloids were observed in thin section.

Interpretation

Based on the thick-bedded, cross-laminated, coarse skeletal grainstone the environmental interpretation of shallow marine shoal deposits is similar to other Mississippian deposits observed in Kansas and Illinois (Cluff 1984; Handford 1988; Smith 2000). Isolated vertical burrows further suggest development of a *Skolithos* ichnofacies where high energy and high sedimentation rates facilitated preservation of vertical dwelling burrows (Gingras 2008; MacEachern et al. 2008;). These depositional features are consistent with an inner ramp where carbonate sand belts develop parallel to strike (Tucker and Wright 1990). Packstone accumulates

on the fringes of sand shoals and in intershoal areas where increased water depth and decreased wave and tidal energy allow for deposition of finer grained sediment (Scholle et al. 1983). A ramp crest positioned on the seaward margin of an inner ramp setting is located above fair-weather wave base where sedimentation is constantly affected through generation of longshore currents and rip currents (Scholle et al. 1983; Burchette 1992).

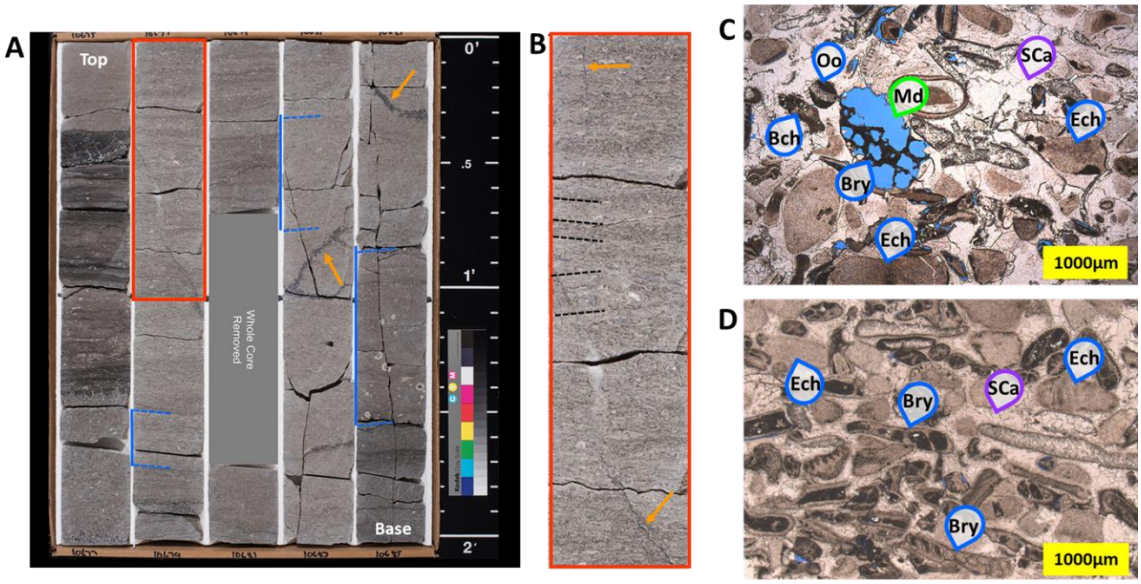

Figure 3. Photographs of the grainstone-packstone facies. A) Thick bedded grainstone (blue brackets) containing abundant natural fractures (orange arrows). Brachiopods, crinoids, and bryozoans are abundant. B) Core photograph (red rectangle) illustrating laminated to cross-laminated structure (black dashes) with natural fractures containing hydrocarbon stain and calcite cement (orange arrow). C, D) Thin section photomicrographs of grainstone. Pink staining represents calcite with blue epoxy filling pore space. Fossil content consists of echinoderms (Ech), bryozoans (Bry), and brachiopods (Bch). Other common constituents are peloids, ooids (Oo), and sparry calcite cement (SCa). Porosity types are moldic (Md), intraparticle, and intercrystalline.

Packstone-Wackestone Facies

The packstone-wackestone facies is composed of light gray packstone with variable amounts of siliciclastic sand grains and gray to dark gray wackestone. Individual packages contain sharp-based, thick-bedded, 10 to 45 cm (0.25 to 1.5 ft) thick, and cross-laminated to planar-laminated packstone that fine upward into thin-bedded, 2 to 10 cm (0.05 to 0.25 ft) thick, intensely bioturbated wackestone. Bioturbation indices range from 3-6 with both horizontal and vertical burrows present. Packstones commonly contain escape burrows that pass vertically into wackestones containing horizontal feeding burrows. *Planolites*, *Teichichnus*, *Phycosiphon, and Chondrites* are the common traces observed. Disarticulated thin-shelled brachiopods are dispersed along bedding planes, and carbonate microbioclastic debris consists of crinoid, brachiopod, and bryozoan fragments (Fig. 4), while peloids, sand-sized quartz and feldspar grains, carbonate cement, and intraparticle porosity within calcareous fossil debris and peloids were also observed in thin section.

Interpretation

Depositional packages composed of thick-bedded, sharp-based, and cross-laminated packstones that fine upward into thin-bedded and intensely bioturbated wackestone are indicative of a mid-ramp environment below fair-weather wave base similar to conditions observed across other Mississippian ramps in southwest Great Britain (Wright et al. 1990). The grains identified are consistent with the carbonate shoal deposits of the grainstone-packstone facies; however, they are more fragmented and mixed with siliciclastic sand grains suggestive of reworking and offshore transport (Burchette 1992). Storm events and sediment gravity flows are interpreted as the major depositional events due to the repetitive stacked occurrence of erosive sharp-based graded beds that contain more silt- and mud-rich sediment in the upper parts containing a diverse trace fossil assemblage (Wright et al. 1990; Cotter 1990; Bracket 1986). Calm episodes between storms

facilitated extensive vertical and horizontal burrowing, and the traces observed are characteristic of a *Cruiziana* ichnofacies (MacEachern et al. 2008).

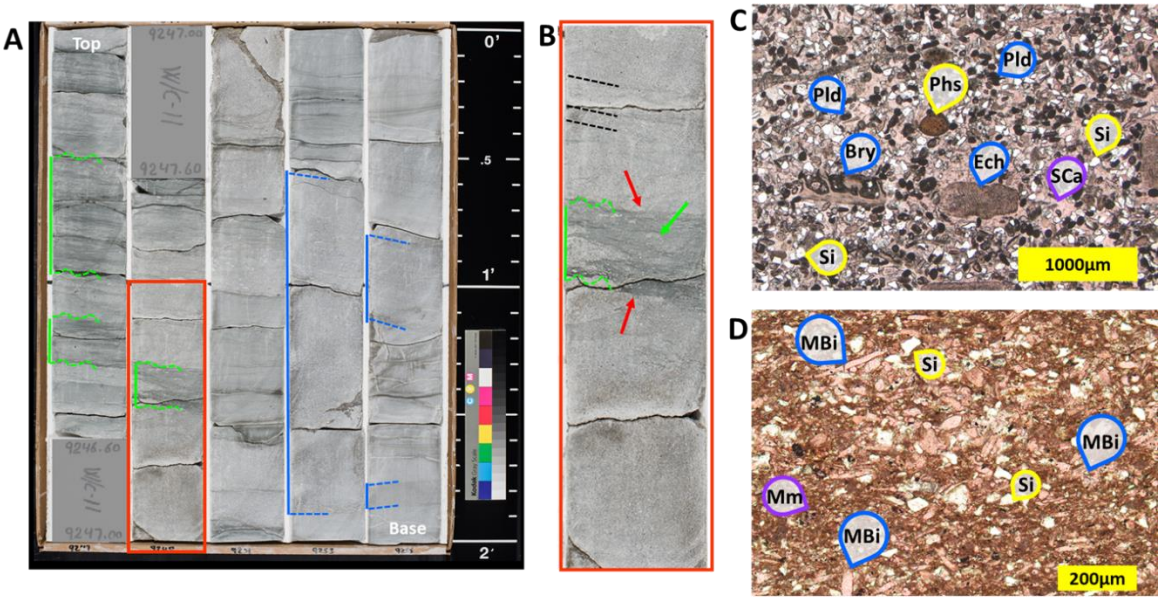

Figure 4. Core photographs of the packstone-wackestone facies. A) Thick bedded sandy packstone and grainstone (blue brackets) with bioturbated wackestone (green brackets). B) Core photograph (red rectangle) illustrating sharp contacts (red arrows) with laminated, cross-laminated (black dashes) and bioturbated (green arrow indicating individual burrow) sedimentary structures. C) Thin section photomicrograph of sandy packstone. Pink staining represents calcite with fossil content consisting of echinoderms (Ech), bryozoans (Bry), and brachiopods (Bch). Other common constituents are peloids (Pld), and sparry calcite cement (SCa), quartz (Si), and phosphate (Phs). D) Thin section photomicrograph of a silty wackestone with burrows containing concentrations of fossil debris. Pink stain represents calcite and microbioclastic debris (MBi). Other common constituents are quartz (Si). The matrix is composed of carbonate mud and clay minerals (Mm).

Biostromal Sponge Facies

The biostromal sponge facies consists of bluish-gray chert with a nodular appearance, which upon closer examination is composed branching siliceous sponges containing abundant monaxon spicules (Fig. 5). Individual sponge branches range between 2-5 cm in width, and are horizontal to subvertical. Interbedded wackestone is laminated to bioturbated with bioturbation indices ranging from 3-5. Common trace fossils are *Planolites, Phycosiphon, Chondrites,* and *Zoophycos.* The biostromal chert can be classified as spiculite within a dolomitic matrix (Fig. 5). Organic inclusions are preserved within the sponge branches, and minor carbonate fossil fragments occur within the matrix. Complex cementation produced multiple generations of calcite, dolomite, and ferroan dolomite that apparently filled voids in the rock framework and replaced primary carbonate. Wackestone in this facies is comprised of microbioclastic debris, peloids, spicules, quartz grains, clay, and carbonate mud (Fig. 5). Porosity types include intraparticle porosity within fossil debris and peloids, along with moldic porosity from dissolution of spicules.

Interpretation

The biostromal cherts consisting of horizontal to subvertical sponge branches and other benthic organisms are interpreted as biocommunal sponge gardens similar to those that formed along Jurassic ramps in Portugal and Spain (Leinfelder 1993; Aurell 2010). The predominance of siliceous sponges indicates low sedimentation rates. The intensity of bioturbation, decrease in the frequency of vertical burrows, and increase in the frequency of horizontal burrows indicate a low energy environment (Leinfelder 1993; Buatois et al. 2011). The occurrence of wackestone composed of microbioclastic debris suggests sediment transported by storms much like that in the calcareous sandstone-siltstone facies. Overall, oxygen and nutrient levels were favorable for a diverse benthic community (MacEachern et al. 2008). The abundance of biogenic silica is suggestive of cool bottom waters that may have been influenced by upwelling from the Rheic

Ocean, which had a major impact on sedimentation during the Late Devonian and Early Mississippian in the Ouachita Embayment and the adjacent shelf (Callner 2014; Cecil 2016; Pashin and Cecil, 2016).

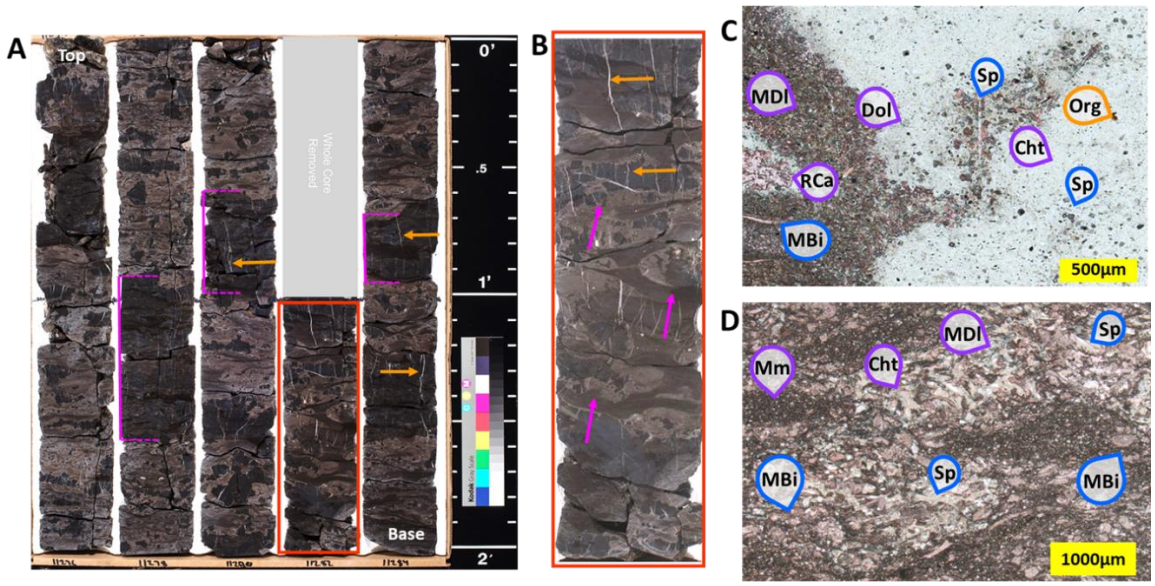

Figure 5. Core photographs of the sponge chert facies. A) Cherty sponge boundstone (pink brackets) interbedded with bioturbated wackestone to packstone. Abundant natural fractures are present (orange arrows). B) Core photograph (red rectangles) illustrating individual sponge branches (pink arrows) that are horizontal to sub-vertical. Natural fractures are typically bound within cherty branches and are filled with silica, calcite, and dolomite (orange arrows). C) Thin section photomicrograph of diagenetically altered sponge boundstone composed of chert (Cht). Sample contains monaxon spicules (Sp) commonly preserved in a dolomitic matrix (MDl). Other constituents include calcareous bioclasts, dolomite rhombs (Dol), organic inclusions (Org), and replacive calcite (RCa). D) Thin section photomicrograph of heavily bioturbated packstone with individual burrows commonly infilled with carbonate mud and clay (Mm). Pink stain marks calcite with abundant microbioclastic debris (MBi). Outlines of sponge spicules (Sp), and complex diagenetic cements composed of chert (Cht) and dolomite (MDl).

Spicular Chert-Wackestone Facies

The spicular facies consists of gray packstone, bluish-gray spicular chert with a granular texture resembling grainstone, gray to dark gray wackestone, and dark gray calcareous mudstone (Fig. 6). Individual beds of packstone and spicular chert have sharp bases and are graded, fining upward to wackestone and calcareous siltstone. These deposits are thin-bedded, 2-10 cm (0.05 to 0.25 ft) thick, and are laminated or bioturbated. Bioturbation indices range from 3-6 where wackestone and calcareous siltstone contain horizontal feeding burrows with *Chondrites*, *Phycosiphon*, and *Zoophycos* traces. The packstone is composed of abundant peloids, microbioclastic debris, along with varying amounts of silt to sand sized quartz and feldspar grains and calcite cement. The spicular chert is composed primarily of sponge spicule debris concentrated in laminae (Fig. 6). Bioturbated beds contain poorly oriented spicules mixed with bioclastic grains, clay, and dolomite. Moldic porosity from dissolution of spicules is common, with silica cement filling parts of the voids. Laminated beds contain more chert than bioturbated beds, but both contain varying proportions of chert, calcite, and dolomite cement.

Interpretation

The thin-bedded, sharp-based, laminated packstone and spicular chert resembling grainstone fining upward to wackestone and calcareous siltstone contain similar sedimentological characteristics to storm deposits in a Silurian mid ramp environment in Pennsylvania (Cotter 1990). The coarser grained rocks in the packstone facies are similar to those described in the packstone-wackestone facies. This compositional link to the more proximal storm deposits and larger volume of fine-grained sediment suggests more distal storm deposits that incorporate detritus derived from the sponge gardens. The coarser strata contain escape burrows with *Planolites* and *Teichichnus* signifying a distal *Cruziana* ichnofacies, whereas the muddy, finer-grained wackestone and calcareous siltstone contain traces indicative of a *Zoophycos* ichnofacies

(MacEachern et al. 2008; Buatois et al. 2011). These depositional characteristics are consistent with a mid-ramp environment below fair-weather wave base.

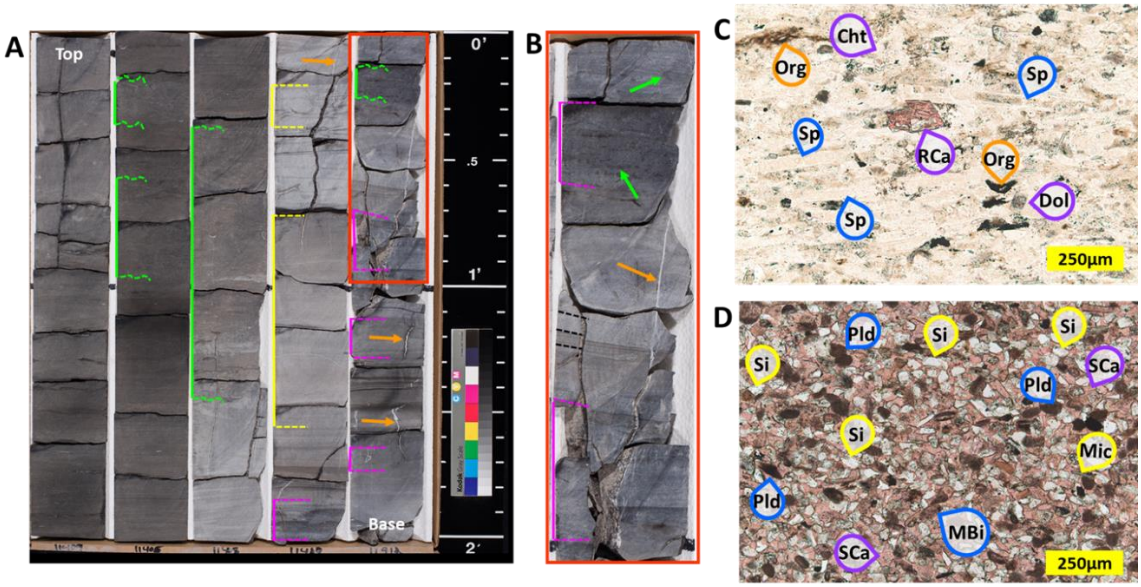

Figure 6. Core photographs of the spicular chert-wackestone facies. A) Packstone-dominated strata containing of thinly laminated spicular chert (pink brackets), laminated to cross-laminated calcareous sandstone (yellow brackets), and laminated to bioturbated peloidal siltstone (green brackets). Beds with the highest silica and calcite content contain intrastratal natural fractures typically filled with calcite (orange arrows). B) Core photograph (red rectangles) illustrating spicular chert beds (pink brackets) with natural fractures filled with calcite cement (orange arrows) and bioturbation (green arrows). Calcareous sandstone beds have sharp bases and are commonly contain cross-laminae (black dashes). C) Thin section photomicrograph of a spicular chert with grainstone texture. Alizarin-red stain marks calcite. Sample contains abundant broken monaxon spicules (Sp), dolomite (Dol), and organic inclusions (Org). This sample has undergone a complex diagenetic history including a conversion of biogenic silica to chert (Cht), an episode of dolomite precipitation, and followed by dolomite dissolution and replacement with calcite (RCa). D) Thin section photomicrograph of calcareous sandstone. Sample contains abundant fine-

to very fine-grained quartz sand (Si) and feldspar (Fld), large mica flakes (Mic), peloids (Pld), microbioclastic debris (MBi), and abundant sparry calcite cement (SCa).

Siliciclastic Facies

Four lithofacies were identified within the Mississippian siliciclastic depositional system: subarkosic sandstone, calcareous sandstone-siltstone, mudstone, and glauconitic/phosphatic sandstone. Transition from the carbonate system to a siliciclastic system started in the Meramecian (Viséan) section, while the frequency and abundance of siliciclastic strata increases up-section (Fig. 2). Facies association identifiers are established to group key lithofacies in order to understand their occurrence within the broader depositional environment context (Table 1).

Subarkosic Sandstone Facies

The subarkosic sandstone facies is composed of brownish-gray subarkosic sandstone and gray to brownish-gray calcareous sandstone, with the most porous beds containing hydrocarbon stain. Individual beds have sharp bases and sharp to gradational tops, are thick-bedded, 15 to 45 cm (0.5-1.5 ft) thick, to well sorted, and are cross-laminated to planar-laminated, and bioturbated (Fig. 7). Bioturbation indices range from 2-4, and vertical burrows predominate. Burrows are typically filled with sediment from the overlying bed. Common trace fossils are *Planolites*, *Cylindrichnus*, and *Thalassinoides*. The sandstone is composed of medium to fine sand composed of quartz and feldspar, with varying amounts of mica, clay, and microbioclastic debris (Fig. 7). The calcareous sandstone consists of similar constituents with an increase in carbonate fragments as peloids, microbioclastic debris, and calcite cement. Interparticle porosity and partially dissolved feldspar grains are present along with intraparticle porosity within peloids and microbioclastic particles.

Interpretation

The nature of thick-bedded, cross-bedded to planar-laminated, well sorted sandstone suggests a high-water energy environment (Pemberton et al. 2012). Compositional and sedimentological characteristics of the subarkosic sandstone and microbioclastic calcareous sandstone are similar to Lower Cretaceous ramp deposits investigated in Egypt (Abdel-Fattah 2018). While the calcareous skeletal component is suggestive of reworked carbonate facies, the medium-grained subarkosic sandstone indicates a basement uplift provenance. Sedimentological characteristics are consistent with a proximal storm dominated ramp environment above fair-weather wave base where sediment is constantly affected by wave agitation associated to storm generated currents (Scholle et al. 1982, Pemberton et al. 2012). The isolated vertical burrowing behaviors observed are suggestive of a *Skolithos* ichnofacies, and further support an interpretation of high-water energy and sedimentation rates (Hasiotis et al. 2012, Pemberton et al. 2012).

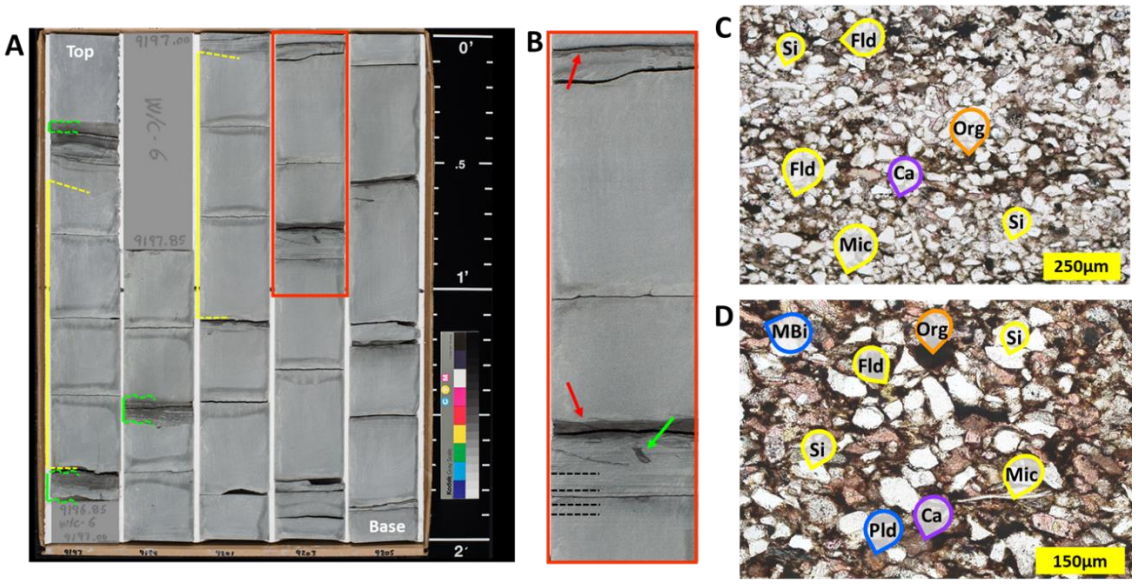

Figure 7. Core photographs of the subarkosic sandstone facies. A) Thick-bedded arkosic and calcareous sandstone (yellow brackets) interbedded with thin beds of bioturbated argillaceous siltstone (green brackets). B) Core photograph (red rectangle) illustrating sharp bases and tops of

sandstone beds (red arrows) along with horizontal laminae (black dashes). Isolated vertical burrows (green arrow) are commonly filled with argillaceous sediment. C) Thin section photomicrograph of arkosic sandstone containing abundant medium- to fine-grained quartz sand (Si) and feldspar (Fld), large mica flakes (Mic), pore-filling organic residue (Org), and minor calcite cement (Ca). D) Thin section photomicrograph of calcareous sandstone. Sample contains abundant medium- to fine-grained sand sized quartz (Si) and feldspar (Fld), large mica flakes (Mic), clays, microbioclastic debris (MBi), pore-filling organic residue (Org), and calcite cement stained pink (Ca).

Calcareous Sandstone-Siltstone Facies

The calcareous sandstone-siltstone facies consist of gray to brownish gray calcareous sandstone, light gray sandy packstone, and dark gray calcareous siltstone. The calcareous sandstone and sandy packstone beds, cross-laminated to planar-laminated, have sharp bases, and fine upward into bioturbated calcareous siltstone (Fig 8.). Bioturbation indices range from 3-5 with *Planolites, Teichichnus, Phycosiphon, and Chondrites* traces being most common. The calcareous sandstone is composed of fine- to very-fine sand composed of quartz and feldspar, with varying amounts of mica, clay, peloids, microbioclastic debris, and calcite cement. The sandy packstone consists of peloids, microbioclastic debris, quartz and feldspar sand grains, carbonate mud, clay, and calcite cement (Fig. 8). Interparticle porosity and partially dissolved feldspar grains are present along with intraparticle porosity within peloids and microbioclastic particles.

Interpretation

The repetitive nature of depositional packages consisting of sharp-based calcareous sandstone and packstone that gradationally fine upward into heavily bioturbated calcareous siltstone indicates episodic high-water energy conditions wanning to lower-water energy conditions, similar to the mixed siliciclastic and carbonate Devonian lower shoreface deposits studied in Morocco

(Lubeseder 2009). The repetitive stacked occurrence of the depositional packages is also indicative of sediment transport mechanisms through storm generated currents (Cotter 1990). The increase in heavily bioturbated calcareous siltstone is suggestive of a more distal position relative to the upper shoreface deposits observed updip (Pemberton et al. 2012). The diverse trace fossil assemblage, with both vertical and horizontal burrowing behaviors, is indicative of a *Cruziana* ichnofacies (MacEachern et al. 2008; Buatois et al. 2011).

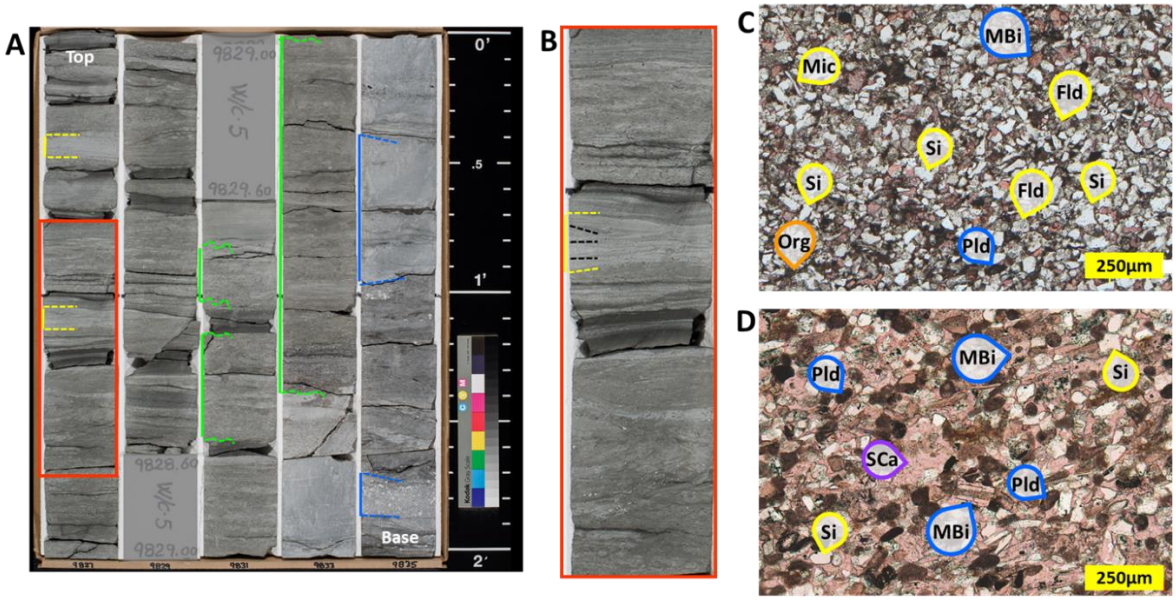

Figure 8. Core photographs of the calcareous sandstone-siltstone facies. A) Interbedded thick bioturbated calcareous sandstone (green brackets), thin cross-laminated calcareous sandstone (yellow brackets), thick laminated sandy packstone (blue brackets), and thin laminated to bioturbated siltstone. B) Core photograph (red rectangle) illustrating thin calcareous sandstone (yellow bracket) and the cross-laminae (black dashes). C) Thin section photomicrograph of calcareous sandstone containing abundant fine- to very fine-grained quartz sand (Si) and feldspar (Fld), large mica flakes (Mic), peloids (Pld), microbioclastic debris (MBi), pore-filling organic residue (Org), and calcite cement (Ca). D) Thin section photomicrograph of a sandy packstone.

Sample contains abundant peloids (Pld) and microbioclastic debris (MBi). Other common components are fine-grained quartz sand (Si), and sparry calcite cement (SCa).

Mudstone Facies

The mudstone facies is composed of gray to dark gray siltstone and dark gray to black mudstone. Thin beds are common, and the strata are typically laminated or bioturbated. Bioturbated siltstone beds are typically more calcareous than surrounding strata (Fig. 9). Bioturbation indices range from 2-4, and *Zoophycos*, *Chondrites*, and *Phycosiphon* traces were observed. Bioturbation indices within mudstone beds range from 1-2, and some *Zoophycos* traces were identified. Disarticulated thin-shelled lingulid brachiopods are present along bedding planes. This facies is comprised of silt to very-fine sand sized quartz and feldspar, mica, and clay. Other common constituents are agglutinated benthic foraminifera, amorphous organic matter, pyrite, conodonts, and varying amounts of carbonate mud and microbioclastic debris (Fig. 9). Interparticle porosity and partially dissolved feldspar grains are typical.

Interpretation

The fine-grained nature of thin-bedded siltstones and organic bearing mudstones is suggestive of outer ramp deposits that formed below storm wave. Similar deposits have been described from Lower Cretaceous strata in Argentina (Moore et al. 2020). The finer grained deposits have low carbonate content, elevated organic richness, preserve benthic foraminifera, conodonts, and exhibit rare horizontal branching burrowing behaviors. Depositional mechanisms are interpreted to be bottom current reworking, suspension settling, and occasional storm induced flow deposits, while bottom current reworking of silt and clay plays a significant role in the development of the mudstone fabric (Schieber 2009; Lazar 2015; Yawar 2017). Sparse, diminutive fossils, pyrite precipitation, accumulation of organic matter, and the low degree of bioturbation indicate that bottom water conditions were stressed (Buatois et al. 2012; Lazar 2015). However, *Zoophycos*

traces, other horizontal burrows, and benthic foraminifera indicate at least episodic conditions favoring pioneering organisms (MacEachern et al. 2008).

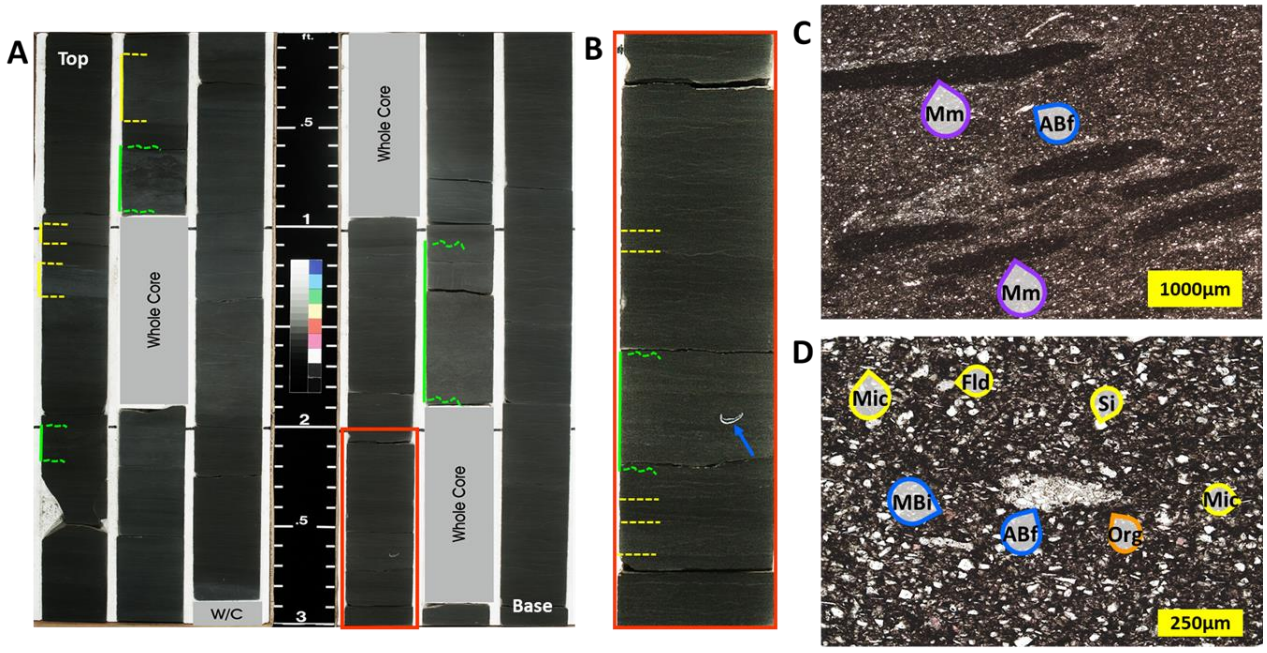

Figure 9. Photographs of the mudstone facies. A) Thin-bedded, bioturbated calcareous siltstone (green brackets), laminated siltstone (yellow brackets) and organic-bearing silty mudstone. B) Core photograph (red rectangles) illustrating bioturbated calcareous siltstone (green bracket) and laminated siltstone (yellow dashes). Scattered thin-shelled brachiopods (blue arrow) and crinoid fragments are present along bedding planes. C) Thin section photomicrograph of a bioturbated calcareous siltstone. Sample contains very fine-grained quartz sand and quartz silt. Other constituents include feldspar, mica, clay, agglutinated benthic foraminifera (ABf), and organic matter. Burrowing organisms often sort fine-grained mud (Mm) and carbonate material around individual burrows. D) Thin section photomicrograph of an organic-bearing silt-rich mudstone. Sample contains quartz (Si) and feldspar (Fld), mica (Mic), clay, agglutinated benthic foraminifera (ABf), organic matter (Org) and minor carbonate microbioclastic debris (MBi).

Glauconitic-Phosphatic Sandstone Facies

The glauconite-phosphate facies consists of green to brown glauconitic and phosphatic sandstone. Bed thicknesses vary between 5-60 cm (0.5 to 2 ft), and are bioturbated or laminated (Fig. 10). The beds have sharp bases that grade upward into finer grained strata. Bioturbation indices typically range from 5-6 with an assemblage including *Teichichnus* and *Thalassinoides*. Vertical burrows are also observed extending into the underlying substrate. Fragmented brachiopod debris along with phosphate nodules and clasts are observed in hand sample and are commonly concentrated at the base of the bed and decrease upward in abundance along with bioturbation. This facies consists of medium- to fine-sand sized glauconite and quartz grains, feldspar, phosphate as bone fragments, conodonts, nodules, clasts, and ooids, ferroan dolomite, carbonate fossil debris, and other clay mineralogies within the matrix. Interparticle porosity is the dominant porosity type, while intraparticle porosity within glauconite grains and ferroan dolomite rhombs are common as well (Fig. 10).

Interpretation

The formation of abundant glauconite and phosphate are indicative of low sedimentation rates (i.e., condensation) on the seafloor under slightly reducing conditions (Leinfelder et al. 1993). However, the high concentration of glauconite and phosphate observed at the base of sandstone beds, which introduces a juxtaposition of contrasting facies, is suggestive of formation of a transgressive ravinement formed by shoreface erosion at the start of condensation (Posamentier and Allen 1999). Infilling of vertical burrows that penetrate the underlying exhumed substrate with concentrated glauconite and phosphate is suggestive of a sequence stratigraphically significant *Glossifungites* surface, and represents a transgressive lag associated with shoreface erosion (MacEachern et al. 2008; Buatois et al. 2011).

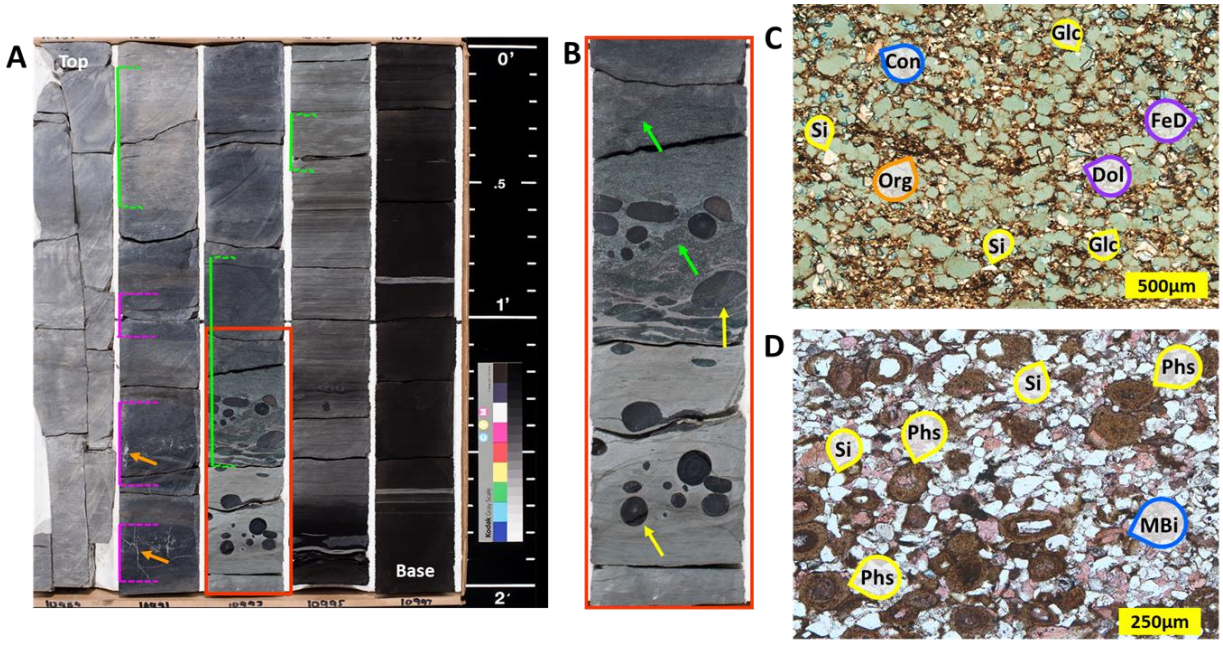

Figure 10. Core photographs of glauconitic-phosphatic sandstone facies. A) Bioturbated to laminated glauconitic and phosphatic sandstone (green bracket) overlain by spicular chert (pink brackets) and bioturbated wackestone (green brackets). B) Core photograph (red rectangle) illustrating intense bioturbation (green arrows) with vertical burrows often extending into the underlying substrate. Other common constituents are phosphate nodules and clasts (yellow arrows), glauconite grains, and brachiopod fragments. C) Thin section photomicrograph of glauconitic sandstone. Sample contains glauconite grains (Glc), quartz grains (Si), conodont fragments (Con), iron-rich dolomite (FeD), dolomite (Dol), organic staining (Org), and clays. D) Thin section photomicrograph of phosphatic sandstone. Sample contains quartz grains (Si), phosphatic ooids and clasts (Phs), microbioclastic debris (MBi), dolomite (Dol), and organic staining (Org).

Depositional Architecture

Integrated facies and gamma-ray logs were utilized for regional correlations across the project area with the lowest gamma ray signatures ranging from 0-25 API units representing the carbonate grainstone, packstone, and biostromal sponge facies due to their low concentration of radioactive minerals. The subarkosic sandstone, and calcareous sandstone-siltstone facies are represented by higher gamma-ray values ranging from 25-75 API units in response to an increase in the radioactive material in the form of clay and feldspar. The wackestone, mudstone, and glauconitic-phosphatic sandstone facies have gamma counts above 75 API units in response to the abundance of radioactive material in the form of organic matter, clay, feldspar, phosphate, and glauconite.

Thick carbonate successions are developed in the northern part of the study area, and siliciclastic sediment is more common in the southern part. The shoal and proximal storm deposits comprised of the carbonate grainstone and packstone facies are observed only in the northern project area, indicating a relatively high position on the carbonate ramp. The distal storm and outer ramp deposits comprising of calcareous sandstone-siltstone, and mudstone facies dominate in the south, indicating a progression to more distal environments over a distance of ~100 km (60 mi). Vertical facies distributions demonstrate an overall shoaling upward through time, with initial deposition characterized by distal storm and outer ramp deposits across the project area. Biostromal sponge facies formed at toe-of-slope on the distal fringes of the ramp crest shoals and proximal storm deposits. The depositional system then transitions from a carbonate dominated system to a siliciclastic dominated system, with proximal storm deposits comprising of subarkosic sandstone facies to the north transitioning to distal storm and outer ramp deposits comprising of calcareous sandstone, siltstone, and mudstone facies to the south.

The depositional architecture of Mississippian strata in the Midcontinent of Oklahoma is characterized by a clinoformal mixed carbonate-siliciclastic ramp system (Fig. 2). Initial deposition was characterized by the establishment of a carbonate system (Fig. 11) that abruptly transitioned to a siliciclastic system. Facies stacking patterns also demonstrate net progradation of the depositional system, with proximal carbonate facies building out from the Burlington shelf in Kansas and Missouri to establish the Boardman ramp margin in north-central Oklahoma. Final deposition is characterized by longshore transport of sediment parallel to the carbonate banks off the Burlington and Boardman margins, which deposited thick successions of siliciclastic strata in the Anadarko Basin influenced by the Wedington and Batesville deltaic systems to the northeast (Fig. 12). These observations are consistent with other regional studies of time equivalent strata, and provide insight into the depositional architecture of Mississippian strata within the Anadarko Basin (Boardman 2013; Franseen 2006; Godwin 2020; Grammer 2020; Hanford 1986, 1988, 1995; Hunt, 2015; Mazzulo 2011, 2013; Stuckey, 2020).

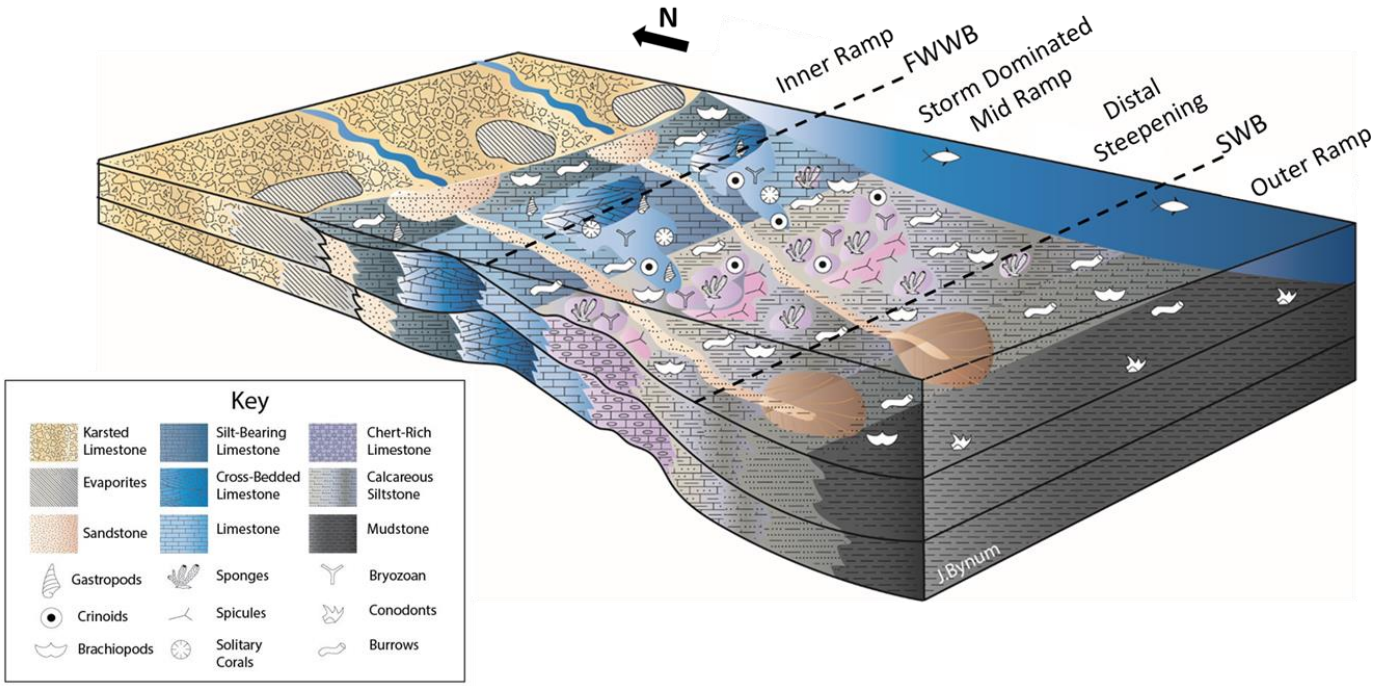

Figure 11. Block diagram of a carbonate-dominated depositional system. The shallowest deposits in the project area are represented by the carbonate shoal deposits observed, and is predominately composed of clean and coarse-grained grainstone textures. Thick-bedded grainstones and packstones are deposited in sheet like geometries down dip from the carbonate shoal deposits on a storm dominated ramp system, and are interbedded with bioturbated wackestones representing deposition between storm events. The distal mid-ramp is located below fair-weather wave base where the biostromal sponge facies is deposited toward the toe of slope of the ramp crest. Deposition then transitions from the distal storm deposit facies to the outer ramp facies where calcareous siltstones and organic-rich mudstones accumulate.

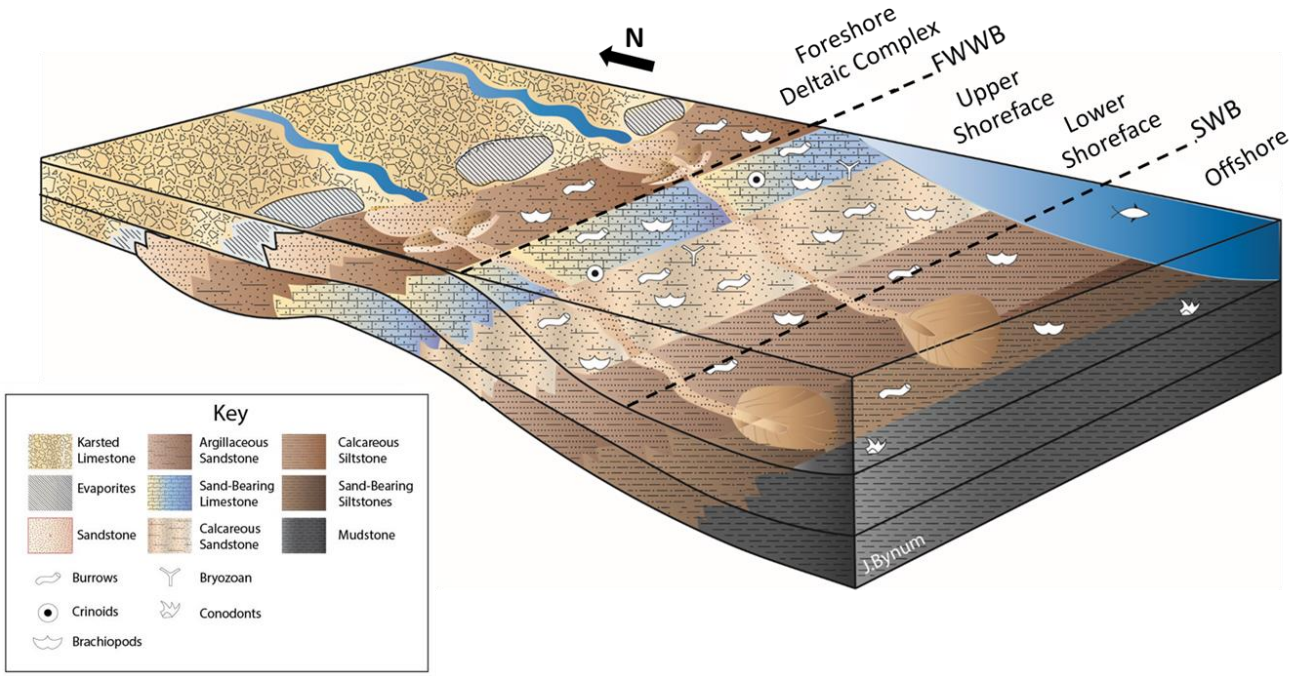

Figure 12. Block diagram of a siliciclastic-dominated depositional system. The proximal deposits in the project area are represented by the subarkosic sandstone facies observed. Deposition occurs predominantly below fair-weather wave base, and transitions down dip to the calcareous sandstone and siltstone facies. The bioturbation intensity is highest within this facies and commonly disrupts all underlying sedimentary structures. However, where preserved sharp based cross-laminated sandstone and packstone represent storm reworked sedimentation, and the distal storm deposit facies increases moving down the ramp. The outer ramp facies observed within the siliciclastic dominated system is less calcareous in nature than the carbonate dominated system, and is composed of sandy siltstone and mudstone.

Stratigraphic Architecture

Lower Mississippian sedimentation is characterized by the formation of a widespread prograding carbonate bank across the US Midcontinent. This event established the Kinderhookian-Osagean (Tournaisian-Viséan) Burlington shelf, which is north of the project area (Boardman 2013; Franseen 2006; Mazzulo 2011, 2013). The age-equivalent strata in this study are designated by biostratigraphic zonation established within Core 1 by Stukey and Godwin (2020), and is represented by outer ramp deposits. Facies analysis indicates the project area is a basinward extension of the Burlington shelf, which is dominated by inner ramp carbonates (Fig. 2). This stratigraphic interval is the thinnest package analyzed in the project area, and continues to thin to the south where it becomes part of a condensed section atop the Devonian Woodford Shale.

Osagean-Meramecian (Viséan) strata are characterized by progradation of the carbonate system from the Burlington shelf, and carbonate rocks represent the bulk of sedimentation in the northern project area (Woodward, Major, and Dewey Counties). This depositional episode establishes a new ramp margin in north-central Oklahoma, which defines the boundary of the Boardman ramp margin, which can be considered as a late-stage extension of the Burlington shelf. Biostratigraphic zonation of Core 1 indicates these strata are Meramecian (Viséan) (Fig. 10), and are represented by formation of carbonate shoals, proximal storm deposits, and biostromal sponge gardens to the north (Woods, Woodward, and Major Counties), and distal storm and outer ramp deposits to the south (Blaine, Kingfisher, and Canadian Counties). This stratigraphic interval is the thickest package analyzed in the northern project area, and represents the establishment of the Boardman ramp margin during Meramecian time. The interval thins to the south from the ramp margin and sits on top of the Lower Mississippian condensed section in the Anadarko Basin.

Upper Mississippian strata are characterized by an abrupt transition to a siliciclastic dominated system, and include the bulk of the section in the southern part of the study area (Blaine,

Kingfisher, and Canadian Counties). This depositional episode is marked by thick siliciclastic packages that accumulated basinward off the Boardman ramp margin. Biostratigraphic zonation of Core 1 indicates these strata are Chesterian (Viséan-Serpukhovian) (Fig. 2), and are represented by proximal storm deposits on the Boardman ramp margin that transition southward to distal storm deposits and muddy outer ramp facies. This stratigraphic interval is the thickest package analyzed in the southern project area and is truncated by the sub-Pennsylvanian unconformity.

Mississippian stratigraphic architecture in the project area is represented by three distinct depositional episodes (Fig. 13). Initial Kinderhookian-Osagean (Tournaisian-Viséan) deposition is distinguished by widespread outer ramp facies in the project area, which are time equivalent to the shallow-water carbonates that accumulated on the Burlington shelf. The second episode is marked by the progradation of the carbonate system basinward from the Burlington shelf, thereby establishing the Boardman ramp margin in north-central Oklahoma during Meramecian (Viséan). The last episode is marked by an abrupt change from a carbonate-dominated system to a siliciclastic-dominated system near the start of the Chesterian (Viséan-Serpukhovian). The Chesterian siliciclastic sediment is preserved mainly basinward of the Boardman ramp margin and is thickest in the Anadarko Basin.

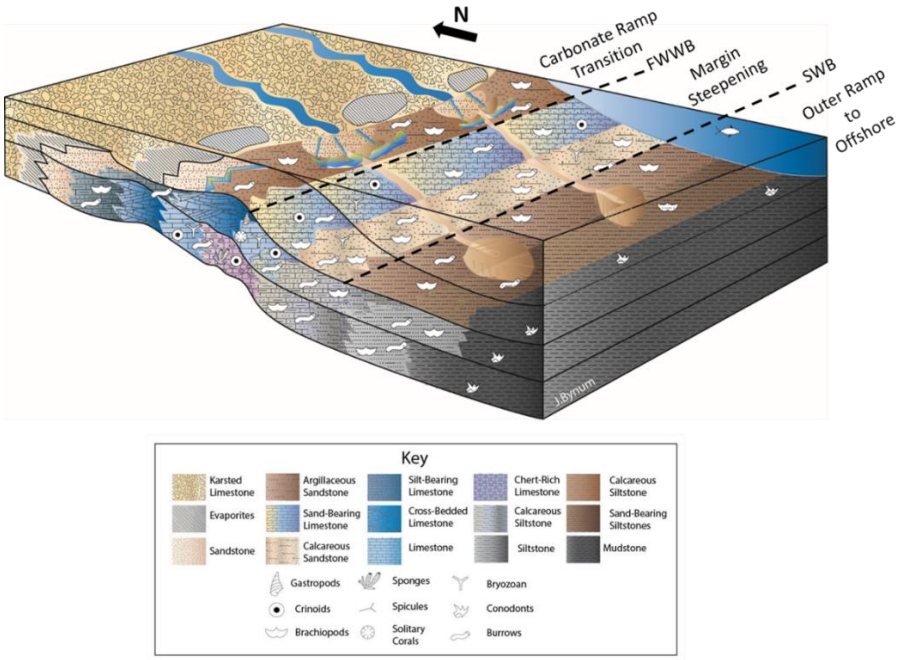

Figure 13. Block diagram demonstrating the stratigraphic transition from a carbonate-dominated system in the Lower Mississippian to a siliciclastic-dominated system in the Upper Mississippian. Stabilization and aggradation of the carbonate ramp system is characteristic of Early Mississippian deposition across the North American craton, and is recognized as the Burlington shelf. Progradation of the carbonate system followed extending the shallow carbonate margin to its furthest basinward location in northern Oklahoma. The carbonate system is abruptly inundated by siliciclastics in the Late Mississippian with siliciclastic sedimentation prograding and depositing thick successions of sandstone and siltstone off the Boardman ramp crest margin.

Discussion

The Mississippian outcrop belt in southwest Missouri, northwest Arkansas, and northeast Oklahoma provides key insights into the depositional processes and stratigraphic framework in the region (Boardman 2013; Frank 2020; Franseen 2006; Hanford 1986, 1988, 1995; Godwin 2020; Grammer 2020; Lindzey 2020; Mazzulo 2011, 2013; Miller 2020). However, a complex stratigraphic nomenclature across the outcrop belt has developed over time, making regional stratigraphic correlations into the subsurface difficult. Biostratigraphic studies of these outcrops have improved stratigraphic control and have revealed additional complexities, such as intraformational unconformities that are related to tectonic and glacio-eustatic events.

Biostratigraphic analysis of Core 1 clarifies the relationship between subsurface strata and the Mississippian outcrop belt of southwest Missouri, northwest Arkansas, and northeast Oklahoma. The distal storm deposit and outer ramp facies associated with the Osagean Stage in Core 1 is time equivalent to the Reed Springs and Bentonville (Burlington-Keokuk) Formations on the Burlington shelf. The thick Meramecian section in Core 1 corresponds to the Ritchey Formation, Moccasin Bend Formation, and Quapaw Limestone and the Bayou Manard Member of the Pryor Creek Formation (lower Mayes Group) in the outcrop belt of northeast Oklahoma. The Meramecian succession at outcrop includes a significant erosional surface called the sub-Mayes unconformity, which occurs in the upper Meramecian above the Quapaw Formation and below the Bayou Manard member of the Mayes Group (Boardman 2013; Godwin 2020; Mazzullo 2013, 2020). The unconformity is readily observed in sections where the Ritchey Formation, Moccasin Bend Formation, and Quapaw Limestone have been eroded and the Bayou Manard member sits directly on top of the Osagean strata of the Reeds Spring Formation in northeast Oklahoma (Boardman 2013; Godwin 2020). This provides insight into the thicker Meramecian strata in the subsurface of the project area with preservation of the lower Meramecian formations along with additional deposition due to the regional sub-Mayes unconformity subaerially exposing and

eroding shallower portions of the Boardman ramp margin and outcrop belt in northeast Oklahoma. This marks the onset of complex depositional controls as tectonic and eustatic events coincide. High frequency depositional cycles interpreted as glacio-eustatic events overlie tectonic influences related to bulge migration during the onset of the Ouachita orogenic event (Ettensohn 2004, 2019; Mazzullo 2013; Pashin 1994, 2009). The progression of the different frequency cycles exhibits significant influence during Chesterian deposition. Thick successions of storm deposits and outer ramp facies in the project area build basinward from the Boardman ramp margin, and appear time-equivalent to the Wedington and Batesville deltaic complexes, which have been identified in northwest Arkansas (Hanford 1986, 1995).

More detailed mapping will provide further insight into the complex tectonic and eustatic controls on Mississippian deposition. Flexural events have been observed and modeled within time equivalent strata of the Appalachian and Black Warrior Basins in response to Ouachita and Neo-Acadian tectonic events, and while high frequency eustatic cycles have been observed, the large-scale influences on sedimentation have been interpreted as flexural events related to foreland basin development (Ettensohn 2004, 2019; Pashin 1994, 2009). Investigating the influences of flexural events in the project area will define the relationship between tectonic and eustatic events in the Midcontinent during the Mississippian as Ouachita and Wichita tectonism progressed.

The workflow used in this project provides an opportunity to investigate the different types of depositional controls on mixed siliciclastic and carbonate systems. The basic stratigraphic and depositional building blocks of these systems should be investigated to gain a better understanding of the factors controlling other mixed carbonate-siliciclastic systems. Furthermore, establishing these building blocks creates an opportunity for developing a holistic research approach for subsequent investigations that includes geochemistry, high-resolution palaeoclimatic and tectonic analysis (Cecil 1993; Pashin 2004).

Conclusions

Facies analysis performed on cores across the project area reveal eight distinct lithofacies. Proximal facies observed in the project area are the grainstone, packstone, and subarkosic sandstone facies, which are coarse-grained, contain high energy depositional features, and have a low response in corresponding gamma-ray logs. Their occurrence and distribution are predominantly confined to the northern project area. Progressing downdip from the more proximal facies deposition are the wackestone, biostromal sponge, and calcareous sandstone-siltstone facies. These facies are indicative of a lower-water energy setting below fair-weather wave base, and provided a more hospitable environment open to a diverse benthic community. These facies contain a variety of rock types and gamma-ray log signatures that range from the lowest gamma response in the chert rich biostromal sponge facies and storm deposited carbonate packstones and spicular chert facies to higher gamma responses in the more clay-enriched bioturbated sandstone and siltstone facies. Distal facies are observed across the project area and are dominated by the outer ramp siltstone and sandstone facies exhibiting the highest gamma-ray responses due to their increase in clay mineralogies, TOC, and phosphate. While the transgressive lag facies is not significant volumetrically, it provides essential stratigraphic context for regional correlations with its distinct gamma-ray signature in response to the elevated phosphate and glauconite content.

The depositional and stratigraphic architecture of the Mississippian strata in the southern Midcontinent of North America is characterized by a mixed carbonate and siliciclastic ramp system. The depositional architecture is characterized by a period of stabilization and aggradation of a widespread carbonate bank across the Midcontinent, established as the Kinderhookian-Osagean (Tournaisian-Viséan) Burlington shelf, and is represented by distal storm deposit and outer ramp facies within the project area. This is followed by a progradational period of the carbonate depositional system out from the Burlington shelf establishing the Meramecian

(Viséan) Boardman ramp margin in north-central Oklahoma, where thick successions of proximal carbonate shoal and carbonate sheet facies accumulate. The closing depositional period is characterized by a thick siliciclastic succession of Chesterian (Viséan-Serpukhovian) sediment building off the Boardman ramp margin into the more distal portions of the Anadarko Basin.

CHAPTER III

MISSISSIPPIAN (LOWER CARBONIFEROUS) FACIES HETEROGENEITY AND DISTRIBUTION WITHIN THE MIXED CARBONATE-SILICICLASTIC RESERVOIRS OF THE MIDCONTINENT STACK PLAY - OKLAHOMA, USA.

Introduction

The study area for this project is in the STACK play in the Anadarko Basin of north-central Oklahoma, where hydrocarbons are produced from Mississippian carbonate and siliciclastic strata. The STACK play is adjacent to the Northwest STACK extension, Mississippi Lime, and Merge plays (Fig 14); it contains a mix of tight carbonate and siliciclastic reservoirs, which represents an emerging reservoir type. As a result, extensive datasets have been collected in an attempt to understand these complex reservoirs. This has provided an opportunity to investigate the stratigraphy and sedimentology of the preserved Lower Carboniferous section, which is present only in the subsurface of the Anadarko Basin; full sections of time-equivalent strata are not exposed in the outcrop belt of northeastern Oklahoma, Arkansas, Kansas, and Missouri. The STACK play refers to a geographic area rather than specific reservoir targets. The STACK acronym stands for the Sooner Trend (oil field), Anadarko (basin), Canadian and Kingfisher (counties).

The Anadarko Basin is the deepest Phanerozoic sedimentary basin in the North American craton (Perry 1989). The basin is asymmetric and structurally deepest along the southwestern margin adjacent to the Wichita and Amarillo uplifts, where the basin contains more than 12 km (~40,000 ft) of sediment ranging in age from Cambrian to Permian. This basin is a giant crustal flexure that is 160 km (100 mi) wide along northwest regional strike and 480 km (300 mi) long along the south-southwest dip direction (Higley 2014). The basin is bounded on the east by the Nemaha Uplift, on the southeast by the Arbuckle Uplift and Ardmore Basin, on the southwest by the Wichita and Amarillo Uplifts, and to the west by the Cimarron Arch (Johnson 1988). The northern part of the basin includes the so-called Anadarko shelf, where basement is less than 1 km deep (~3,000 ft) (Ball 1991).

During the Late Devonian through mid Carboniferous, the Anadarko Basin was located in the western intracontinental portion of the Laurussian Plate between 10 and 20°S. This location produced nutrient-rich upwelling currents that originated in the Ouachita Embayment, particularly during the Famennian and Tournaisian (Gutschick 1983). This upwelling resulted in high organic productivity, including siliceous plankton blooms (i.e., radiolarians) and siliceous bottom fauna (sponges). However, as the Gondwanan and Laurussian plates continued to collide through the mid to Late Carboniferous, the closing of the Rheic Ocean cut off the strong upwelling zones to create the more isolated Midcontinent Sea (Algeo 2008) leading to a drastic decrease in biogenic silica production. The mid Carboniferous marks the transition to an icehouse world as Pangaea formed and Gondwanan glaciation drove high-frequency sea-level change in the Milankovitch band (Crowley 1993; Fielding 2007; Frakes 1992; Saunders 1986; Smith 2000).

Thick Lower Carboniferous (Mississippian) carbonate successions were deposited across North America in the Appalachian, Black Warrior, Illinois, Eastern Interior, Michigan, Arkoma, Anadarko, Williston, and Permian Basins (Ettensohn et al. 2004; Grammer et al. 2018, 2020; Pashin 1994; Pashin et al. 2009; Silberling 1995; Smith 2000; 2019). The composition of the

carbonate bank that developed on the western Laurussian craton during the early Carboniferous changed abruptly in response to orogenic events, which increased the input of siliciclastic sediment (Ettensohn et al. 2019; Sandberg 1982). The Neo-Acadian and Alleghanian synorogenic clastic wedges contain mosaics of open marine, marginal marine, and terrestrial facies that built outward from the eastern highlands onto the stable craton (Ettensohn 2004; Friedman 1988; Meckel 1970; Pashin et al. 2009). Similar thick clastic successions, such as the Humbug Delta, prograded cratonward from the west, and were sourced by the Antler and Ancestral Rocky Mountain highlands (Sandberg 1982). In proximity to the study area, the Early Carboniferous Batesville and Wedington deltaic complexes were apparently sourced from the northern Appalachians and prograded onto the Arkoma shelf (Hanford 1988; 1995). Sediment was transported along fluvial axes through the Michigan and Illinois Basins and was ultimately deposited in the Arkoma and Black Warrior Basins via the Mississippi Valley Graben (Craddock 2013; Hanford 1995; Pashin et al. 2009; Xie et al. 2016).

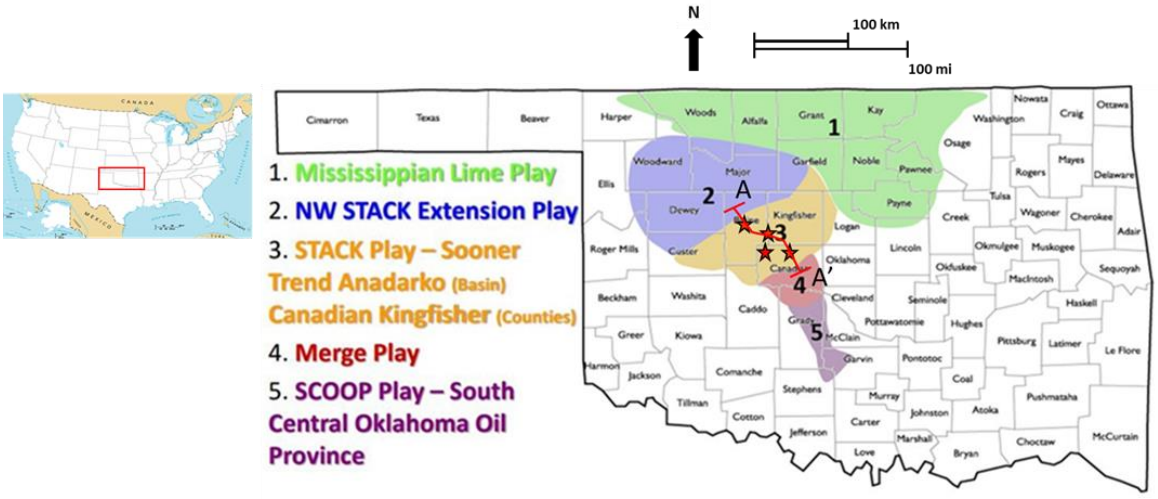

Fig. 14 — Map of study area showing geographic areas and hydrocarbon industry play nomenclature for Mississippian (Lower Carboniferous) oil and gas reservoirs. Cores evaluated for this study are highlighted by red stars, and located in Blaine, Kingfisher, and Canadian Counties within the STACK play, which is highlighted in orange.

Methods

The data used in this study come from subsurface cores and geophysical well logs taken from a transect across the Anadarko Basin and Anadarko shelf (Fig. 1). Core plug samples were extracted for x-ray diffraction (XRD), total organic carbon (TOC), porosity, permeability, and thin section analysis. Descriptive work was performed on clean polished viewing slabs and butt slabs of the cores for recording lithology, sedimentary structures, body fossils, and trace fossils. Framework mineralogy and grain size were analyzed in XRD and thin section using the standard Udden-Wentworth grain-size scale. The intensity of bioturbation was characterized using the ichnofabric index of MacEachern and Bann (2008). Thin sections were analyzed under a petrographic microscope to identify sedimentary structures, rock texture, fabric, mineralogy, fossils, and pore types. Thin sections were impregnated with UV-epifluorescence dye to aid micro-pore identification under UV light. Thin sections were stained on half of the slide with alizarian red S and potassium ferricyanide to aid in distinguishing calcite, ferroan calcite, ferroan dolomite, and feldspar. The Folk classification scheme was used for siliciclastic rock types (Folk 1980), the Dunham classification scheme was used on carbonate rock types (Dunham 1962), and the Choquette and Pray scheme was used to classify pore types (Choquette and Pray 1970).

Facies analysis was performed for each core described in the project area, and the facies are distinguished by their spatial relationships and internal characteristics. This analysis provides the fundamental building blocks for interpreting the Mississippian sedimentary succession (Noel 2010). Each facies is defined by lithology, sedimentary structures, and fossil content in order to provide insight into the genetic relationships between the sedimentary succession and depositional environment. Digital lithofacies logs were generated for each core described in the project area and are defined by the facies scheme that was developed. Each facies is designated by a specific number and assigned to the corresponding depth at which it was observed within core at 15cm (~0.5 ft) intervals. The facies logs were then calibrated to core spectral gamma logs

for integrating the facies logs with geophysical log signatures. These facies logs were then analyzed using JewelSuite subsurface modeling software to make regional correlations and statistical analysis of facies distributions. Statistical analysis of the facies logs was performed to investigate the facies thickness distributions and recurrence patterns. The facies logs were utilized to calculate facies occurrences, gross probability, bed thicknesses. The bed thickness frequency was investigated to provide insight on the depositional hierarchy, and a Markov chain was constructed to determine the transitional probability of one facies succeeding another. This workflow provides insight into the lateral and vertical variability of the facies to discern key lithologic associations, rhythmic, and cyclic accumulation patterns and follows the basic methodology of Wilkinson et al. (2003).

Results

Results from this project were produced through integration of geologic datasets provided from core and geophysical well log analyses for the purposes of investigating the lithofacies distributions across the Mississippian (lower Carboniferous) reservoirs in the STACK play in central Oklahoma. Carbonate and siliciclastic lithofacies were identified within the project area, and they are defined by their genetic relationship in regard to composition, distribution, geometry, and depositional process. The depositional architecture of lower Carboniferous (Mississippian) strata in the Midcontinent of Oklahoma is characterized by a clinoform, mixed carbonate-siliciclastic ramp system. These observations are consistent with other regional studies of time equivalent strata, and clarify the depositional architecture of Lower Carboniferous (Mississippian) strata within the Anadarko Basin (Bynum, 2022; Boardman 2013; Franseen 2006; Godwin 2020; Grammer 2020; Hanford 1986, 1988, 1995; Hunt, 2015; Mazzulo 2011, 2013; Stuckey, 2020). Integration of the lithofacies analysis performed on core and geophysical well logs provides key insights into depositional and stratigraphic architecture, and establishes the basis for investigating the temporal changes of lithofacies distribution. Lithofacies distribution

was investigated within three distinct depositional systems during the Osagean, Meramecian, and Chesterian. Carbonate lithofacies dominate deposition within the Osagean-Meramecian (Tournaisian-Visean) section and decrease in abundance upward into the Chesterian (Serpukhovian) section. The depositional system transitions from a carbonate system to a siliciclastic system starting in the Meramecian (Visean) section, and siliciclastic sediment predominates in the Chesterian (Serpukhovian) section.

Lithofacies Definitions. Seven lithofacies were identified within the cores in the project area. The three carbonate lithofacies characterized are sandy peloidal packstone, wackestone, and spicular chert. Four siliciclastic lithofacies were characterized and include calcareous sandstone, siltstone, mudstone, and glauconitic-phosphatic sandstone.

Carbonate Strata. *Sandy Peloidal Packstone.* This lithofacies is composed of light gray packstone and contains variable amounts of siliciclastic sand and silt (Fig. 15). Individual beds are sharp-based, 10 to 45 cm (0.25 to 1.5 ft) thick, cross-laminated to planar-laminated, and overlain by finer-grained lithofacies. Bioturbation indices range from 3-5 where trace fossils are present; *Planolites, Teichichnus, Phycosiphon, and Chondrites* are common trace fossils. Carbonate microbioclastic debris consists of crinoid, brachiopod, and bryozoan fragments (Fig. 15). Peloids, sand-sized quartz and feldspar grains, carbonate cement, and intraparticle porosity within calcareous fossil debris and peloids also were observed in thin section. This lithofacies contains some of the highest natural fracture density ranging from 1-5 fractures per 30 cm (~1 ft). Fractures are typically strata bound, terminating near bedding surfaces. Gamma-ray signatures from the core gamma-log for this lithofacies range from 0-25 API units in response to their lower concentration of radioactive minerals. These rocks are interpreted to represent deposition below fair weather wave base evidenced by alternating periods of high-energy, cross-bedded carbonate deposition and of low-energy, fine-grained sedimentation and bioturbation (Scholle, 1983). Deposition is consistent with a proximal mid-ramp environment where sediment reworking and

basinward transport of carbonate debris from the inner ramp occurs by way of storm events and sediment gravity flows (Burchette, 1992; Wright, 1990; Cotter 1990; Bracket 1986).

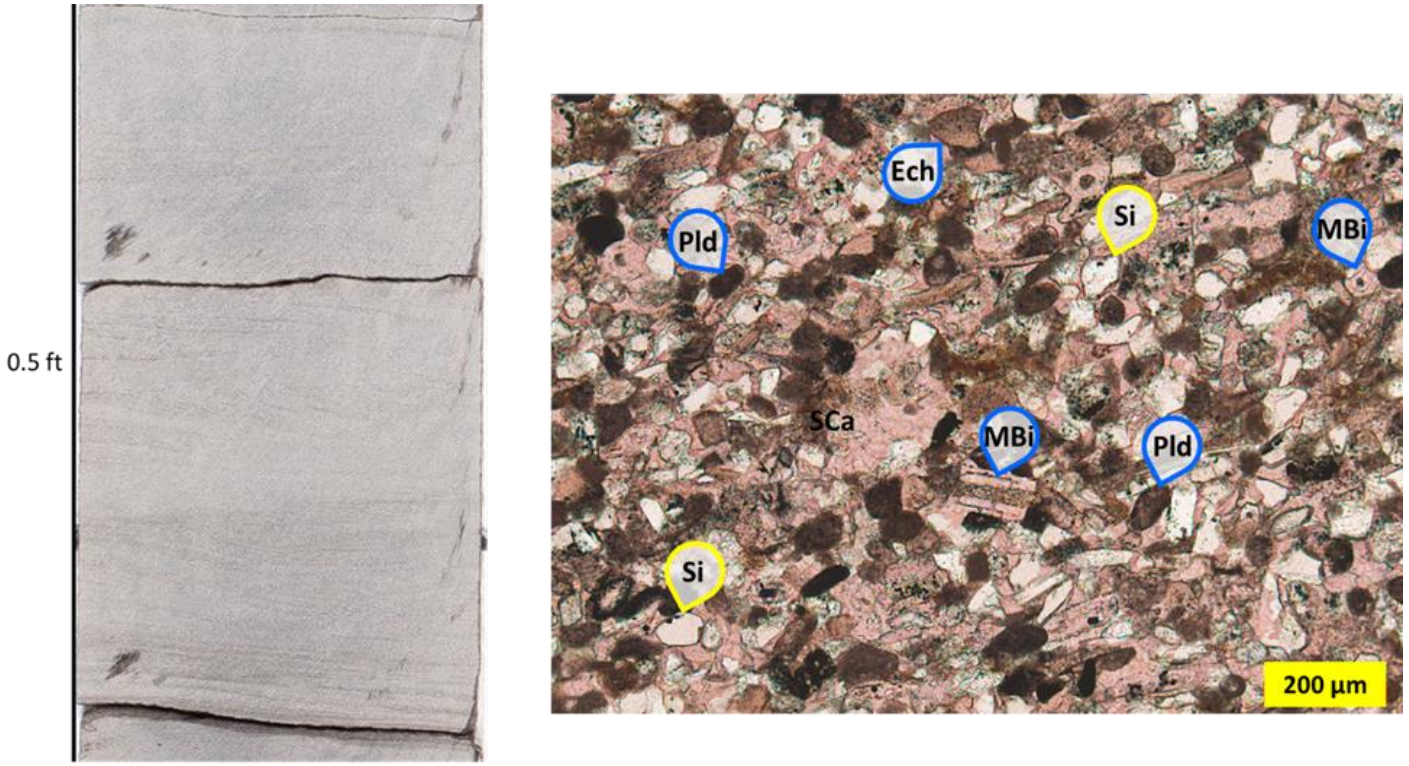

Figure 15. Left image is a core photograph of sandy grainstone containing ripple cross-laminae and horizontal laminae. Right image is a thin section photomicrograph of a sand-bearing grainstone. Alizarin-red stain marks pink calcite. Grains consists of microbioclastic debris (Mbi), peloids (Pld), quartz (Si), and feldspar. Feldspar grains contain dissolution porosity that is commonly filled with organic residue. Spary calcite (SCa) cementation is also observed.

Wackestone. This lithofacies is composed of gray to dark gray wackestone (Fig. 16). Individual beds typically fine upward from packstone to wackestone, are 2 to 10 cm (0.05 to 0.25 ft) thick, and intensely bioturbated. Bioturbation indices range from 3-6, and horizontal feeding burrows predominate. Common trace fossils are *Phycosiphon*, *Chondrites*, and *Zoophycos*. Disarticulated thin-shelled brachiopods are dispersed along bedding planes. The wackestone is composed of microbioclastic debris, peloids, spicules, quartz grains, clay, and carbonate mud. Minor ferroan dolomite occurs within the matrix. Porosity types include intraparticle porosity within fossil debris and peloids, along with moldic porosity from dissolution of spicules. Natural fractures are commonly ptygmatic and terminate where clay content increases (Wang et al., 2019). Gamma-ray signatures from the core gamma-log for this lithofacies are above 75 API units in response to the abundance of radioactive material in the form of organic matter and clay minerals within the matrix. These rocks are interpreted to represent deposition below fair-weather wave base due to the increase in fine-grained sedimentation and horizontal burrows indicative of lower energy settings (Scholle, 1983). Deposition is consistent with a mid-ramp environment where storm-transported microbioclastic sediment is reworked and mixed with finer-grained sediment by burrowing organisms (Burchette, 1992; MacEachern et al. 2008).

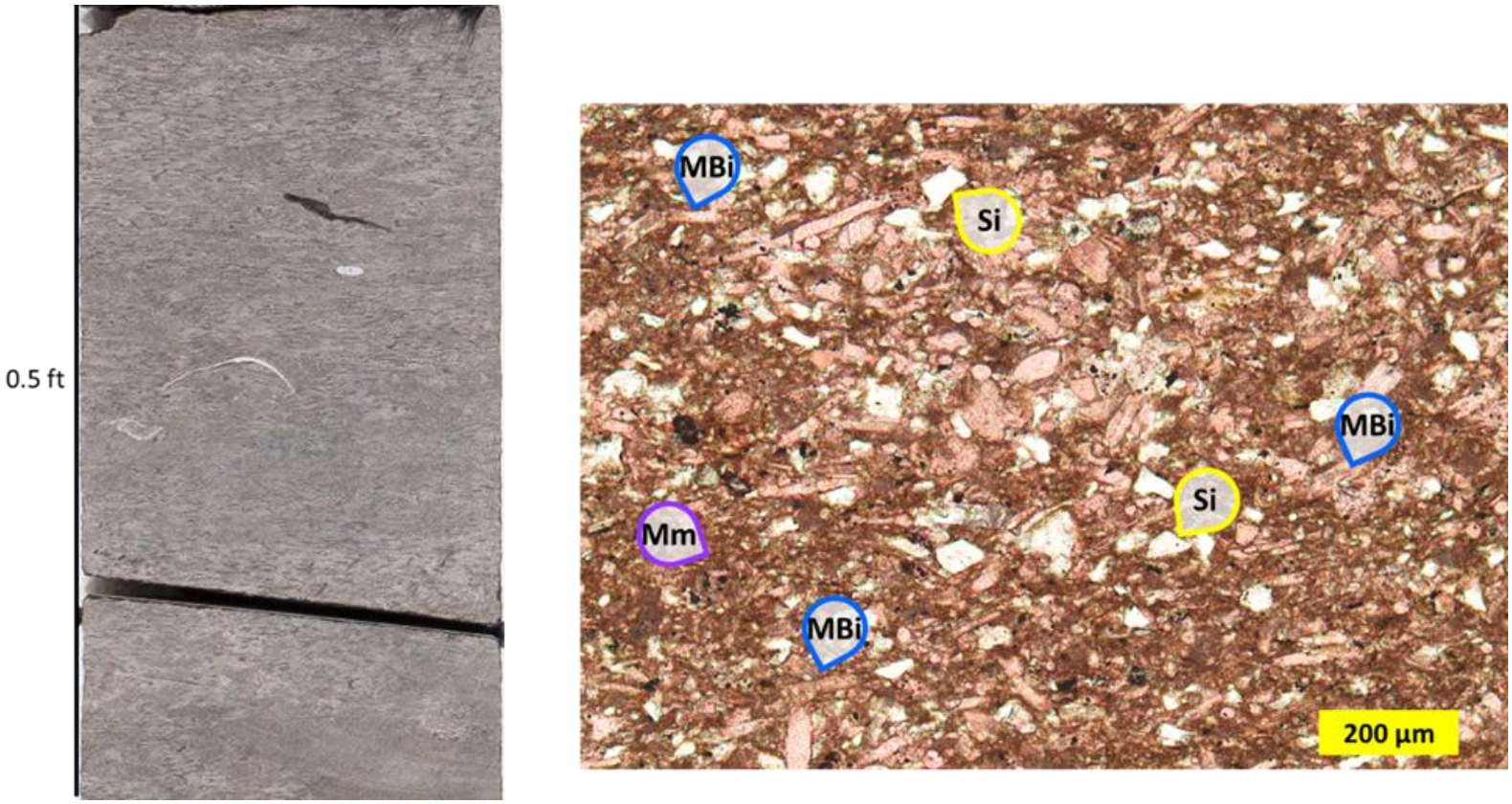

Figure 16. Left image is a core photograph of a shelly, arenaceous packstone. Bioturbation is common within this lithofacies with indices ranging from 3-6. *Chondrites* and *Phycosiphon* are the most abundant ichnofossils, and thin-shelled brachiopods and crinoid ossicles are present. Right image is a thin section photomicrograph of a sandy packstone. Alizarin-red stain marks calcite. Grains consist of microbioclastic debris (Mbi), peloids, quartz (Si), feldspar, and the matrix is composed of carbonate mud and clay minerals (Mm).

Spicular Chert. The spicular chert lithofacies is composed of bluish-gray chert with a granular texture resembling grainstone (Fig. 17). Individual beds are sharp-based, are 2-10 cm (0.05 to 0.25 ft) thick, are planar-laminated or bioturbated, and are overlain by silt-rich wackestones. Where bioturbation is present, indices range from 3-6 with horizontal and vertical burrows being typical. Common traces are *Planolites*, *Teichichnus*, *Chondrites*, *Phycosiphon*, and *Zoophycos*. The spicular chert is composed primarily of sponge spicule debris with imbricate spicules concentrated in laminae. Bioturbated beds contain poorly oriented spicules mixed with other bioclastic grains, clay, and dolomite. Moldic porosity from dissolution of spicules is present, with silica cement being the most common. Laminated beds contain more chert than bioturbated beds, but both contain varying proportions of chert, calcite cement, and dolomite cement. This lithofacies contains the highest natural fracture density with greater than 10 fractures per 30 cm (1 ft) being common. Fractures are typically strata-bound and terminate near bedding surfaces. Gamma-ray signatures from the core gamma-log for this lithofacies range from 0-25 API units in response to their lower concentration of radioactive material. These rocks are interpreted to represent deposition below wave base due to the concentration and imbrication of thin spicular debris beds, increase in fine-grained sediment, and common reworking of spicule and microbioclastic debris with the finer-grained sediment by burrowing organisms. The characteristic trace fossils like *Phycosiphon, Chondrites,* and *Zoophycos* are indicative of a *Zoophycos* ichnofacies occurring in predominately lower water energy settings. Deposition is consistent with a distal mid-ramp environment where storm transported spicule and microbioclastic beds exhibit erosive bases with higher energy sedimentological features and sharp tops where not bioturbated similar to characteristics observed in storm deposits of a Silurian mid ramp environment in Pennsylvania (Cotter 1990; Nakashima, 2007.

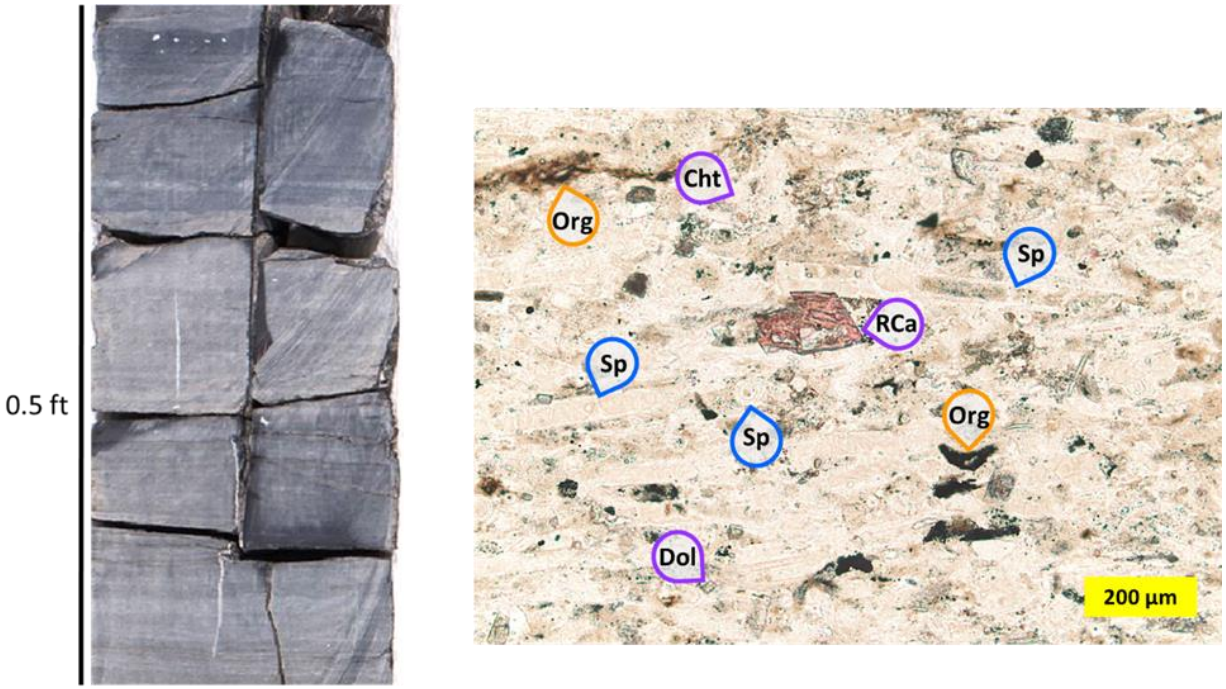

Figure 17. Left image is a core photograph of spicular chert. Individual beds are laminated with scattered crinoid fragments. Beds with the highest silica content contain intrastratal natural fractures typically filled with calcite. Right image is a thin section photomicrograph of spicular chert with grainstone texture. Alizarin-red stain helps identify calcite. Sample contains abundant broken monaxon spicules (Sp), dolomite (Dol), and organic inclusions (Org). This sample has undergone a complex diagenetic history including a conversion of biogenic silica to chert (Cht), an episode of dolomite precipitation, and followed by dolomite dissolution and replacement with calcite (RCa).

Siliciclastic Strata. *Calcareous Sandstone.* This lithofacies is characterized as a calcareous sandstone that is gray to brownish-gray with the most porous beds containing hydrocarbon stain (Fig. 18). Individual beds have sharp bases that grade upward into siltstone, are thick bedded, and are cross-bedded, laminated, or bioturbated. Bioturbation indices range from 2-4. Burrows commonly descend and are filled with sediment from the overlying bed. The calcareous sandstone is composed of fine to very fine-grained sand composed of quartz, feldspar, peloids, microbioclastic debris, and varying amounts of clay and carbonate cement. Interparticle porosity and intraparticle porosity within partially dissolved feldspar grains are present along with intraparticle porosity within peloids and microbioclastic debris. While organics in the form of migrated hydrocarbons are observed staining the pore system. Gamma-ray signatures from the core gamma-log for this lithofacies range from 25-75 API units in response to an increase in the radioactive material in the form of organic matter, clay and feldspar minerals. These rocks are interpreted to represent deposition below fair-weather wave base base due to the sharp-based sandstone beds that grade upward into siltstone (Pemberton, 2012). Deposition is consistent with a storm-dominated mid-ramp environment. Vertical escape burrows provide evidence for periods of rapid sedimentation alternating with periods of lower sedimentation rate between recorded by fine-grained background sedimentation and extensive burrowing. *Planolites*, *Teichichnus*, and *Phycosiphon* traces are present and interpreted as a *Cruiziana* ichnofacies, which is typical of mid ramp environments (MacEachern, 2008).

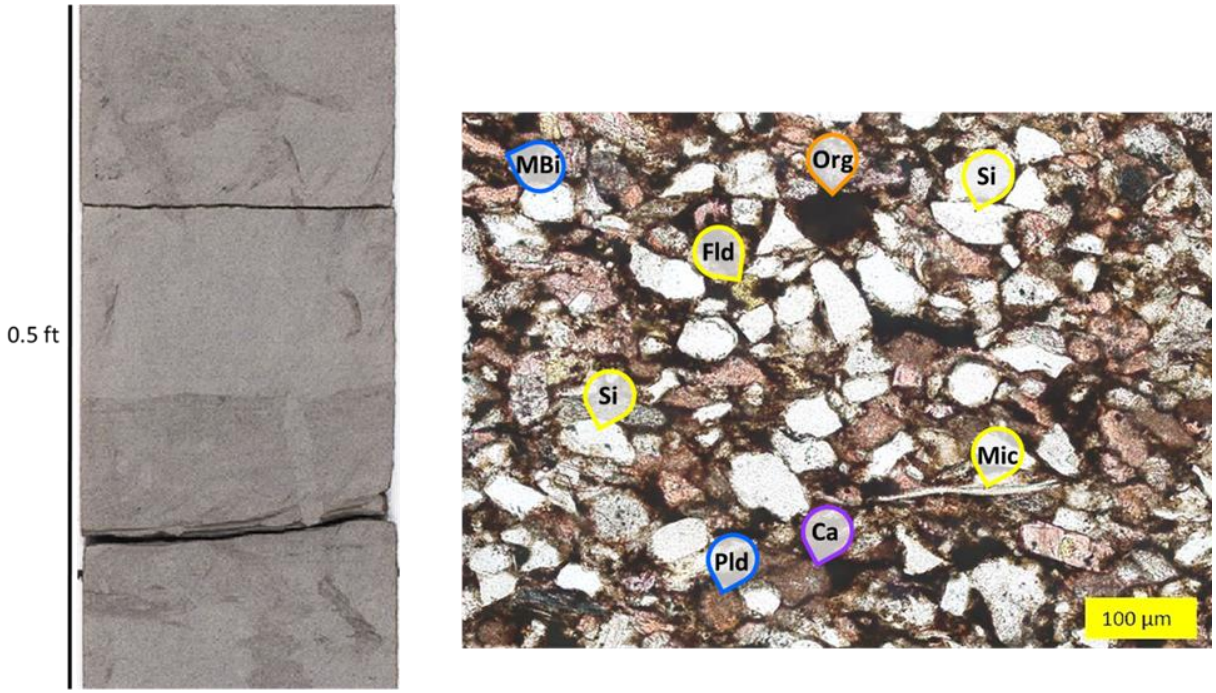

Figure 18. Left image is a core photograph of calcareous sandstone. Individual beds have sharp bases that transition from massive to laminated. Beds typically gradationally fine upward and are bioturbated. Vertical burrows are common. They are either filled with coarser sand from above or contain more clay than the adjacent sandstone. Right image is a thin section photomicrograph of calcareous sandstone. Sample contains abundant medium- to fine-grained sand sized quartz (Si) and feldspar (Fld), large mica flakes (Mic), clays, microbioclastic debris (MBi), pore-filling organic residue (Org), and calcite cement stained pink (Ca).

Siltstone. This lithofacies is composed of gray to dark gray siltstone (Fig. 19). Individual beds are typically laminated or bioturbated and thinly bedded. Bioturbated beds are typically more calcareous than surrounding strata, and bioturbation indices range from 2-4. Common traces are *Zoophycos, Chondrites*, and *Phycosiphon*. Disarticulated thin-shelled brachiopods occur along bedding planes. The siltstone is composed of quartz, feldspar, mica, clay, agglutinated benthic foraminifera, amorphous organic matter, conodonts, and varying amounts of carbonate mud and microbioclastic particles. Interparticle porosity between grains and intraparticle porosity within feldspar grains are typical. Gamma-ray signatures from the core gamma-log for this lithofacies are above 75 API units in response to the abundance of radioactive material in the form of organic matter, clay, phosphate, and feldspar minerals. These rocks are interpreted to represent deposition below wave base due to the increase in fine-grained sedimentation, decrease in carbonate content, and the transition to more horizontal and branching burrowing behaviors indicative of lower energy settings. Deposition is consistent with a distal mid ramp to outer ramp environment. The fining upward siltstone layers have scoured bases, are coarser and laminated at the base, then capped by either bioturbated muddy siltstone or silty laminae reworked by bottom currents. Sparse diminutive fossils and the low degree of bioturbation demonstrating a *Zoophycos* ichnofacies indicate that bottom water conditions may have been oxygen-stressed (MacEachern, 2007). However, bioturbation indicates episodic oxygenation, which is typical of the distal mid ramp to outer ramp environments.

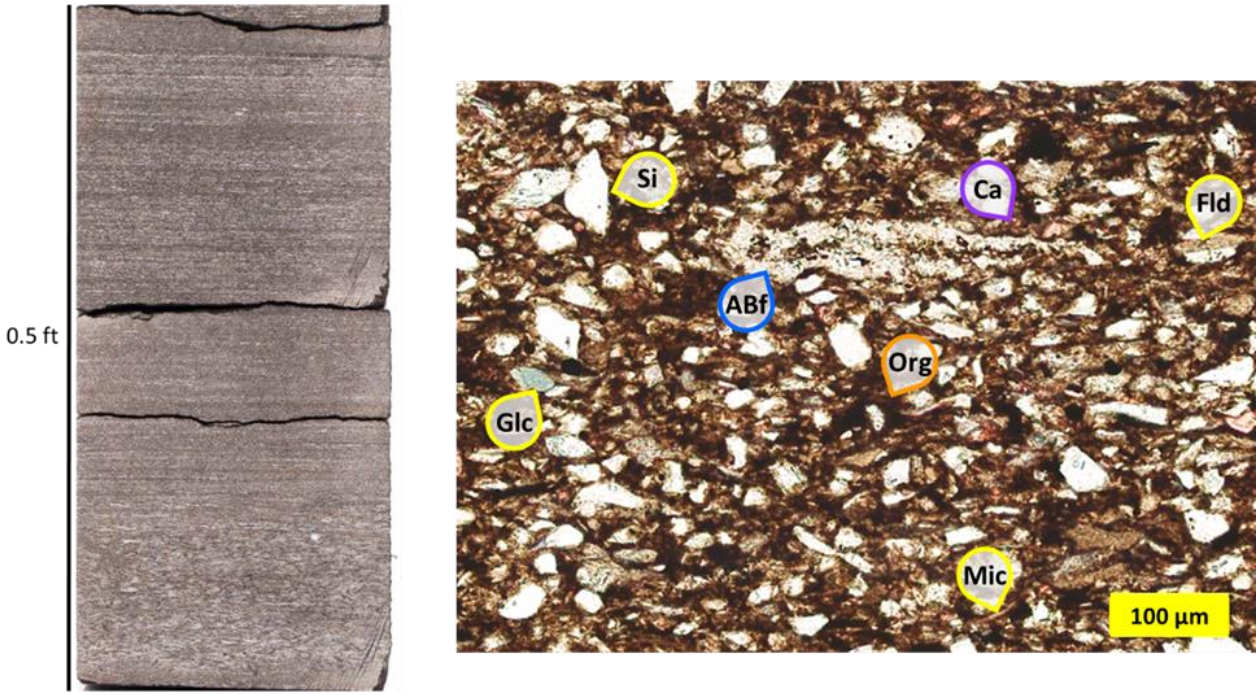

Figure 19. Left image is a core photograph of siltstone that is laminated and bioturbated. Bioturbated beds have higher calcite content than laminated beds. Scattered thin-shelled brachiopods and crinoid fragments are present, and most commonly observed along bedding planes. *Chondrites*, *Phycosiphon*, and *Zoophycos* are the most common ichnofossils. Right image is a thin section photomicrograph of siltstone. Sample contains very fine-grained quartz sand and quartz silt (Si). Other constituents include feldspar (Fld), mica (Mic), clay, agglutinated benthic foraminifera (ABf), organic matter (Org), and minor glauconite (Glc).

Mudstone. This lithofacies is composed of dark gray argillaceous and silty mudstone (Fig. 20). Individual beds are typically laminated, ripple cross-laminated, and thinly bedded. Bioturbation indices range from 1-2. Rare *Zoophycos* traces were observed, and disarticulated thin-shelled brachiopods are present along bedding planes. The mudstone is composed of quartz, feldspar, mica, clay, pyrite, agglutinated benthic foraminifera, conodonts, amorphous organic matter, and compacted clay floccules. Porosity is hard to identify at this scale except for intraparticle porosity within feldspar grains. Gamma-ray signatures from the core gamma-log for this lithofacies are above 75 API units in response to the abundance of radioactive material in the form of organic matter, clay and feldspar minerals. These rocks are interpreted to represent deposition below wave base due to fine grain size, increased organic matter content, decreased carbonate content, and a fossil assemblage of benthic foraminifera and conodonts. Deposition is consistent with the outer ramp. Depositional mechanisms are interpreted to be suspension settling, storm-induced flows, and bottom current reworking of silt and clay. Bottom current reworking of silt and clay plays a significant role in the development of the mudstone fabric. Silt and clay migrate as ripples generated by bottom currents, and were deposited as thin veneers of interlaminated silt and clay (Yawar, 2017; Schieber, 2009). Sparse, diminutive fossils, pyrite precipitation, and the low degree of bioturbation indicate that bottom water conditions were stressed. However, *Zoophycos* traces, other horizontal burrows, and benthic foraminifera indicate at least episodic conditions hospitable to pioneering organisms (e.g., Seilacher, 2007; Bann, 2008).

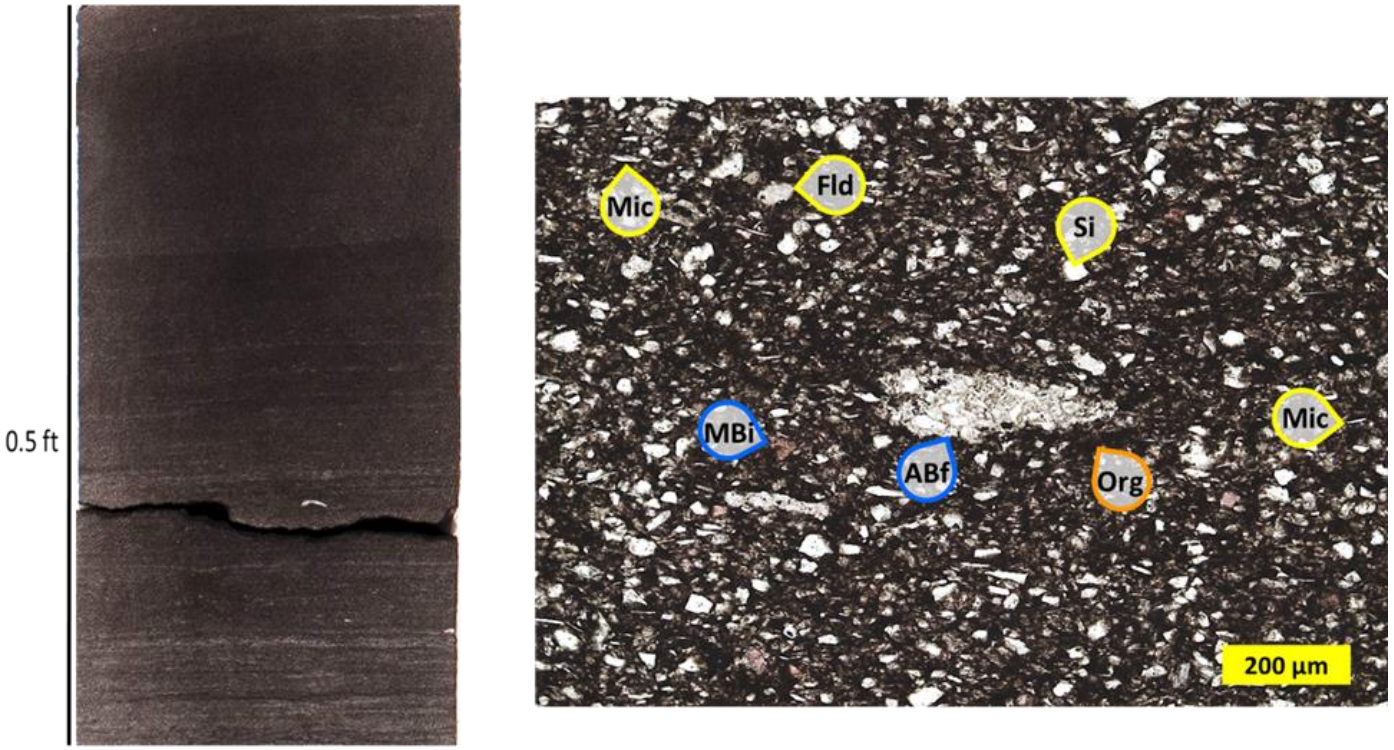

Figure 20. Left image is a core photograph of organic-bearing silt-rich mudstone. Individual beds are laminated to faintly laminated. Rare observations of bioturbation and thin-shelled brachiopod fragments. Right image is a thin section photomicrograph of an organic-bearing silt-rich mudstone. Sample contains quartz (Si) and feldspars (Fld), mica, clays, compacted agglutinated benthic foraminifera (ABf), organics (Org) and minor carbonate microbioclastic debris (MBi).

Glauconitic-Phosphatic Sandstone. This lithofacies is composed of greenish to brownish sandstone (Fig. 21) Bed thickness ranges from 5-60 cm (0.5 to 2 ft), and the beds are bioturbated to laminated. The beds have sharp bases that gradationally transition upward into a finer grained siltstone or wackestone lithofacies. Bioturbation indices range from 5-6 with an assemblage including *Teichichnus* and *Thalassinoides*. These complex vertical burrows are also observed extending into the underlying substrate. Fragmented brachiopod debris along with phosphate nodules and abraded bone fragments are commonly concentrated at the base of the bed and decrease upward. Burrowing intensity decreases upward, and laminae are visible in the upper part of the sandstone beds. The sandstone consist of medium- to fine-sand sized glauconite and quartz grains, ferroan dolomite, quartz, feldspar, phosphatic clasts, bone fragments, carbonate fossil debris, conodonts, and other clay minerals. Interparticle porosity is the dominant porosity type, while intraparticle porosity within glauconite grains and ferroan dolomite rhombs are common as well. Gamma-ray signatures from the core gamma-log for this lithofacies are above 75 API units in response to the abundance of radioactive material in the form of organic matter, clay, feldspar, glauconite, and phosphate. These rocks are interpreted to represent transgressive deposition associated with ravinement development (e.g., Liu and Gastaldo, 1992; Miller and West, 1998) due to their sharp bases and vertical burrows extending into the underlying substrate, which are filled with the glauconitic sandstone. This burrowing behavior is interpreted as a *Glossifungites* surface. These types of features are consistent with deposition of a transgressive sandstone associated with shoreface erosion and subsequent stratigraphic condensation (MacEachern, 2007).

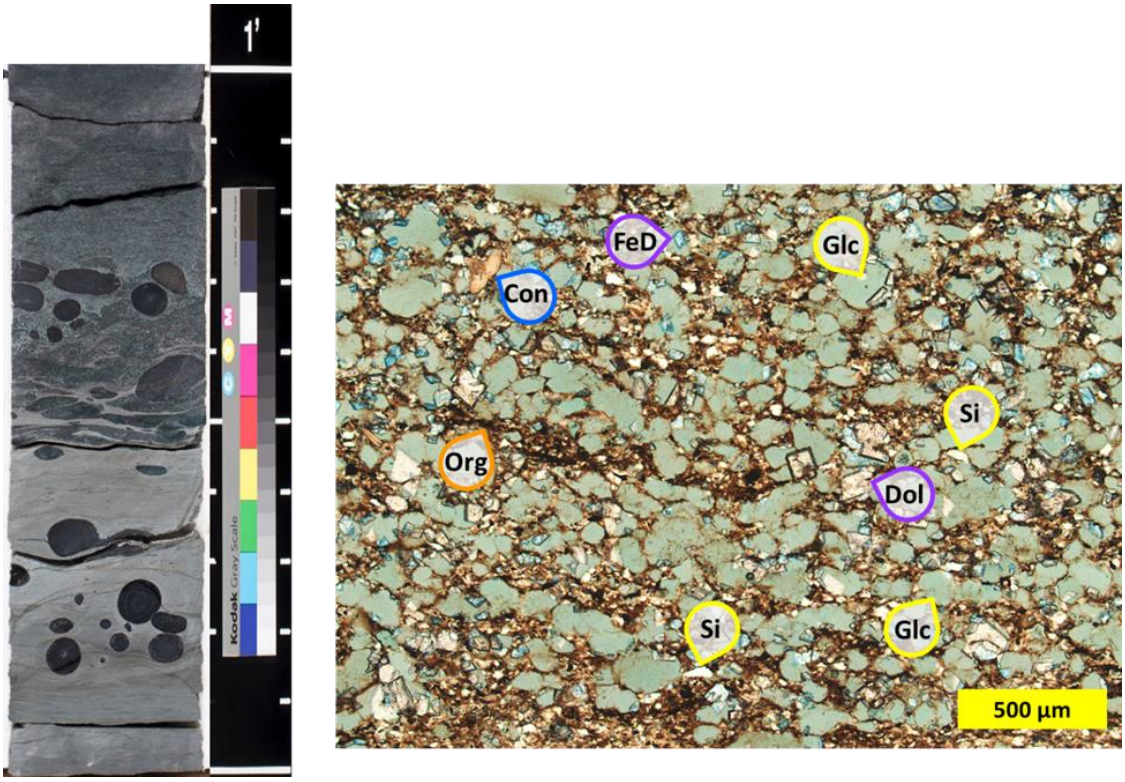

Figure 21. Left image is a core photograph of glauconitic sandstone. Intense bioturbation is common with vertical burrows extending into the underlying substrate. Phosphate nodules, glauconite grains, and brachiopod fragments are also observed. Right image is a thin section photomicrograph of a glauconitic sandstone. Sample contains glauconite grains (Glc), quartz grains (Si), conodont fragments (Con), iron-rich dolomite (FeD), dolomite (Dol), organic staining (Org), and clays.

Lithofacies Distributions. Facies heterogeneity and distribution across the STACK play are related to variations in the depositional system of the Mississippian (Lower Carboniferous), where thick carbonate successions were deposited across the North American craton. The widespread carbonate bank changed abruptly in response to orogenic events, which increased siliciclastic sediment flux (Ettensohn et al., 2019; Sandberg, 2009), and is represented proximal to the project area by the Batesville and Wedington deltaic complexes sourced from the Appalachians (Hanford, 1995; Pashin, 2009, Craddock, 2013; Xie et al., 2016). The depositional succession observed in the Anadarko Basin and Shelf can be subdivided into 3 distinct depositional systems and parasequence sets (Fig. 22). The first is represented by stabilization and aggradation of the carbonate and sponge biocommunities during the Osagean. This was followed by a period of carbonate progradation during the Meramecian, when the first observable siliciclastic mixing occurred. After this transitional period, Chesterian influx of siliciclastics supplanted carbonate production, and only reworked and transported carbonate is observed in the project area.

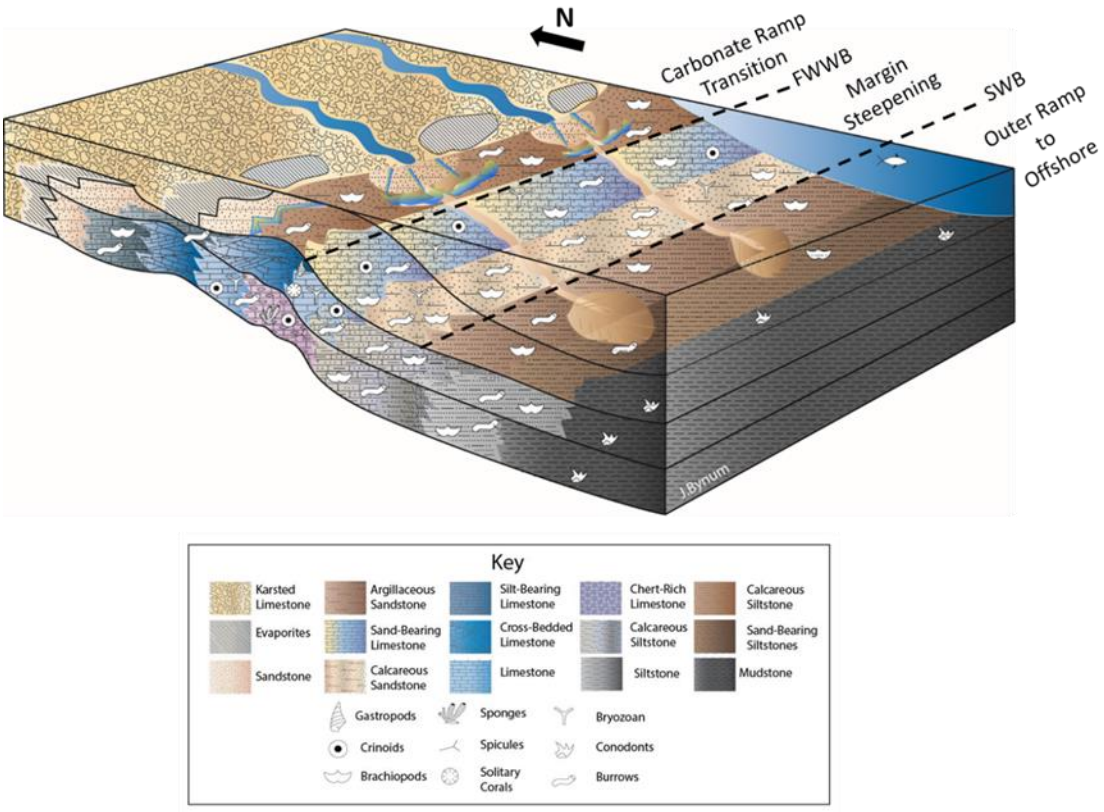

Fig. 22 — Block diagram showing the transition from a carbonate-dominated system to a siliciclastic-dominated system (Bynum, 2022). The depositional environments observed for the carbonate system range from grainstone dominated inner-ramp deposits to calcareous siltstone dominated outer-ramp deposits. While the siliciclastic depositional environments range from arkosic sandstone dominated upper shoreface deposits to siltstone dominated offshore deposits. Depositional stacking patterns are identified across the Anadarko Basin & Shelf, and stratigraphically record progradational packages at different scales within the Lower Carboniferous (Mississippian) strata.

Parasequences observed in core subdivide the Osagean, Meramecian, and Chesterian strata into clinoform parasequence sets, which are correlatable across the STACK play using integrated facies and geophysical logs (Fig. 23). The parasequences are shoaling-upward successions bounded by marine flooding surfaces. The complete succession in the study area appears to be

subaqueous, and any evidence for exposure has been obscured by reworking of sediment below the ravinement surfaces forming the base of the glauconitic sandstone lithofacies. The clinoform parasquence stacking pattern defines an overall shoaling-upward succession with offshore shaly strata most common at the bottom of the section and ramp-shelf carbonate and sandstone most common at the top. Wells in the northwest contain strata enriched in calcareous fossil debris and bioturbation, as well as coarser grained siliciclastic deposits. Wells to the southeast, by contrast, contain deeper water depositional facies enriched in organic matter, clay, and silt and carbonate. Indeed, proximal depositional environments of the Oklahoma Shelf are recorded in the northwestern part of the cross section (Core 1), and distal shelf environments are recorded in the southeastern part (Core 4).

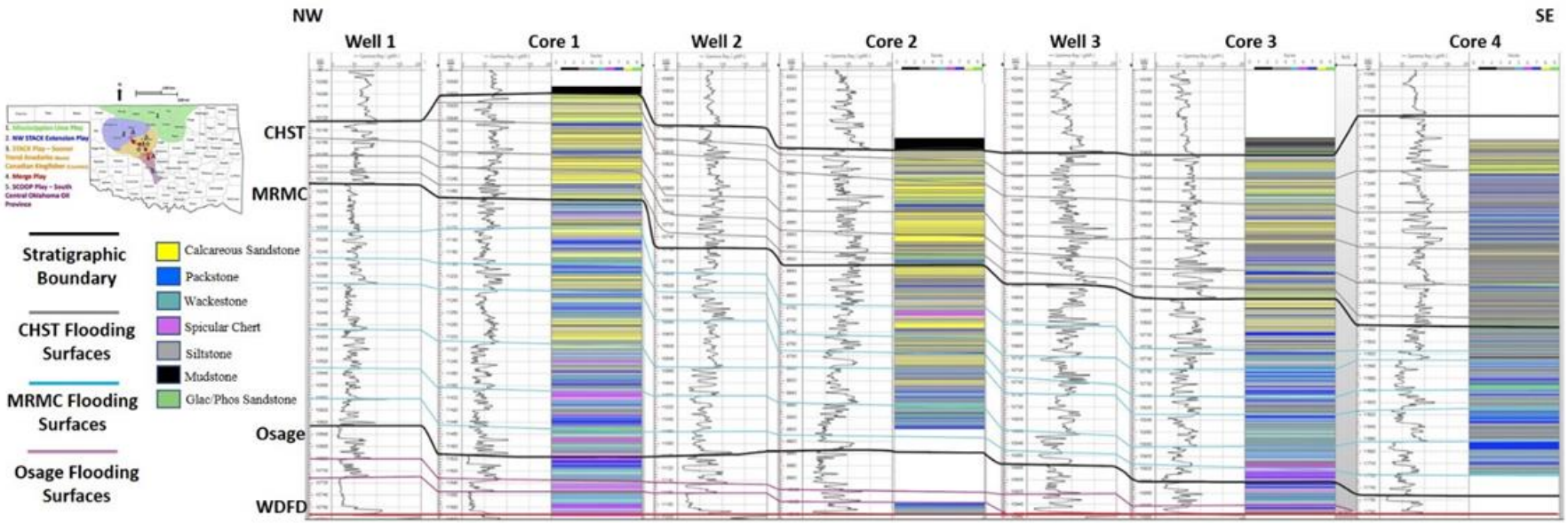

Fig. 23 — Cross-section showing correlatable parasequence packages using gamma ray and facies logs. Facies distributions vary laterally and vertically due to the changes in depositional environments and eustatic sea-level fluctuations. Osagean strata are predominately composed of carbonate and spicular chert in the northwest that thin basinward, passing to laminated siltstone and mudstone. The Meramec strata are characterized by a mixed carbonate-siliciclastic succession, with an increase in siliciclastic facies in the upper section. Chesterian strata are predominately composed of siliciclastic facies with an overall increase in sandstone content.

Lithofacies Statistics.

Osagean. The Osagean section in the STACK area contains the highest percentage of carbonate facies (47%) compared to the other stratigraphic sections with 27% wackestone, and 20% packstone (Fig. 24). It also contains the highest percentage of spicular chert (23%). The siltstone facies compose 24% of the rock observed in the cores. The histogram shows a bimodal distribution of sediment in which wackestone, siltstone, specular chert, and packstone are dominant and glauconitic-phosphatic sandstone, mudstone, and calcareous sandstone are subordinate. However, 25% of the Osage section was not cored, and likely would alter the histogram. Wackestone has the highest gross probability (40%) while packstone has the highest mean bed thickness of 1.11 ft. (Table 2). The bed thicknesses for the major lithofacies all demonstrate a power function distribution with the majority of thicknesses occurring in the 0.5 to 1 ft. range (Fig. 25), which is a salient characteristic of stochastic rather than deterministic systems. Calcareous sandstone, mudstone, and glauconitic-phosphatic sandstone were under sampled and so were not included in the thickness-frequency analysis. The Markov chain analysis demonstrates the transitional probability for each facies (Table 3). Results indicate that the highest and most consistent transitional probability is that any given facies will be overlain by siltstone (33-100%), which defines a rhythmic aspect of Osagean sedimentation. Interestingly, siltstone is most likely to be succeeded by wackestone (50%), specular chert (31%), or less commonly, packstone (16%). This result indicates that Osagean facies development was not cyclic, and regional facies relationships indicate that transitional probability favors carbonate sedimentation in the upper part of the ramp and siltstone deposition in the outer ramp. While lithologic transitions help define and correlate individual parasequences as thin shoaling-upward packages, the most consistent relationship within the Osagean parasequence set is that any given facies will most likely be overlain by siltstone.

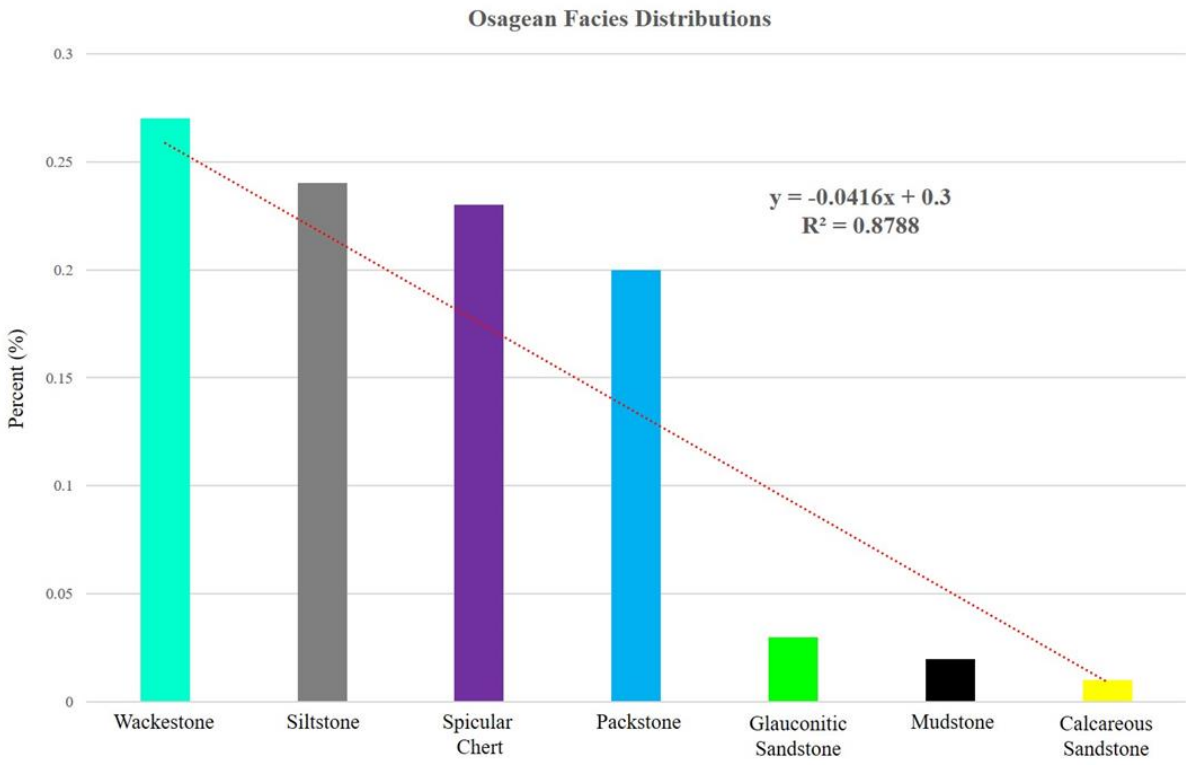

Fig. 24— Histogram of the combined Osagean facies distribution from the studied cores across the STACK play. The rock volume consists of: 47% carbonate facies, 23% spicular chert facies, 24% siliciclastic facies. The most common facies is wackestone (27%) with the spicular chert making up nearly a quarter of the rock volume. The Osagean lithofacies demonstrate a linear distribution relationship with an R^2 value of 0.88.

.

Facies	Occurrences	Gross Probability	Total Thickness (ft)	Mean Thickness (ft)
Siltstone	101	0.20	49.5	0.77
Packstone	82	0.17	41	1.11
Wackestone	197	0.40	55.5	0.86
Calcareous Sandstone	2	0.00	1	0.50
Spicular Chert	94	0.19	46.5	0.67
Glauc/Phos Sandstone	8	0.02	5.5	0.81
Mudstone	11	0.02	4.5	0.75

Table 2—Demonstrating for each lithofacies the number of occurrences, gross probability, total thickness associated with occurrences, and the mean thickness of each occurrence within the Osagean strata. The carbonate facies have a combined gross probability of 57%, with spicular chert and siltstone gross probabilities occurring near 20% each. The packstone lithofacies has the highest mean bed thickness of 1.11 ft., and the calcareous sandstone has the lowest mean bed thickness of 0.5 ft.

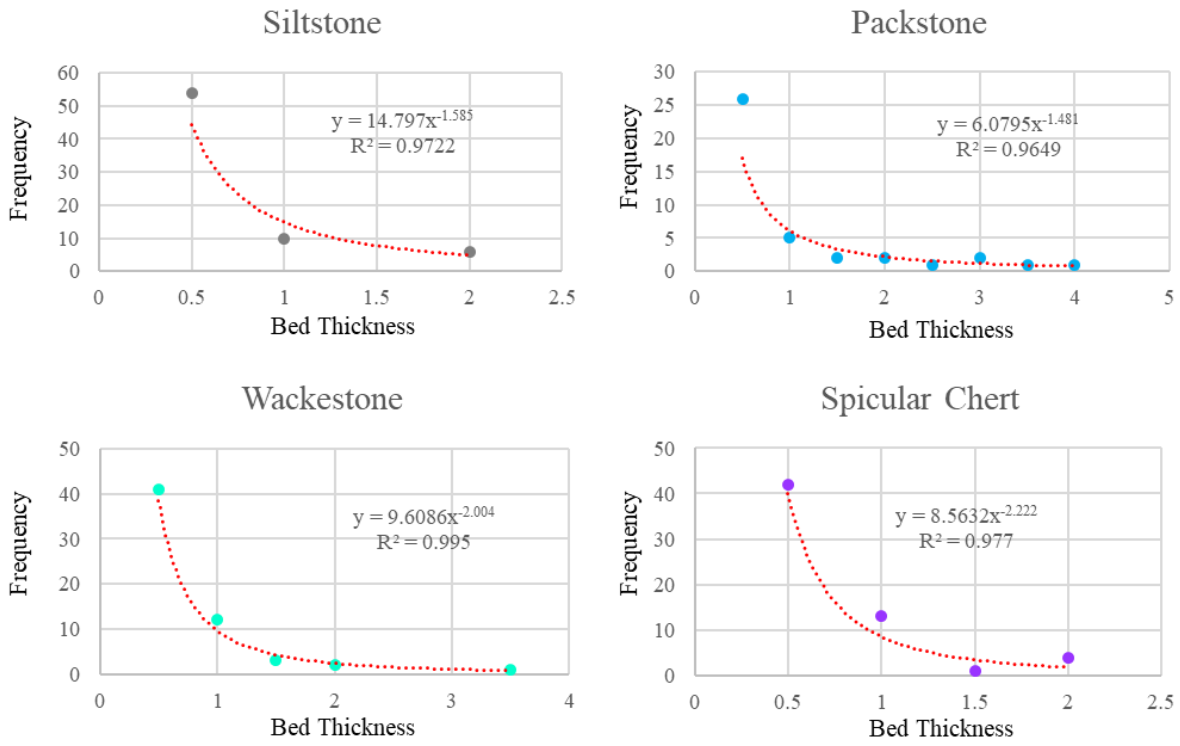

Fig. 25— Thickness frequency distributions of the Osagean strata with bed thickness on the x-axis and frequency on the y-axis. The siltstone contains the highest number occurrences of 0.5 ft thickness with 54 while the wackestone (41) and spicular chert (42) demonstrate similar thickness frequencies. The packstone contains the thickest occurrence at 4 ft, while the other lithofacies maximum occurrence thickness is approximately 2 ft. Thickness frequency distributions are observed as power functions with an R^2 value greater than 0.95. The calcareous sandstone, glauconitic sandstone, and mudstone are rare and under sampled statistically so no distribution could be defined.

Succeeding Beds

Underlying Beds Facies	Siltstone	Packstone	Wackestone	Calcareous SS	Spicular Chert	Glauc/Phos SS	Mudstone
Siltstone	x	0.16	0.5	0.02	0.31	0.01	0
Packstone	0.36	x	0.3	0	0.34	0	0
Wackestone	0.44	0.19	x	0	0.23	0.1	0.04
Calcareous Sandstone	1	0	0	x	0	0	0
Spicular Chert	0.57	0.21	0.18	0	x	0	0.04
Glauc/Phos Sandstone	0.61	0.17	0	0	0.11	x	0.11
Mudstone	0.33	0.49	0	0	0.09	0.09	x

Table 3—Demonstrating a Markov chain of transitional probability for each lithofacies within the Osagean strata. Overall, siltstone has the highest transition probability while the calcareous sandstone has the lowest and is only observed within one core. The dark orange color represents transition probabilities greater than 0.5, orange represents 0.4-0.49, yellow represents 0.3-0.39, green represents 0.2-0.29, teal represents 0.1-0.19, blue represents 0.01-0.09, and grey represents no facies succeeding relationship was observed.

Meramecian. The Meramecian section is the most common target for hydrocarbon production in the STACK area. Overall, the siltstone facies is the most common facies observed (52%) with the combined carbonate facies constituting 30% of the strata (Fig. 26). The lateral facies distribution in Meramecian strata among the cores shows that the siltstone facies is the most common facies ranging from 44-64%. The spicular chert is most abundant in the northwest (Core 1 = 6%) and decreases southeastward so that no specular chert is present in core 4. The calcareous sandstone facies exhibit the same distribution pattern with a maximum percentage in the northwest (Core 2 = 17%). In Core 4, which is in the southeastern part of the transect, none of the facies is observed. The siltstone has the highest gross probability (37%) and the highest mean bed thickness of 1.63 ft. (Table 4). The bed thickness-frequency distribution for the major occurring lithofacies all demonstrate a power function distribution with the majority of thicknesses occurring in the 0.5 to 1 ft. range (Fig. 27), demonstrating a dominant stochastic component of sedimentation. The Markov chain analysis demonstrates the transitional probability for each facies (Table 5). As in the Osagean section, transitional probability in Meramecian strata indicates that any given facies

is most likely overlain by siltstone, indicating a strong rhythmic component of sedimentation (transitional typically between 44 and 74%). Transitional probabilities among siltstone, packstone, wackestone, and calcareous sandstone typically range from 18-33%, indicating a random component of sedimentation. Measured sections demonstrate a vertical tendency favoring a transitional from carbonate to siliciclastic sedimentation and a lateral tendency for packstone and sandstone to pass down-ramp into wackestone, siltstone, and mudstone. These patterns indicate that vertical facies transition is stochastic, and that trends among mudstone, siltstone, sandstone, and carbonate beds can be used to define shoaling-upward parasequences within the Meramecian section. The northwestern cores are dominated by sandstone and siltstone, whereas carbonate content increases and sandstone content decreases southeastward in the outer ramp. As in the Meramecian section, vertical changes in the distribution of mudstone, siltstone, sandstone, and carbonate can be used to define and correlate parasequences.

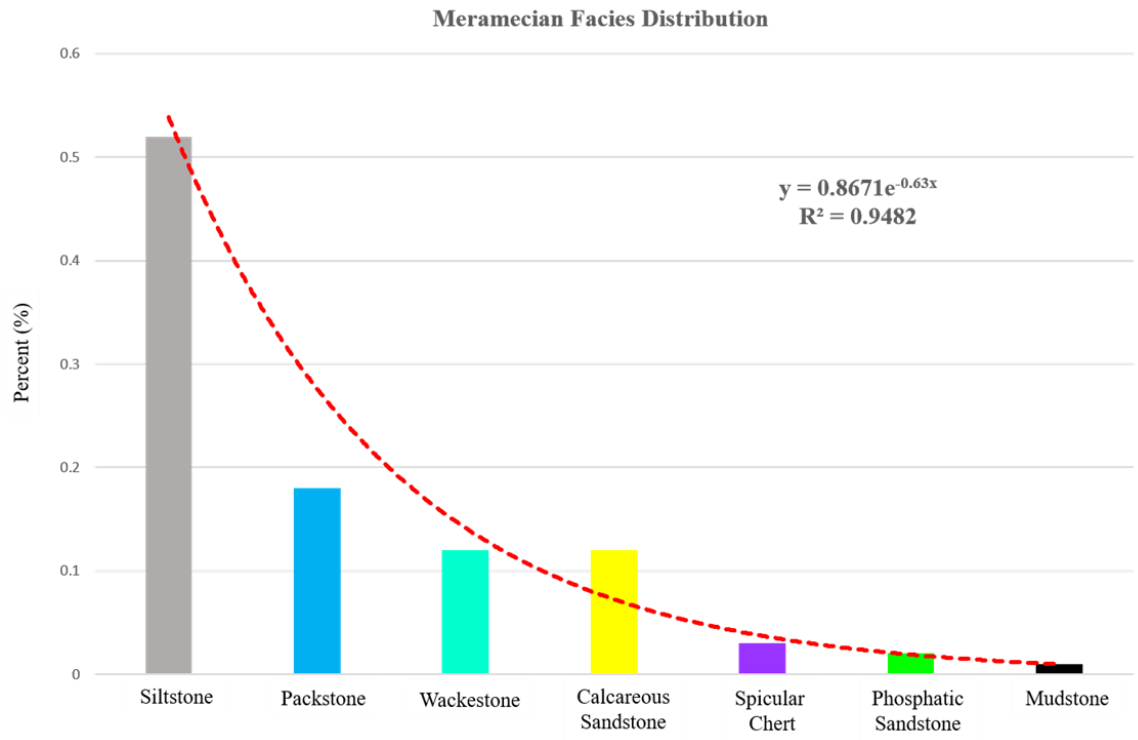

Fig. 26— Histogram of the Meramecian strata facies distribution combined from the studied cores across the STACK play consists of: 64% siliciclastic facies, 30% carbonate facies, and 3% spicular chert. The most common facies is the siltstone (52%), while the sandstone facies increased by a factor of 11 compared to the underlying Osagean section. The lithofacies distribution is represented by an exponential relationship with an R^2 value of 0.95.

Facies	Occurrences	Gross Probability	Total Thickness (ft)	Mean Thickness (ft)
Siltstone	469	0.37	652.5	1.63
Packstone	257	0.20	238	0.94
Wackestone	257	0.20	158.5	0.61
Calcareous Sandstone	182	0.14	146	0.80
Spicular Chert	53	0.04	39.5	0.66
Glauc/Phos Sandstone	26	0.02	19.5	0.74
Mudstone	30	0.02	17.5	0.63

Table 4— Demonstrating for each lithofacies the number of occurrences, gross probability, total thickness associated with occurrences, and the mean thickness of each occurrence within the Meramecian strata. The carbonate facies have a combined gross probability of 40%, while siltstone gross probabilities occurring at 37%. The siltstone lithofacies has the highest mean bed thickness of 1.63 ft., and the wackestone has the lowest mean bed thickness of 0.61 ft.

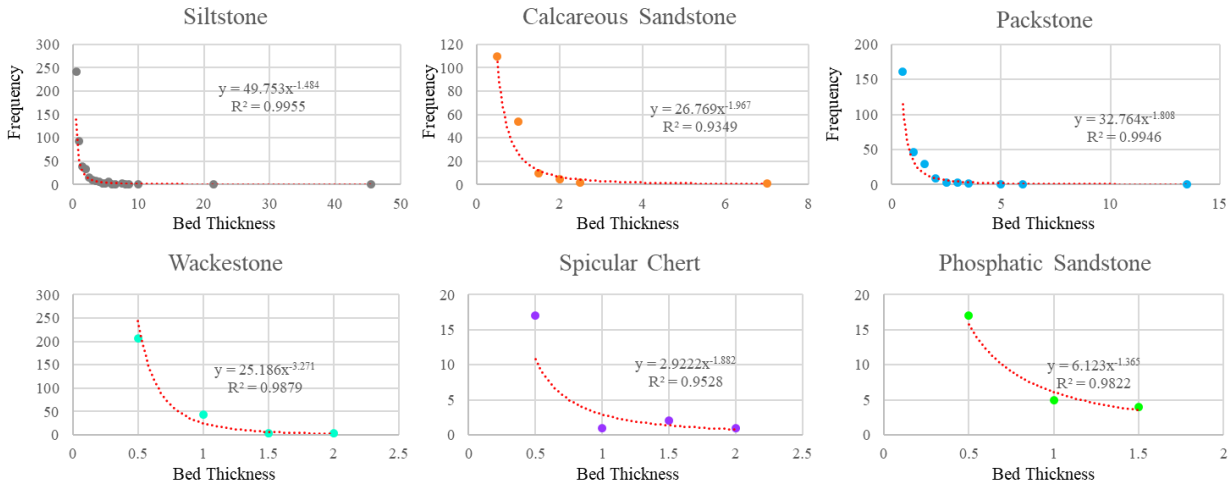

Fig. 27 — Thickness frequency distributions of the Meramecian strata with bed thickness on the x-axis and frequency on the y-axis. The siltstone contains the highest number occurrences of 0.5 ft thickness with 242 while the wackestone (207) and packstone (161) demonstrate similar thickness frequencies. The siltstone contains the thickest occurrence at 45.5 ft, while the other

lithofacies maximum occurrence thickness is approximately 2 ft. Thickness frequency distributions are observed as power functions with an R^2 value greater than 0.93. The mudstone is rare and under sampled statistically so no distribution could be defined.

		Succeeding Beds						
	Facies	Siltstone	Packstone	Wackestone	Calcareous SS	Spicular Chert	Glauc/Phos SS	Mudstone
Underlying Beds	Siltstone	x	0.29	0.33	0.23	0.06	0.04	0.05
	Packstone	0.44	x	0.33	0.18	0.02	0.02	0.01
	Wackestone	0.6	0.3	x	0.04	0.04	0.01	0.01
	Calcareous Sandstone	0.68	0.24	0.05	x	0.01	0	0.02
	Spicular Chert	0.74	0.03	0.22	0	x	0	0.01
	Glauc/Phos Sandstone	0.56	0.22	0.06	0.08	0	x	0.08
	Mudstone	1	0	0	0	0	0	x

Table 5 — Demonstrating a Markov chain of transitional probability for each lithofacies within the Meramecian strata. Overall, siltstone has the highest transition probability while the glauconitic sandstone has the lowest transition probability. The dark orange color represents transition probabilities greater than 0.5, orange represents 0.4-0.49, yellow represents 0.3-0.39, green represents 0.2-0.29, teal represents 0.1-0.19, blue represents 0.01-0.09, and grey represents no facies succeeding relationship was observed.

Chesterian. The Chesterian section in the STACK area is predominantly composed of siliciclastic facies (83%) containing 60% siltstone and 23% calcareous sandstone (Fig. 28). Overall, the siliciclastic facies is approximately 20% more abundant than in the underlying Meramecian section, while the calcareous sandstone facies nearly doubled in occurrence. Chesterian strata mark the completion of the transition from a carbonate dominated system to a siliciclastic dominated system. The most significant contribution to reservoir quality is the increase in sand content in the distal portions of the Oklahoma Shelf. The Chesterian section is thickest in the southeast (Core 4 = 280 ft) where it is predominantly composed of siltstone. It is thinnest to the northwest (Core 1 = 125 ft) where it is mainly composed of sandstone. The lateral facies distributions for Chesterian strata among the cores indicate that the bioturbated and

laminated strata of the siltstone facies are most common in the STACK area. The siltstone facies constitutes 36-78% of the strata with the percentage increasing toward the southeast. The calcareous sandstone facies ranges in abundance from 6-47% with abundance decreasing from northwest to southeast. The carbonate facies is relatively uncommon in the STACK play, never composing more than 15% of the Chesterian section; spicular chert is absent. While the sand content is highest in the north and northwest, the overall thickness of the Chesterian section decreases, offsetting the gain in reservoir quality. The siltstone has the highest gross probability (60%) and the highest mean bed thickness of 1.9 ft. (Table 6). The bed thicknesses for the major occurring lithofacies again demonstrate a stochastic power function distribution with the majority of thicknesses occurring in the 0.5 to 1 ft. range (Fig. 29). The Markov chain analysis demonstrates the transitional probability for each facies (Table 7). Again, the Markov chain indicates that the dominant successional probability is that any given facies tends to be overlain by siltstone (52-100%), defining a dominance of rhythmic sedimentation. For siltstone, the dominant successional probability is that it will be overlain by calcareous sandstone (61%) or packstone (20%). Successional probability among the other rock types is >17%, again indicating that facies succession is part of a stochastic system. Indeed, sediment composition, thickness, and distribution was apparently regulated by a broad range of stochastic processes rather than any deterministic type of cyclicity.

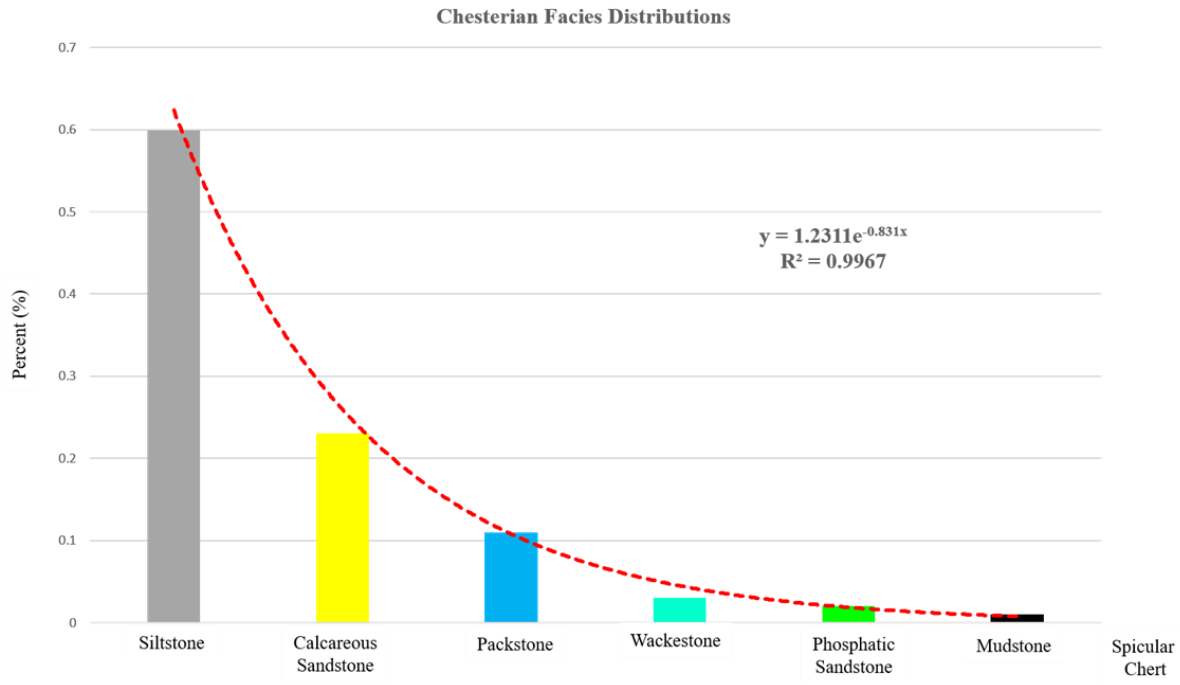

Fig. 28— Histogram of the Chesterian strata facies distribution combined from the studied cores across the STACK play consists of 83% siliciclastic facies, 14% carbonate facies. The most common facies is the siltstone (60%), while the carbonate facies decreased by a factor of 2 compared to the underlying Meramecian and Osagean sections. The spicular chert facies was not observed in any of the Chesterian cored sections. The lithofacies distribution is represented by an exponential relationship with an R^2 value of 0.99.

Facies	Occurrences	Gross Probability	Total Thickness (ft)	Mean Thickness (ft)
Siltstone	1035	0.60	462	1.90
Packstone	244	0.14	72	0.87
Wackestone	35	0.02	15	0.46
Calcareous Sandstone	355	0.21	174.5	0.97
Spicular Chert	-	-	-	-
Glauconitic/Phosphatic	41	0.02	20.5	0.77
Mudstone	3	0.00	1.5	0.13

Table 6— Demonstrating for each lithofacies the number of occurrences, gross probability, total thickness associated with occurrences, and the mean thickness of each occurrence within the Chesterian strata. The siliciclastic facies have a combined gross probability of 81%, while carbonate facies have a combined gross probabilities of 16%. The siltstone lithofacies has the highest mean bed thickness of 1.90 ft., and the mudstone has the lowest mean bed thickness of 0.13 ft.

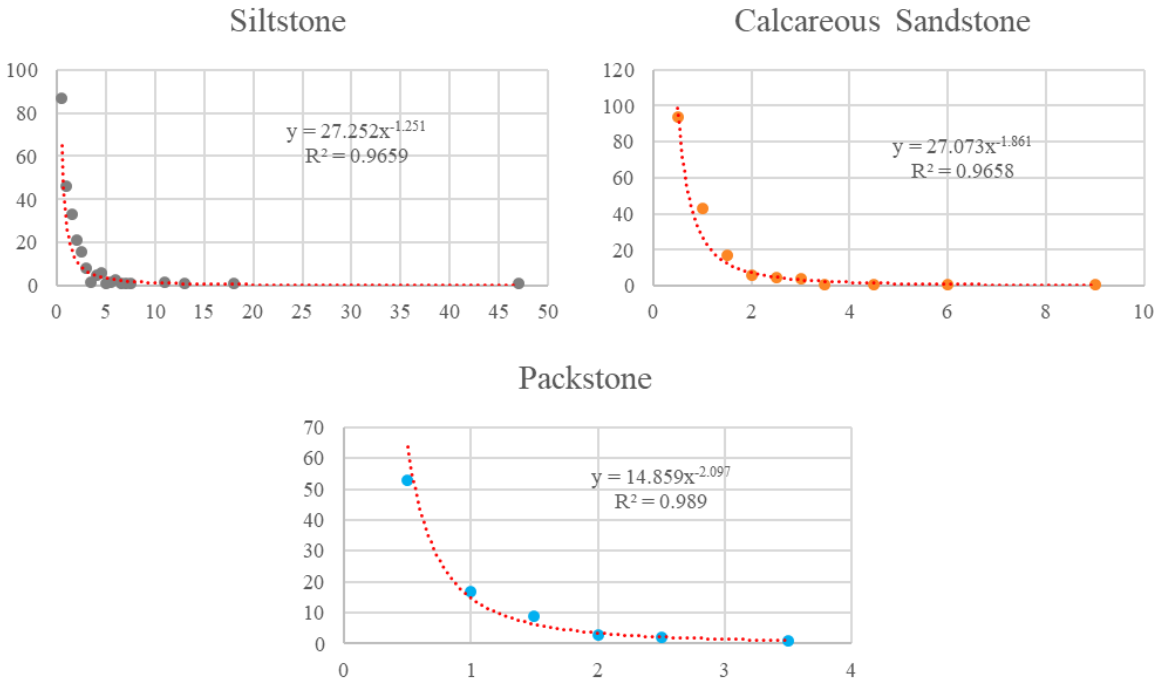

Fig. 29— Thickness frequency distributions of the Chesterian strata with bed thickness on the x-axis and frequency on the y-axis. The calcareous sandstone contains the highest number occurrences of 0.5 ft thickness with 94 while the siltstone (87) demonstrate similar thickness frequencies. The siltstone contains the thickest occurrence at 45.5 ft, while the other lithofacies maximum occurrence thickness is approximately 2 ft. The mudstone contains only a single core observation while the phosphatic sandstone and wackestone, demonstrate linear relationship in part due to the low sample density of the lithofacies. The siltstone, calcareous sandstone, and packstone lithofacies thickness frequency distributions are observed as power functions with an R^2 value greater than 0.96.

Succeeding Beds

Underlying Beds Facies	Siltstone	Packstone	Wackestone	Calcareous SS	Spicular Chert	Glauc/Phos SS	Mudstone
Siltstone	x	0.29	0.33	0.23	0.06	0.04	0.05
Packstone	0.44	x	0.33	0.18	0.02	0.02	0.01
Wackestone	0.6	0.3	x	0.04	0.04	0.01	0.01
Calcareous Sandstone	0.68	0.24	0.05	x	0.01	0	0.02
Spicular Chert	0.74	0.03	0.22	0	x	0	0.01
Glauc/Phos Sandstone	0.56	0.22	0.06	0.08	0	x	0.08
Mudstone	1	0	0	0	0	0	x

Table 7— Demonstrating a Markov chain of transitional probability for each lithofacies within the Chesterian strata. Overall, siltstone has the highest transition probability while the mudstone has the lowest transition probability. The dark orange color represents transition probabilities greater than 0.5, orange represents 0.4-0.49, yellow represents 0.3-0.39, green represents 0.2-0.29, teal represents 0.1-0.19, blue represents 0.01-0.09, and grey represents no facies succeeding relationship was observed.

Discussion

Statistical analysis indicates that Mississippian strata in the STACK play of the Anadarko Basin are dominated by diverse rhythms in which siltstone succeeds a range of rock types. Each series can be considered as a parasequence set, and vertical changes in rock types, bed thickness, and sedimentary and biogenic structures can be used to define and correlate the constituent shoaling-upward successions, marine flooding surfaces, and condensed sections that define parasequences. The parasequences and the larger parsequence sets reflect relative sea level change, and the overall clinoform stratigraphic architecture reflects southward progradation of a ramp system. The clearest temporal change is a transition from carbonate- to siliciclastic-dominated sedimentation, and the primary product of this transition is a highly layered system composed of relatively thin carbonate, chert, mudstone, siltstone, and sandstone beds. This has a strong impact on reservoir distribution and heterogeneity and provides critical insight for hydrocarbon development.

The Osagean section is not typically targeted for hydrocarbon production, but potentially contributes to the overlying reservoirs by providing migration pathways from the underlying Woodford Formation through natural fractures. The highest probability of this type of contribution is in the northwest area of the STACK play, where thicker accumulations of carbonate are preserved. As the section thins to the southeast, the Osagean section becomes less rich in carbonate, and the contribution of production to overlying reservoirs would be less significant. The best reservoir potential in the Osagean section would be in the northwest portion of the STACK play and in the NW STACK Extension acreage (Fig 1). The higher variability in lithofacies distribution and the thin layering within the Meramecian section indicate potential for higher drilling risks and production differences across the STACK area when compared to the Chesterian section. Target zones with a higher concentration of carbonate might negatively affect drilling parameters like rate of penetration, produce circulation issues due to open fracture networks, and decrease producibility where authigenic cementation has lowered porosity and permeability. Other potential effects could be in target zones where bioturbated siltstone contains elevated clay content that could reduce permeability and contribute to formation damage related to fluid interactions, or where argillaceous zones act as frac barriers potentially mitigating completion strategies. The Chesterian section would likely have lower drilling risks and production variability compared to the Meramecian strata due to increased lithologic consistency and continuity. The increase in deposition of coarser grained sandstone may indicate additional target zones in the upper portion of the Mississippian section that are not typically targeted for hydrocarbon production. Conducting economic evaluations of reservoir thickness and the relationship to production will delineate areas with lower economic risk. Well locations to the southeast contain less sand and more clay-rich bioturbated siltstone. Target zones that contain a higher percentage of laminated siltstone and a lower percentage of bioturbated siltstone in this area will likely facilitate more productive wells. Similar to the potential Meramecian targets, the

composition of the parasequence provides insight into which target zones will be the most productive in a particular area.

Conclusions

Statistical analysis indicates that the Mississippian System in the Anadarko Basin is fundamentally a highly layered rhythmic succession in which a variety of carbonate rock types, siliciclastic rock types, and chert tend to form couplets with siltstone. Thickness-frequency distributions and Markov chain analysis indicate that sediment thickness and lithologic transitions were stochastically regulated and that lithologic cyclicity is not apparent. Overall lithologic trends indicate a transition from carbonate to sandstone in the mid ramp and from carbonate to mudstone and siltstone in the outer ramp. Stratal geometry defines a series of south-prograding clinoforms, and detailed analysis of vertical trends in the distribution of mudstone, siltstone, sandstone, chert, and carbonate facilitates identification of shoaling-upward parasequences that can be correlated regionally.

The depositional succession observed in the STACK play in the Anadarko Basin and Shelf can be broken into 3 distinct depositional systems and corresponding parasequence sets. The first is represented by a period of stabilization and aggradation of carbonate and siliceous sponge biocommunities during the Osagean. This is followed by an episode of carbonate progradation during the Meramecian, when the first major influx of siliciclastic sediment occurred. After this time, influx of Chesterian siliciclastics terminated carbonate production, and only reworked/transported carbonate was preserved. Shoaling-upward successions observed in core subdivide each series into parasequence packages, which are correlatable across the STACK play using integrated lithofacies logs and geophysical well logs. Wells in the northwestern part of the study area record relatively shallow water facies enriched in calcareous fossil debris, bioturbation, and siliciclastic sand grains. Wells in the southeastern part, by contrast, record deeper water

facies enriched in organic matter, clay, and siliciclastic silt. Parasequence packages are composed of deeper water facies at the base of the package that pass upward into shallower water facies at the top. The parasequences have a well defined clinoform geometry and progradational stacking pattern. Facies within each parasequence are variable and are a key source of reservoir heterogeneity, and overall the Mississippian section can be characterized as a thinly layered system. Understanding this heterogeneity requires detailed mapping and facies analysis of specific target zones. This helps facilitate an understanding the geologic parameters influencing rate of drill-bit penetration, the distribution of natural and induced fractures, hydraulic communication among wells, and production performance.

The Osagean section is the thinnest interval within the STACK play. In the northwest it reaches a maximum thickness of 85 ft and thins southeast to 25 ft. in the. Osagean strata are dominated by carbonate (47%) and spicular chert (23%), which have the highest concentration of natural fractures and hence the highest brittleness of all the facies observed. While the Osage would not be designated as a primary production target, it is probable that it contributes to production from the overlying reservoirs by providing hydrocarbon migration pathways from the underlying Woodford Formation through natural fractures. The Meramecian section is the thickest interval within the STACK play, having an average thickness of 300 ft. It is predominantly composed of siliciclastic strata (67%), which increase in abundance by a factor of 2 in comparison to the underlying Osagean strata. The Meramecian exhibits the highest facies variability in the play area due to the transition from the carbonate-dominated Osagean section to the siliciclastic-dominated Chesterian section. The calcareous sandstone facies increases to 12% within the Meramecian section and contributes to reservoir quality in the upper part of the section, where sandstone content is highest. The Chesterian section is thickest in the southeastern part of the project area, reaching a maximum thickness of 246 ft. This section is thinnest in the northwestern part of the project area, where it is as thin as 155 ft. thick. Chesterian strata are predominantly composed of

siliciclastic strata (86%) in which the overall calcareous sandstone facies contribution reaches 23%. The increase in sand content within the Chesterian has the largest impact on reservoir quality by increasing porosity and permeability.

The facies distribution in the Meramecian section demonstrates that the siltstone facies is the most common facies ranging in abundance from 24-34% with a mean bed thicknesses of 1.63 ft, and a gross probability of 37%. The transition probability from siltstone to wackestone is highest with 33%, and for all other lithofacies the succeeding bed probability for siltstone averages 67%. The spicular chert is more abundant in the lower portion of the Meramecian in the northwest at 6%, and decreases to the southeast where none of the facies is observed. The calcareous sandstone facies exhibits the same distribution pattern with a maximum abundance in the northwest at 17% and decreases to the southeast where the laminated siltstone facies dominates with an abundance of 32%. The lateral facies distribution within the Chester section demonstrates that the siltstone facies ranges from 44-75% in abundance and that the abundance increases from northwest to southeast. The calcareous sandstone facies ranges in abundance from 6-47% with distribution opposite that of the siltstone. While the sandstone facies percentage is highest in the north and northwest, the net thickness of the Chestererian section decreases. Overall, the Chesterian section is dominated by siliciclastic lithofacies (86%) with the calcareous sandstone increases by a factor of 2 with a mean bed thickness of 0.97 ft. The most common lithofacies that occurs is siltstone (60%) with a 61% probability of transitioning to a calcareous sandstone. All other lithofacies have an average of 75% transition probability that the succeeding bed will be siltstone.

CHAPTER IV

TECTONIC AND EUSTATIC CONTROLS ON A MIXED CARBONATE-SILICICLASTIC DEPOSITIONAL SYSTEM, MISSISSIPPIAN (LOWER CARBONIFEROUS), SOUTHERN MIDCONTINENT USA.

Introduction

The Anadarko Basin is the deepest Phanerozoic sedimentary basin in the North American craton (Perry 1989). The basin is asymmetric and structurally deepest along the southwestern margin adjacent to the Wichita and Amarillo uplifts, where the basin contains more than 12 km (~40,000 ft) of sediment ranging in age from Cambrian to Permian (Perry 1989). This basin is 160 km (100 mi) wide along regional northwest strike and 480 km (300 mi) long along the south-southwest dip direction (Higley 2014). The basin is bounded on the east by the Nemaha Uplift, on the southeast by the Arbuckle Uplift and Ardmore Basin, on the southwest by the Wichita and Amarillo Uplifts, and to the west by the Cimarron Arch (Johnson 1988). The northern part of the basin includes the so-called Anadarko shelf, where basement is less than 1 km deep (~3,000 ft) (Ball 1991).

During the Late Devonian through mid Carboniferous, the Anadarko Basin was within the western part of the Laurussian craton between 10 and 20°S. This location was prone to nutrient-rich upwelling currents that originated in the Ouachita Embayment (Gutschick 1983). This upwelling resulted in high organic productivity, including siliceous plankton blooms (i.e., radiolarians) and siliceous bottom fauna (sponges)

However, as the Gondwanan and Laurussian plates continued to collide thru the mid to late Carboniferous, the closing of the Rheic Ocean cut off the strong upwelling zones to create the more isolated Midcontinent Sea (Algeo 2008) leading to a drastic decrease in biogenic silica production. The mid Carboniferous marks the transition to an icehouse world as Pangaea formed and glaciation drove high-frequency sea-level change in the Milankovitch band (Crowley 1993; Fielding 2007; Frakes 1992; Saunders 1986; Smith 2000).

Thick carbonate successions of the lower Carboniferous (Mississippian) were deposited across North America in the Appalachian, Black Warrior, Illinois, Eastern Interior, Michigan, Arkoma, Anadarko, Williston, and Permian Basins (Ettensohn et al. 2004; Grammer et al. 2018, 2020; Pashin 1994; Pashin et al. 2009; Silberling 1995; Smith 2000; 2019). The composition of the carbonate bank that developed on the western Laurussian craton during the early Carboniferous changed abruptly in response to orogenic events, which increased the input of siliciclastic sediment (Ettensohn et al. 2019; Sandberg 1982). The Neo-Acadian and Alleghanian synorogenic clastic wedges contain mosaics of open marine, marginal marine, and terrestrial facies that built out from the eastern highlands onto parts of the stable craton (Ettensohn 2004; Friedman 1988; Meckel 1970; Pashin et al. 2009). Similar thick clastic successions, such as the Humbug Delta, prograded cratonward from the west, and were sourced by the Antler and Ancestral Rocky Mountain highlands (Sandberg 1982). In proximity to the study area, the early Carboniferous Batesville and Wedington deltaic complexes were apparently sourced from the northern Appalachians and prograded onto the Arkoma shelf (Fig. 30) (Hanford 1988; 1995). Sediment was transported along fluvial axes through the Michigan and Illinois Basins and was ultimately deposited in the Arkoma and Black Warrior Basins via the Mississippi Valley Graben (Craddock 2013; Hanford 1995; Pashin et al. 2009; Xie et al. 2016).

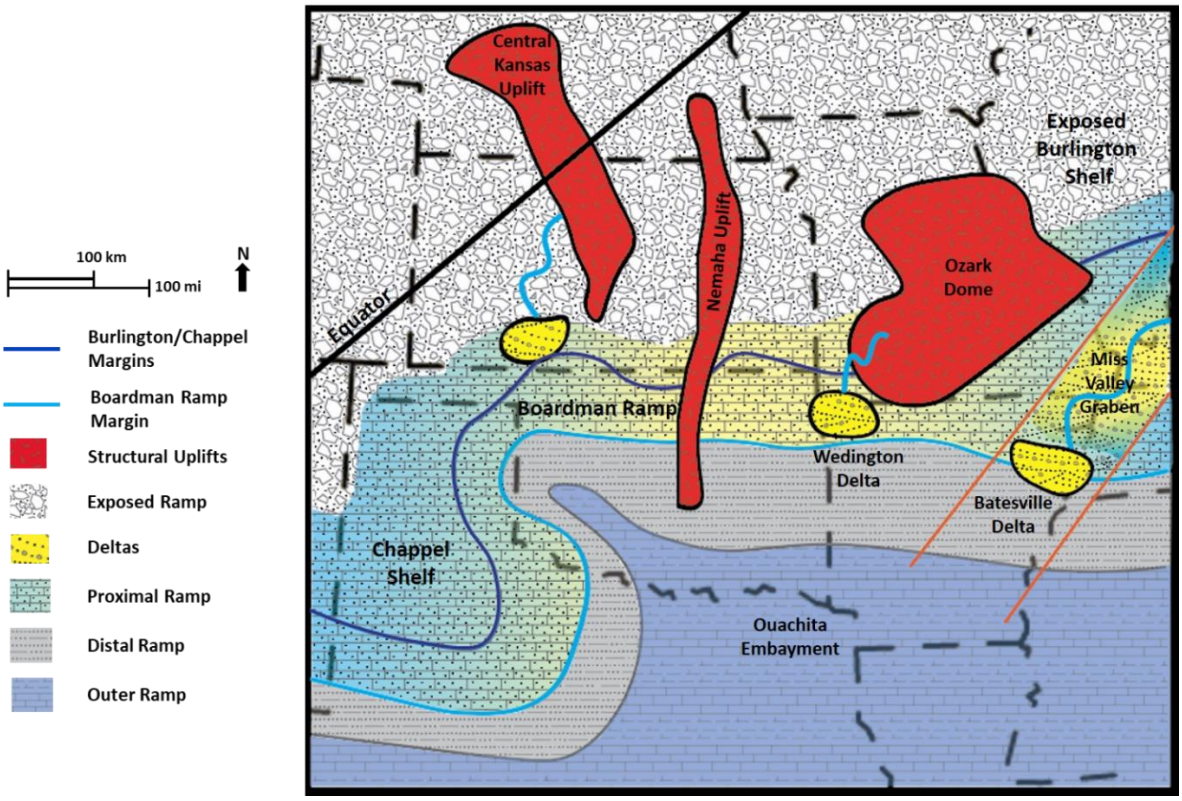

Figure 30. Regional paleogeographic reconstruction of the late Mississippian within the midcontinent. During the late Mississippian the carbonate ramp prograded basinward from the Burlington and Chappel shelves. An influx of siliciclastics encroached upon the carbonate system from the Mississippi Valley Graben and local structural highs with development of the Wedington and Batesville deltas in the Late Mississippian. Carbonate and siliciclastic mixing are prevalent on the Boardman ramp and is reflected in the transition to siliciclastic siltstone and sandstone downdip. The deeper water environments within the Southern Oklahoma Transform Zone and Ouachita embayment are characterized by calcareous mudstone with interbedded muddy limestone.

Methods and Datasets

The data used in this study come from subsurface cores and geophysical well logs taken across the Anadarko Basin and Anadarko Shelf (Fig. 1). Core plug samples were extracted for XRD, TOC, porosity, permeability, and thin section analysis. Clean polished slabs and butt slabs of the cores were described to record lithology, texture, bedding, physical sedimentary structures and biogenic structures. Framework mineralogy and grain size were analyzed in XRD and thin section using the standard Udden-Wentworth grain-size scale.

Thin sections were analyzed under a petrographic microscope to identify sedimentary structures, rock texture, fabric, mineralogy, fossils, and pore types. Thin sections were impregnated with UV-epifluorescence dye to aid micro-pore identification under UV light. Thin sections were stained on half of the slide with Alizarian Red S and potassium ferricyanide to aid in distinguishing calcite, ferroan calcite, ferroan dolomite, and feldspar. The Folk classification scheme was used for siliciclastic rock types (Folk, 1980), the Dunham classification scheme was used for carbonate rock types (Dunham, 1962), and the Choquette and Pray scheme was used to classify pore types (Choquette and Pray, 1970).

Facies analysis was performed for each core described in the project area. This analysis provides the fundamental building blocks for interpreting the Mississippian sedimentary succession (Noel and Dalrymple, 2010). Each facies has been defined in terms of distinctive variations in composition, texture, sedimentary structure in order to provide insight into depositional processes and environment.

Digital logs showing facies were generated for each core described in the project area. Each facies is designated by a number and is assigned to the corresponding depth at 0.5 ft intervals. These facies logs were then calibrated to core spectral gamma logs for correlating facies

characteristics with geophysical log signatures. This provides insight into the lateral and vertical distribution of the facies and characterizing depositional and stratigraphic architecture.

Results

Lithofacies Analysis: A total of eight lithofacies were identified in the cores. Five carbonate lithofacies characterized are: grainstone, sandy peloidal packstone, wackestone, and spicular chert lithofacies. While four siliciclastic lithofacies were characterized: subarkosic sandstone, calcareous sandstone, siltstone, and mudstone.

Carbonates. Grainstone. The grainstone lithofacies is comprised of light gray to brownish gray grainstone with the most porous beds containing hydrocarbon stain. Individual beds have sharp bases and tops, are thick bedded (10 to 30 cm; ~0.25 to 1ft) thick, and are cross-laminated to planar-laminated. Bioturbation constitutes isolated vertical burrows. Calcareous fossil fragments consist of very coarse sand-size crinoids, brachiopods, and bryozoans (Fig. 31). Peloids and ooids were observed along with abundant interparticle calcite cement. Moldic and intraparticle porosity within carbonate fossil debris and peloids were observed in thin section (Fig 32.). Gamma-ray signatures from the core gamma-log for this lithofacies range from 0-25 API units in response to their lower concentration of radioactive minerals. These rocks are interpreted to represent shallow marine shoal deposits and are similar to other Lower Carboniferous deposits in Kansas and Illinois (Cluff 1984; Handford 1988; Smith 2000). A ramp crest positioned on the seaward margin of an inner ramp setting is located above fair-weather wave base where sedimentation is strongly affected by longshore currents and rip currents (Scholle et al. 1983; Burchette 1992).

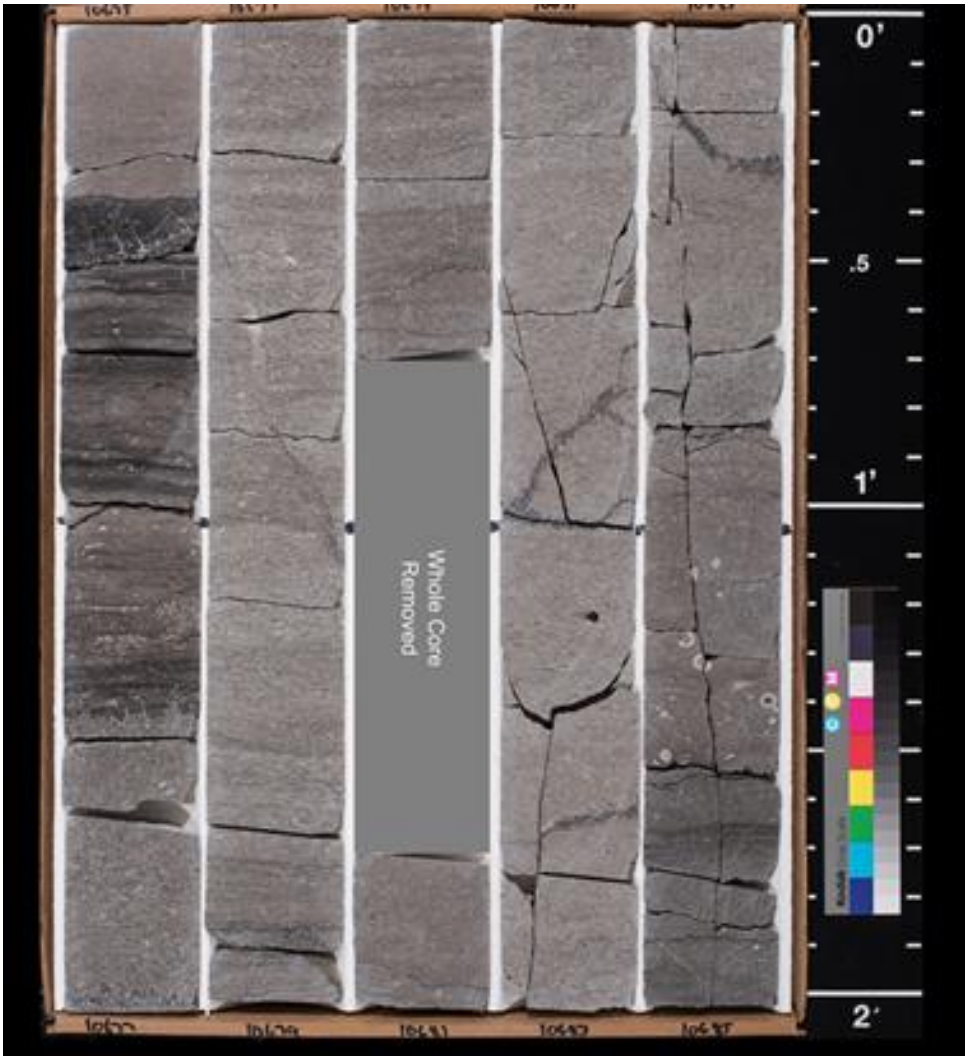

Figure 31. Core photograph of thick bedded, cross to planar-laminated grainstone facies. Crinoidal and bryozoan fossil fragments observed along with large natural fractures.

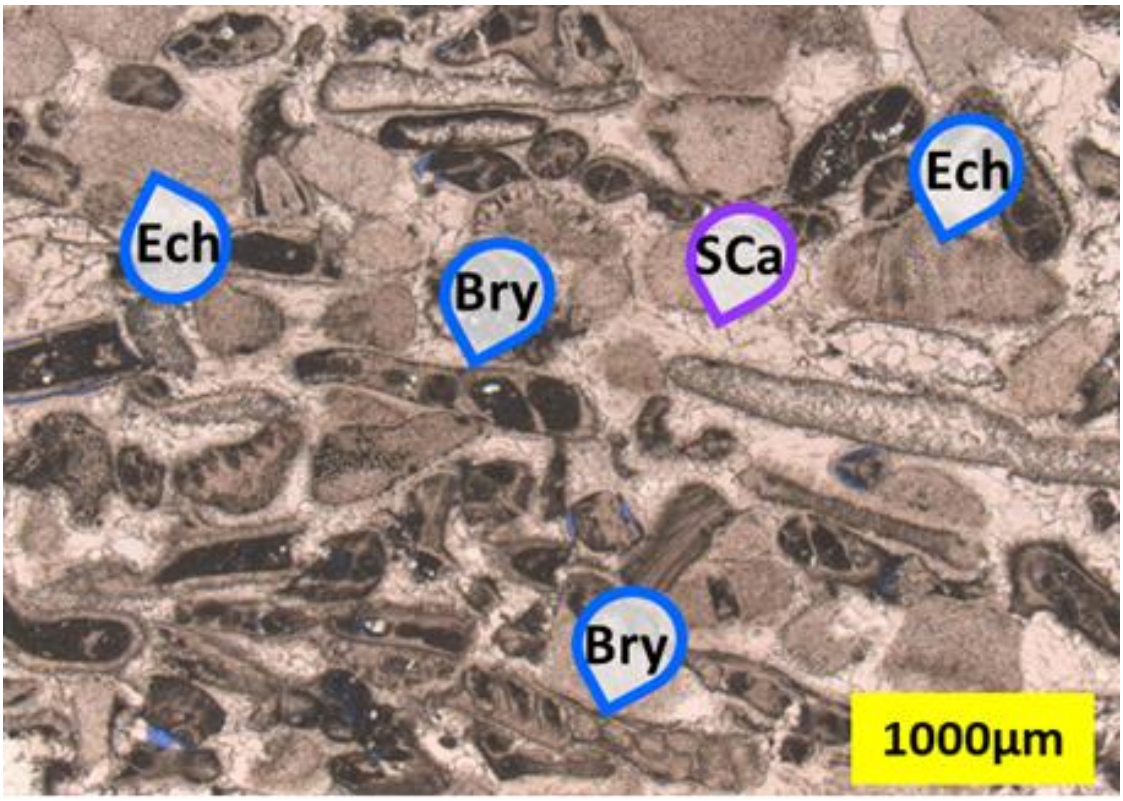

Figure 32. Thin section photomicrograph with Alizarin-red stain marks pink calcite. Grains consists of bryozoan and echinoderms.

Sandy Peloidal Packstone. This lithofacies is composed of light gray packstone and contains variable amounts of siliciclastic sand and silt (Fig. 33). Individual beds are sharp-based, 10 to 45 cm (0.25 to 1.5 ft) thick, cross-laminated to planar-laminated, and overlain by finer-grained lithofacies. Bioturbation indices range from 3-5 where trace fossils are present; *Planolites, Teichichnus, Phycosiphon, and Chondrites* are the common traces observed. Carbonate microbioclastic debris consists of crinoid, brachiopod, and bryozoan fragments (Fig. 34). Peloids, sand-sized quartz and feldspar grains, interparticle carbonate cement, and intraparticle porosity within calcareous fossil debris and peloids were also observed in thin section. Gamma-ray signatures from the core gamma-log for this lithofacies range from 0-25 API units in response to a low concentration of radioactive minerals. These rocks are interpreted to represent deposition

below fair-weather wave base evidenced by alternating cross-bedded arenaceous calcarenite deposits and fine-grained strata with diverse trace fossil assemblages (Scholle, 1983). Deposition is consistent with a proximal mid-ramp environment where storm reworking and basinward transport of carbonate debris from the inner ramp occurs by way of storm waves, storm-generated longshore currents, and offshore-directed gravity flows (Burchette, 1992; Wright, 1990; Cotter 1990; Bracket 1986).

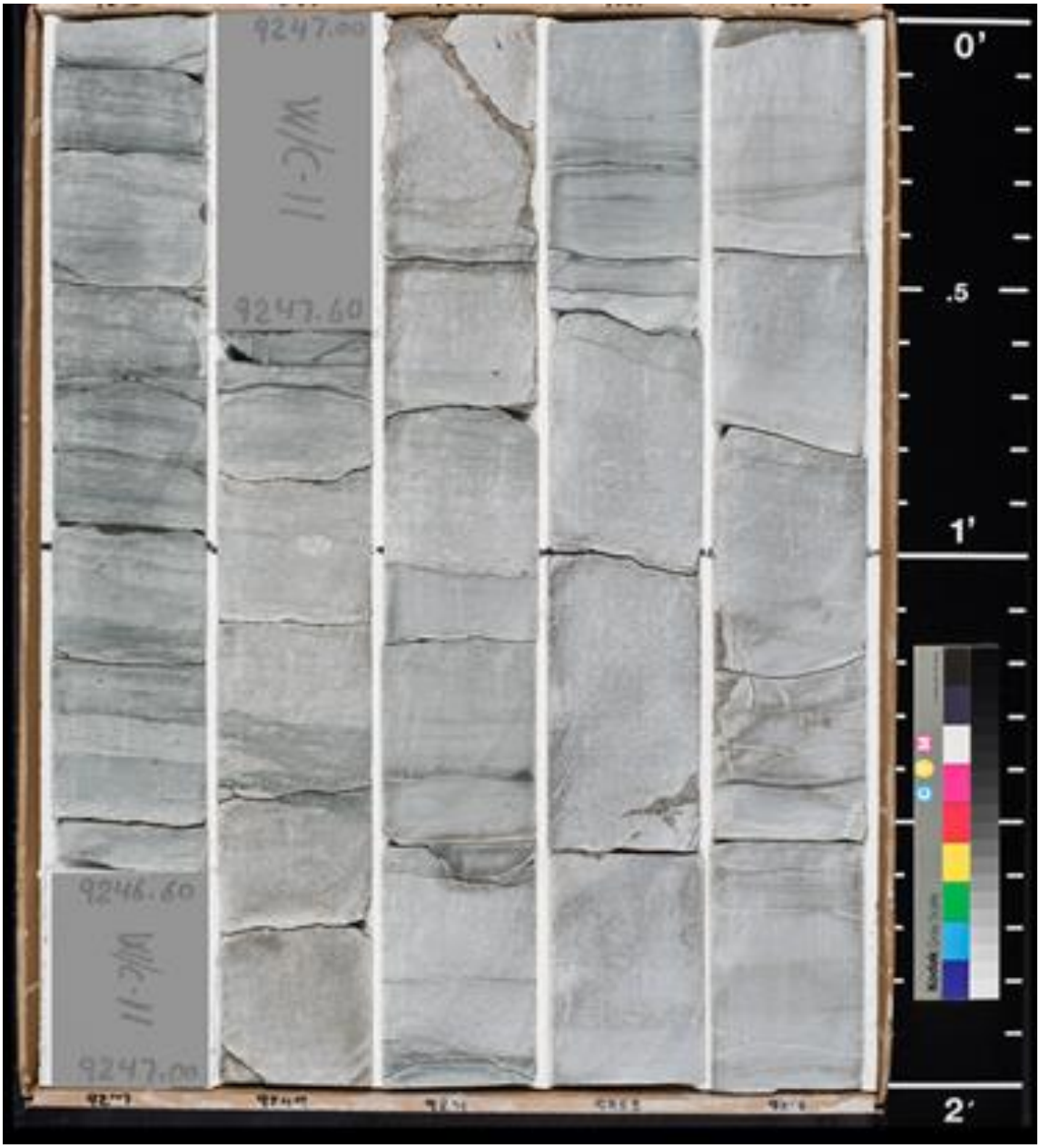

Figure 33. Core photograph of a sandy packstone to grainstone facies interbedded with silty wackestone. Sandy packstone to grainstone are thick bedded and are cross to planar laminated.

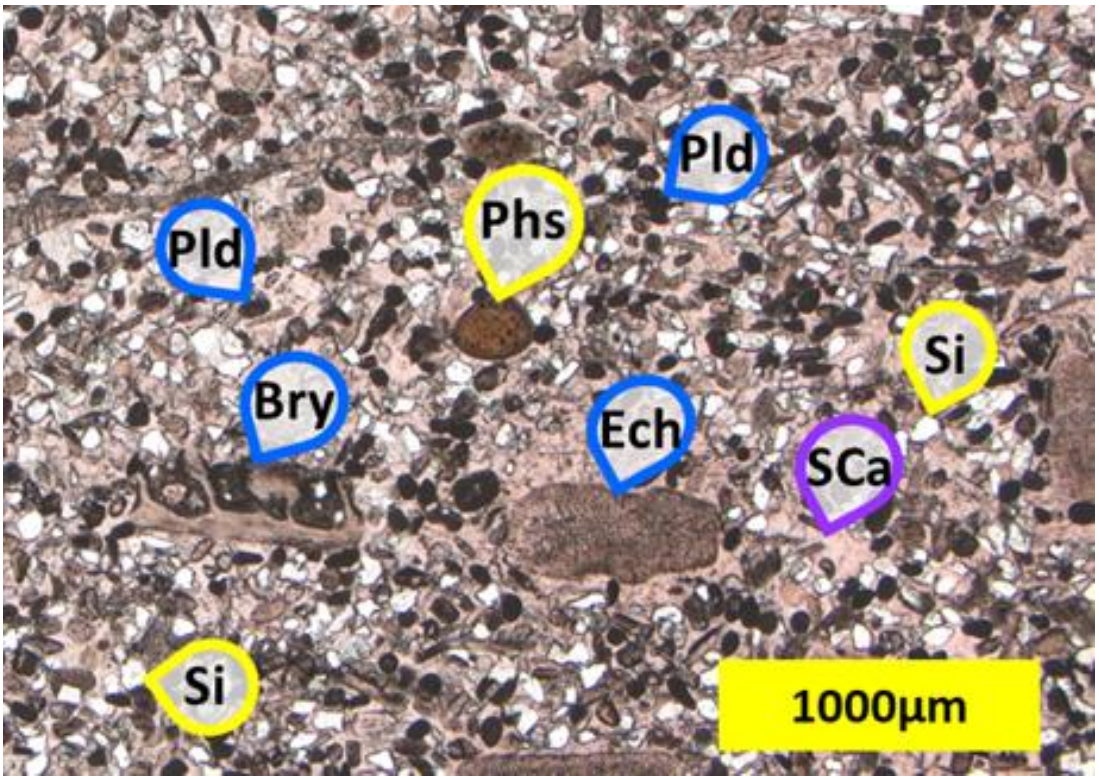

Figure 34. Thin section photomicrograph of sandy grainstone to packstone facies with Alizarin-red stain marks pink calcite. Grains consists bryozoan, echinoderms, microbioclastic debris, peloids, quartz, and feldspar.

Wackestone. This lithofacies is composed of gray to dark gray wackestone (Fig. 35). Individual beds typically fine upward from packstone to wackestone, are 2 to 10 cm (0.05 to 0.25 ft) thick, and are intensely bioturbated. Bioturbation indices ranging from 3-6 and the trace fossil assemblage is dominated by horizontal feeding burrows with a broad range of morphology. Indeed, common traces include *Phycosiphon*, *Chondrites*, and *Zoophycos*. Disarticulated, thin-shelled brachiopods are dispersed along bedding planes. The wackestone is composed of microbioclastic debris, peloids, spicules, silt to very-fine sand- sized quartz grains, clay, and carbonate mud (Fig .36). Minor ferroan dolomite is present within the matrix. Porosity types include intraparticle porosity within fossil debris and peloids, along with moldic porosity from dissolution of spicules. Gamma-ray signatures from the core gamma-log for this lithofacies are

above 75 API units, indicating significant radiogenic elements in the clay and organic matter. These rocks are interpreted to represent deposition below fair-weather wave base due to the increase in fine-grained sedimentation and bioturbation behaviors indicative of lower energy settings (Scholle, 1983). Deposition is consistent with a mid-ramp environment where storm-transported microbioclastic sediment is reworked and mixed with finer-grained sediment by burrowing (Burchette, 1992; MacEachern et al. 2008).

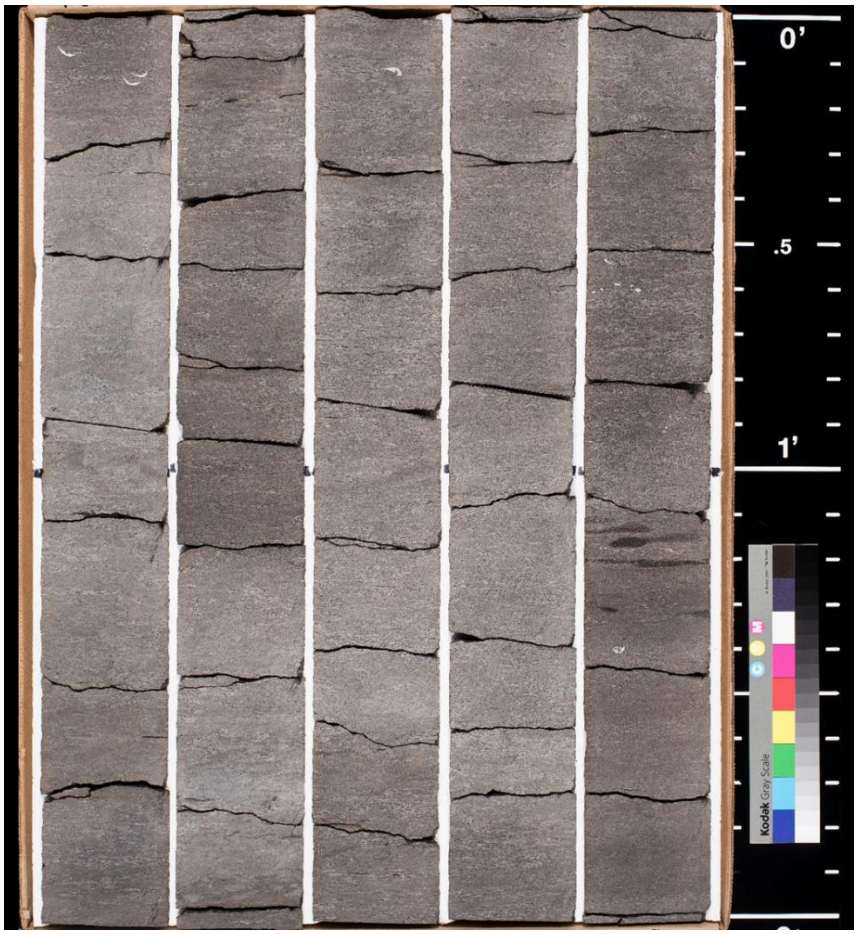

Figure 35. Core photograph of shelly, arenaceous packstone. Bioturbation is common within this lithofacies with indices ranging from 3-6. *Chondrites* and *Phycosiphon* are the most abundant ichnofossils, and thin-shelled brachiopods and crinoid ossicles are present.

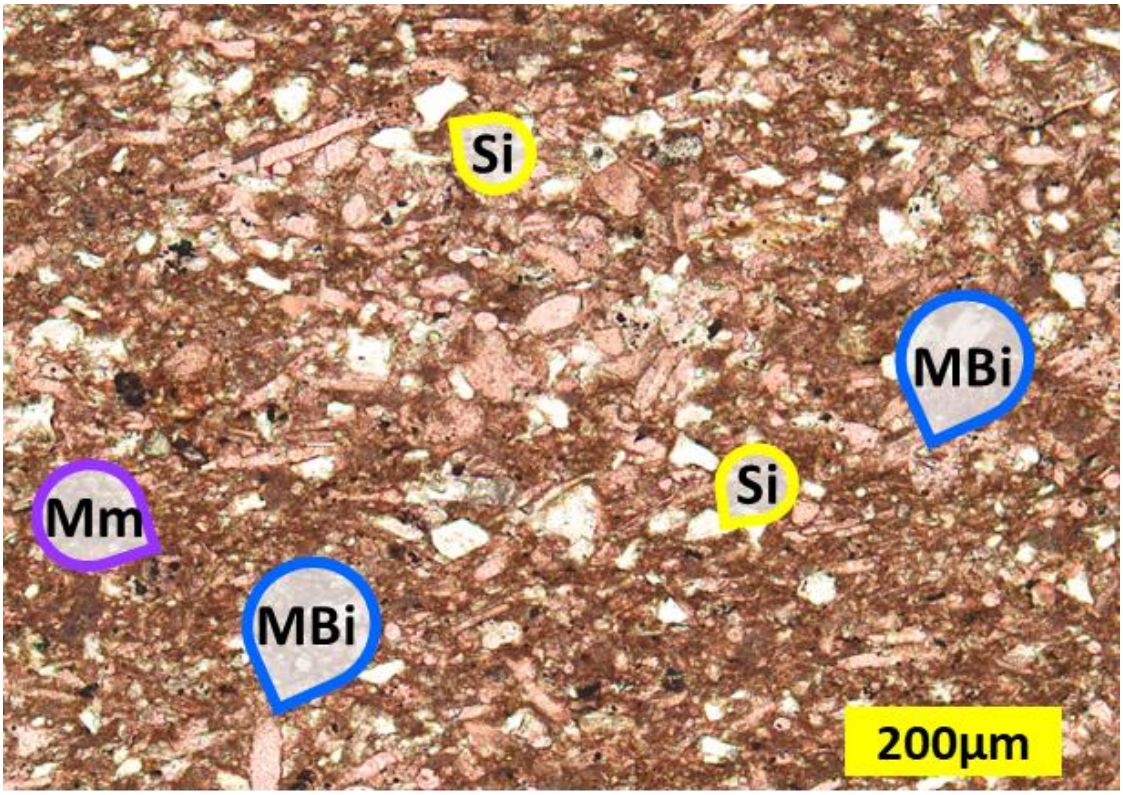

Figure 36. Image is a thin section photomicrograph of a sandy packstone. Alizarin-red stain marks calcite. Grains consist of microbioclastic debris (Mbi), peloids, quartz (Si), feldspar, and the matrix is composed of carbonate mud and clay minerals (Mm).

Spicular Chert. The spicular chert lithofacies is composed of bluish-gray chert with a granular texture resembling grainstone (Fig. 37). Individual beds are sharp-based, are 2-10 cm (0.05 to 0.25 ft) thick, are planar-laminated or bioturbated, and are overlain by silt-rich wackestone. Where bioturbation is present, bioturbation index ranges from 3-6 with a variety of horizontal and vertical burrows present. Common traces are *Planolites*, *Teichichnus*, *Chondrites*, *Phycosiphon*, and *Zoophycos*. The spicular chert is composed primarily of sponge spicule debris with imbricate spicules concentrated in laminae. Bioturbated beds contain poorly oriented spicules mixed with other bioclastic grains, clay, and dolomite. Moldic porosity from dissolution of spicules is present, with silica cement being the most common. Laminated beds contain more chert than

bioturbated beds, but both contain varying proportions of chert, calcite cement, and dolomite cement (Fig. 38). Gamma-ray signatures from the core gamma-log for this lithofacies range from only 0-25 API units. These rocks are interpreted to represent deposition near storm wave base due to the concentration of spicular debris, increase in fine-grained sediment, and common reworking of spicule and microbioclastic debris by burrowing. The trace fossils are define a *Zoophycos* ichnofacies, which is common in low energy settings. Deposition is consistent with a distal mid-ramp environment where storm transported spicule and microbioclastic beds exhibit erosive bases and sharp tops. These beds are similar to some Silurian storm deposits in Pennsylvania that are interpreted to have accumulated in a mid ramp environment (Cotter 1990; Nakashima, 2007).

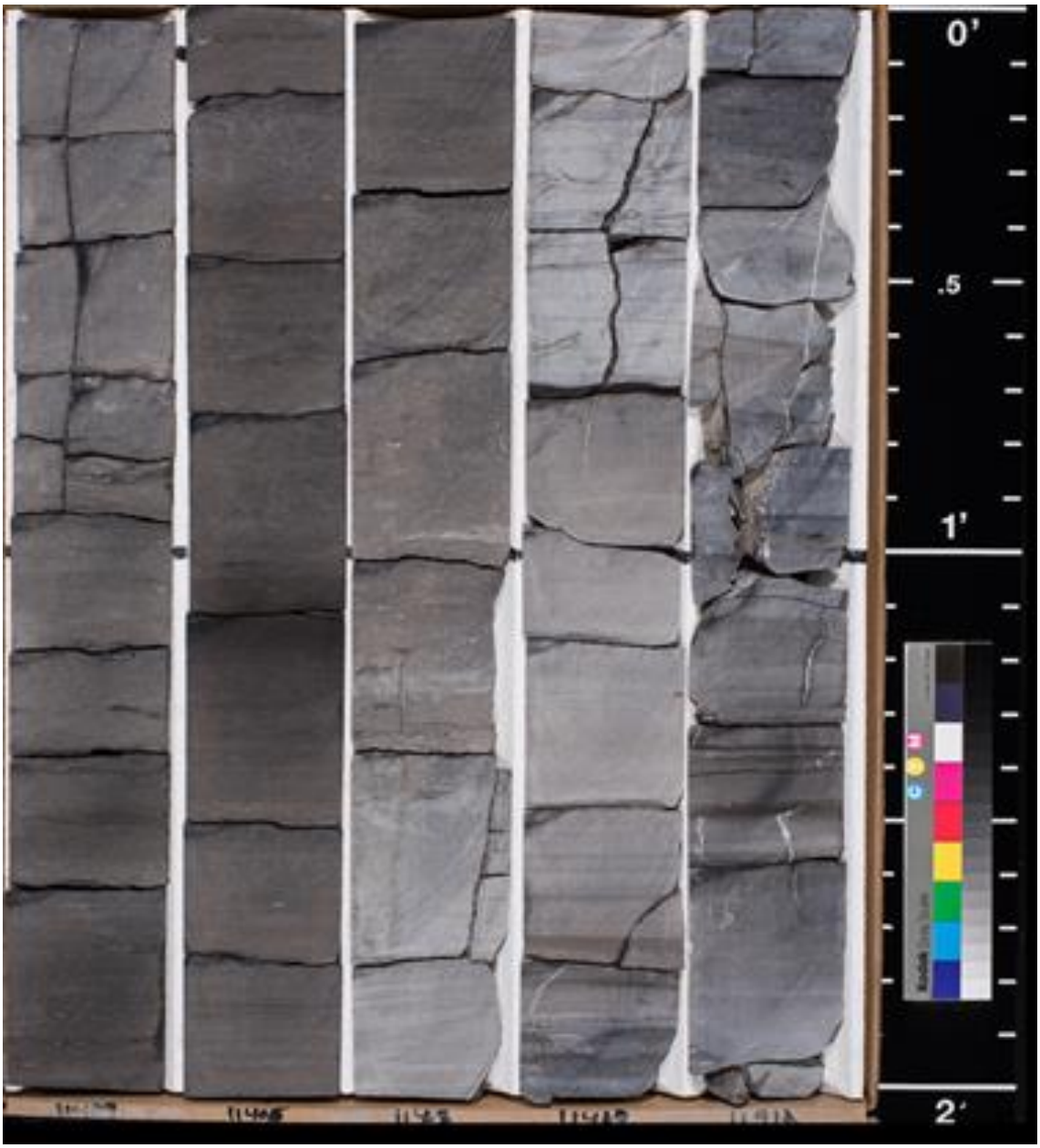

Figure 37. Core photograph of spicular chert facies interbedded with silty wackestone to mudstone facies. Chert beds are sharp based and planar laminated. Bed bound natural fractures commonly observed within chert beds.

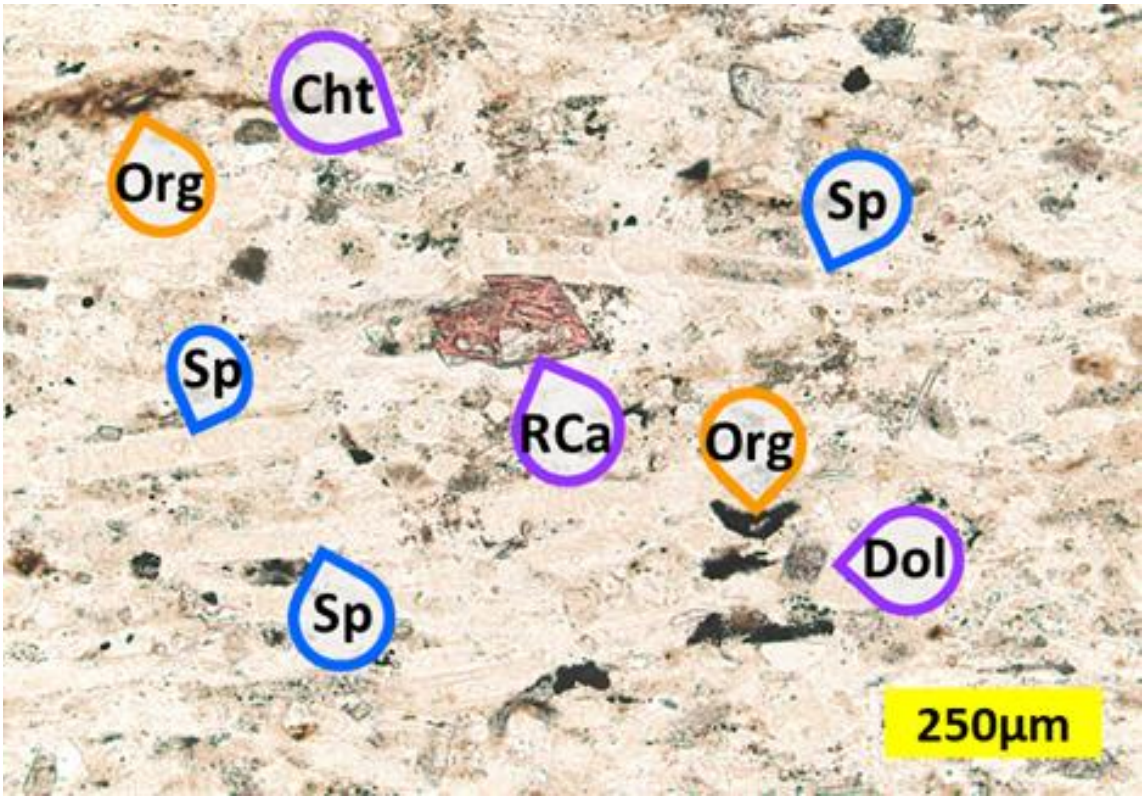

Figure 38. Thin section photomicrograph of a spicular chert with grainstone texture. Sample contains abundant broken monaxon spicules, dolomite, and organic inclusions.

Siliciclastics. *Subarkosic Sandstone.* This lithofacies is composed of brownish-gray subarkosic sandstone, with the most porous beds containing hydrocarbon stain. Individual beds have sharp bases and sharp to gradational tops, are thick-bedded (15 to 45 cm; 0.5-1.5 ft), well sorted, and are cross-laminated, planar-laminated, and bioturbated (Fig. 39). Burrows are typically filled with sediment from the overlying bed. The sandstone is composed of medium to fine sand composed of quartz and feldspar, with varying amounts of mica, clay, and microbioclastic debris (Fig. 40). The calcareous sandstone consists of similar constituents with an increase in carbonate fragments as peloids, microbioclastic debris, and calcite cement. Interparticle porosity and partially dissolved feldspar grains are present along with intraparticle porosity within peloids and microbioclastic particles. Interpretation of the sedimentological characteristics are consistent with

a proximal mid ramp environment where sediment is affected by wave agitation associated storm generated currents (Scholle et al. 1982, Pemberton et al. 2012).

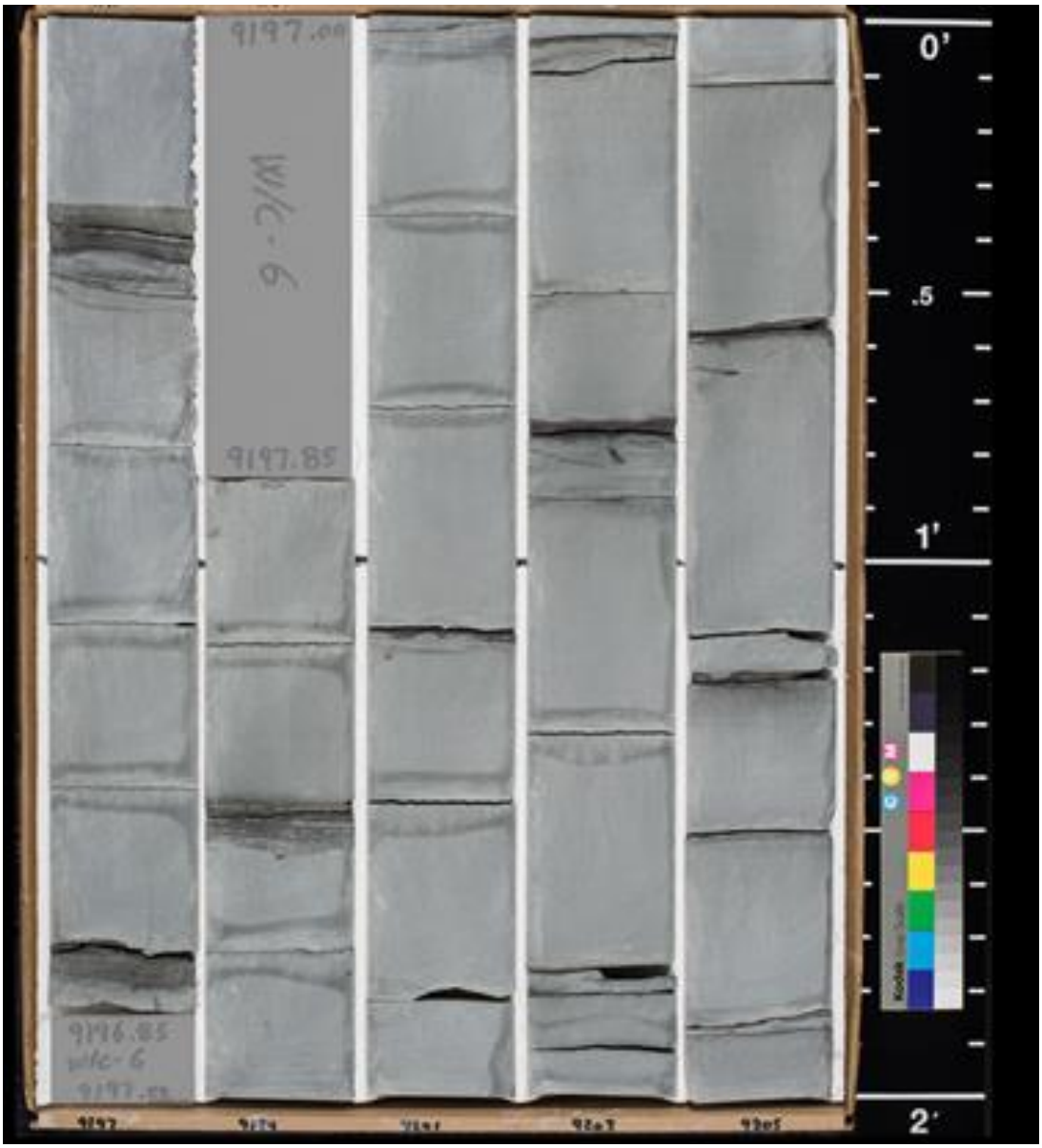

Figure 39. Core photograph of sandstone facies that are thick bedded and cross to planar-laminated. Thin interbedded silty mudstones are observed and contain bioturbation with some vertical burrowing into underlying sandstone bed.

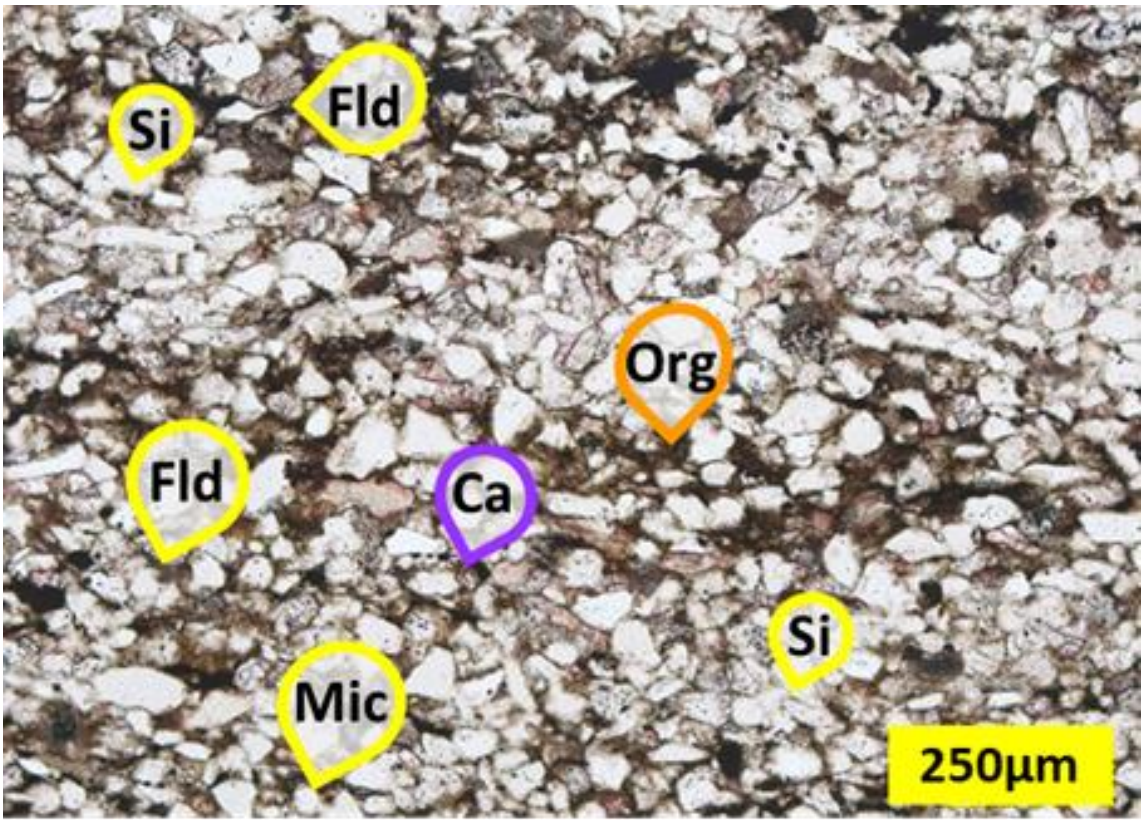

Figure 40. Thin section photomicrograph containing abundant medium- to fine-grained quartz sand and feldspar, large mica flakes, pore-filling organic residue, and minor calcite cement.

Calcareous Sandstone. This lithofacies is characterized as a calcareous sandstone that is gray to brownish-gray with the most porous beds containing hydrocarbon stain (Fig. 41). Individual beds have sharp bases and grade upward from sandstone to siltstone, are thick bedded, and are cross-bedded, horizontally laminated, and bioturbated. Bioturbation indices range from 2-4. Burrows commonly descend and are filled with sediment from the overlying bed. The calcareous sandstone is composed of fine to very fine-grained sand composed of quartz, feldspar, peloids, microbioclastic debris, and varying amounts of clay and carbonate cement (Fig 42). Interparticle porosity and intraparticle porosity within partially dissolved feldspar grains are present along with intraparticle porosity within peloids and microbioclastic debris. While organics in the form of migrated hydrocarbons are observed staining the pore system. Gamma count ranges from 25-75

API units, reflecting increased clay and feldspar content. These rocks are interpreted to represent deposition below fair-weather wave base due to the sharp-based sandstone beds that grade upward into siltstone (Pemberton, 2012). Deposition is consistent with a storm-dominated mid-ramp environment. Vertical escape burrows provide evidence for periods of rapid sedimentation alternating with periods of lower sedimentation rate between recorded by fine-grained background sedimentation and extensive burrowing. *Planolites*, *Teichichnus*, and *Phycosiphon* traces are present and interpreted as a *Cruiziana* ichnofacies, which is typical of mid ramp environments (MacEachern, 2008).

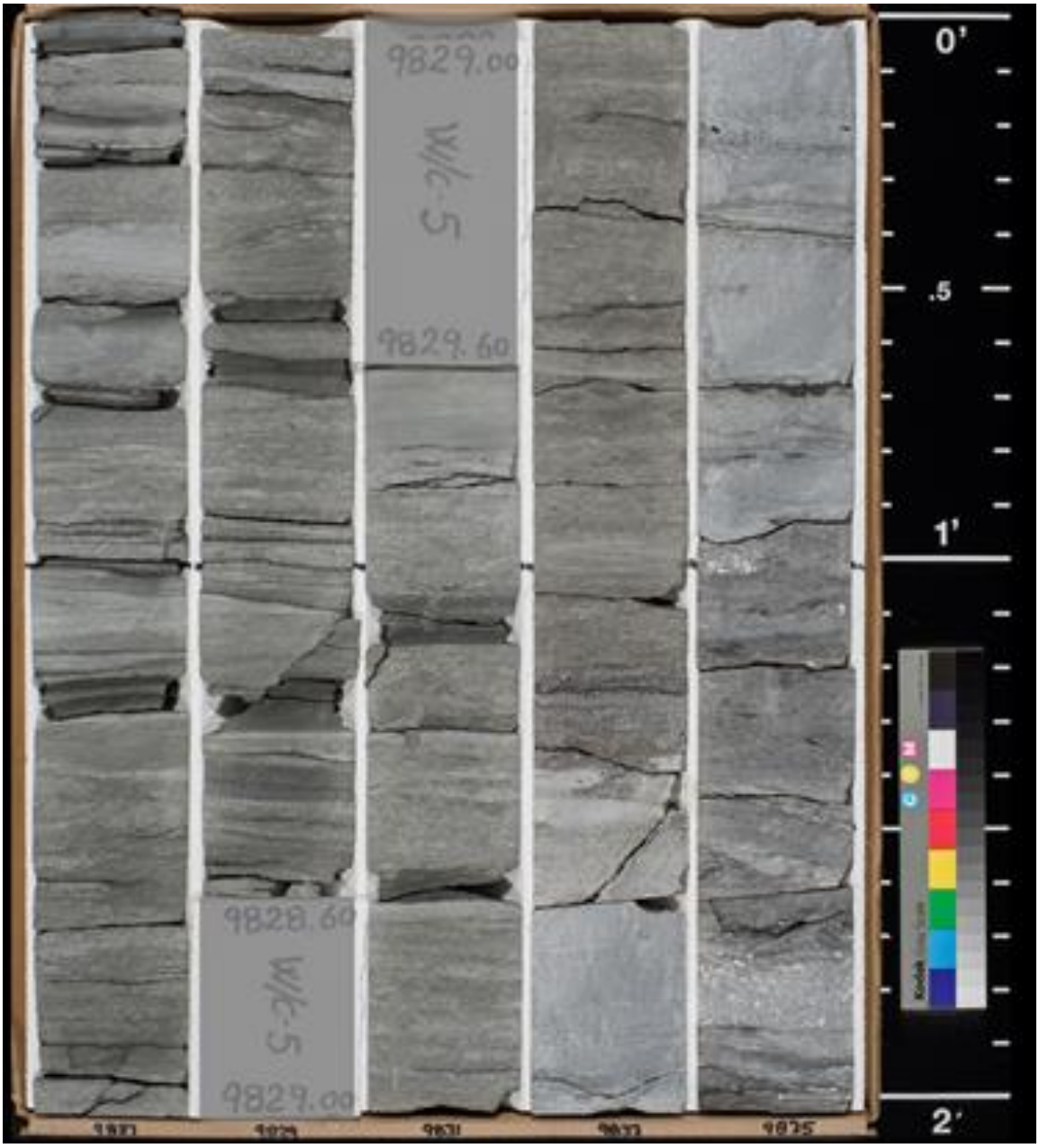

Figure 41. Core photograph of a calcareous sandstone facies interbedded with silty mudstone. Individual beds contain sharp bases and are highly bioturbated. Both horizontal and vertical burrows are observed and indicate a diverse trace fossil assemblage.

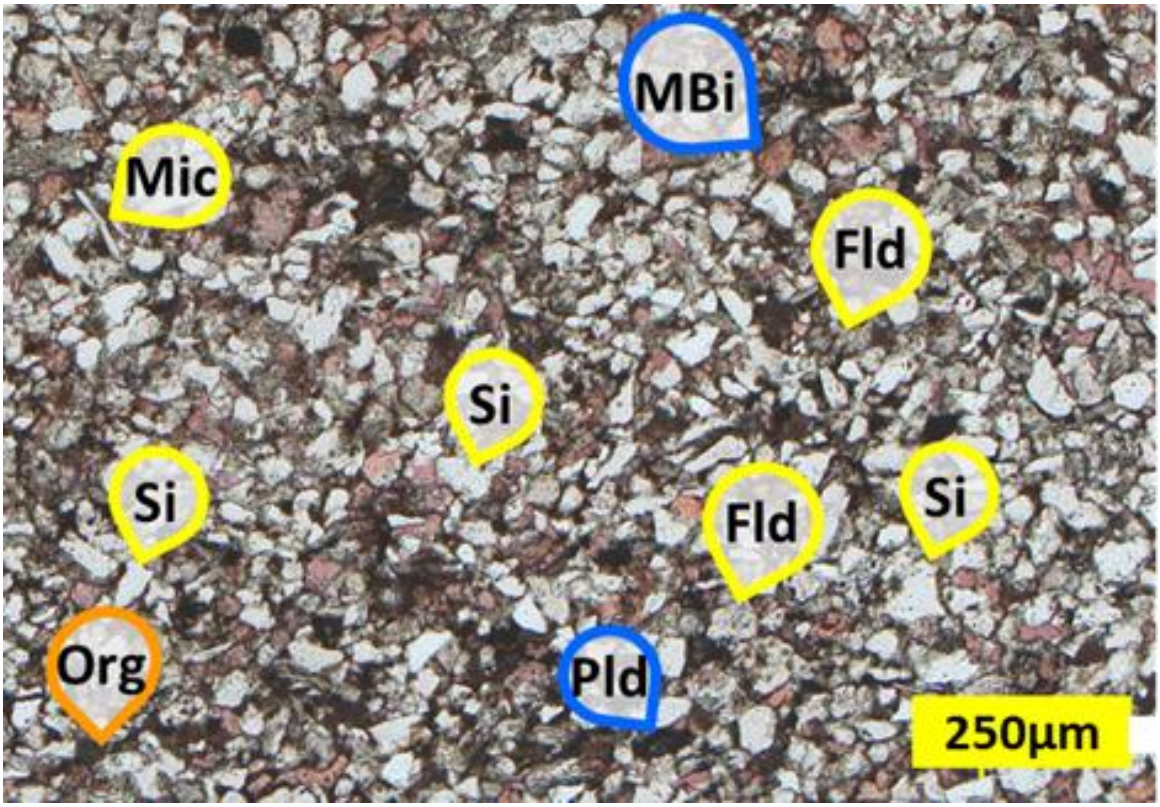

Figure 42. Thin section photomicrograph containing abundant fine- to very fine-grained quartz sand and feldspar, large mica flakes, peloids, microbioclastic debris, pore-filling organic residue, and calcite cement.

Siltstone. This lithofacies is composed of gray to dark gray siltstone (Fig. 43). Individual beds are horizontally laminated to bioturbated and thinly bedded. The siltstone beds fine upwards, are coarser and laminated at the base, then capped by either bioturbated muddy siltstones or silty laminae reworked by bottom currents. Bioturbated beds are typically more calcareous than surrounding strata, and bioturbation index ranges from 2-4. Common traces are *Zoophycos*, *Chondrites*, and *Phycosiphon*. Disarticulated thin-shelled brachiopods occur along bedding planes. The siltstone is composed of quartz, feldspar, mica, clay, agglutinated benthic foraminifera, amorphous organic matter, conodonts, and varying amounts of carbonate mud and microbioclastic particles (Fig. 44). Interparticle porosity between grains and intraparticle porosity within feldspar grains are typical. Core gamma count in this lithofacies is above 75 API units.

These rocks are interpreted to represent deposition within a distal mid ramp to outer ramp environment. This environment is supported by the sedimentologic characteristics of upward fining beds, and the sparse diminutive fossils and the low degree of bioturbation demonstrating a *Zoophycos* ichnofacies indicate that bottom conditions were oxygen-stressed (MacEachern, 2007). However, bioturbation indicates episodic oxygenation, probably after major storm events, which is typical of distal environments.

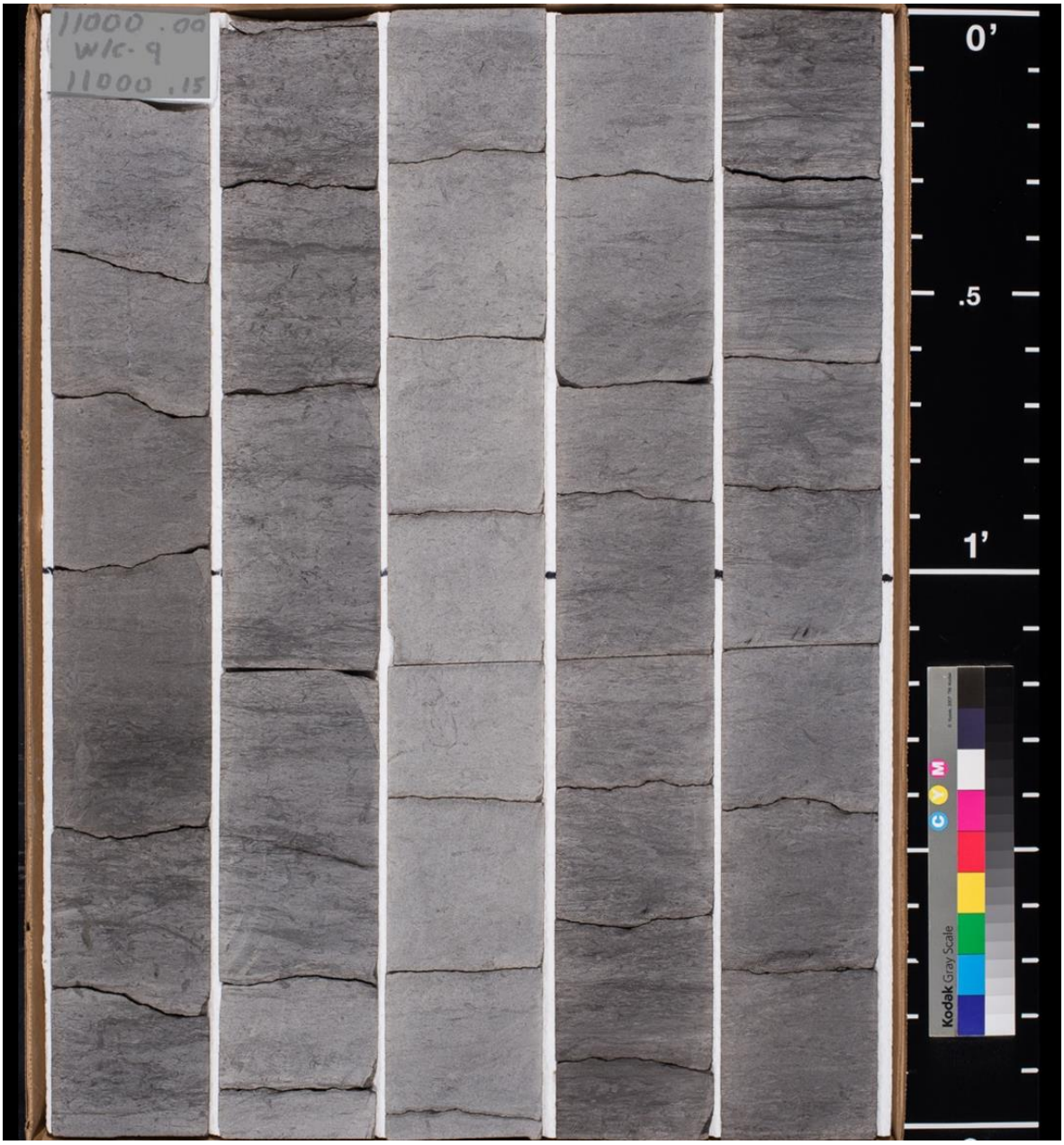

Figure 43. Image is a core photograph of siltstone that is laminated and bioturbated. Bioturbated beds have higher calcite content than laminated beds. Scattered thin-shelled brachiopods and crinoid fragments are present, and most commonly observed along bedding planes. *Chondrites*, *Phycosiphon*, and *Zoophycos* are the most common ichnofossils.

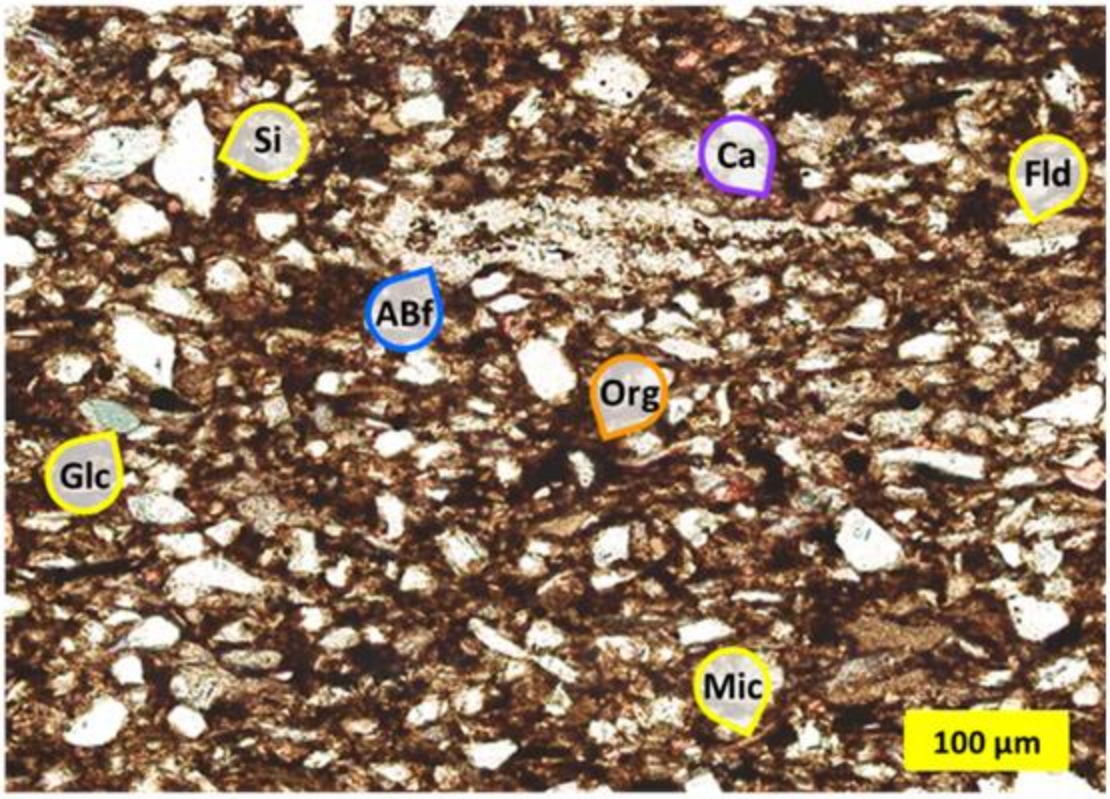

Figure 44. Image is a thin section photomicrograph of siltstone. Sample contains very fine-grained quartz sand and quartz silt (Si). Other constituents include feldspar (Fld), mica (Mic), clay, agglutinated benthic foraminifera (ABf), organic matter (Org), and minor glauconite (Glc).

Mudstone. This lithofacies is composed of dark gray mudstone (Fig. 45). Individual beds are typically laminated, ripple cross-laminated, and thinly bedded. Bioturbation indices range from 1-2. Rare *Zoophycos* traces were observed, and disarticulated phosphatic thin-shelled brachiopods are present along bedding planes. The mudstone is composed of quartz, feldspar, mica, clay, pyrite, agglutinated benthic foraminifera, conodonts, amorphous organic matter, and compacted clay floccules (Fig. 46). Porosity is hard to identify at this scale except for intraparticle porosity within feldspar grains. Gamma-ray count is above 75 API units in the mudstone. These rocks are interpreted to represent distal sedimentation below wave base due to fine grain size, increased organic matter content, decreased carbonate content, and a fossil assemblage restricted to benthic

foraminifera and conodonts. Deposition is consistent with the distal outer ramp. Depositional mechanisms are interpreted to be suspension settling, and episodic reworking of silt and clay by bottom currents. Current reworking of silt and clay plays a significant role in the development of the mudstone fabric. Silt and clay migrate as ripples in bedload generated by bottom currents, and deposit as thin veneers of interlaminated silt and clay (Yawar, 2017; Schieber, 2009). Sparse, diminutive fossils, pyrite precipitation, and the low degree of bioturbation indicate that bottom water conditions were stressed. However, *Zoophycos* traces, other horizontal burrows, and benthic foraminifera indicate at least episodic conditions hospitable to pioneering organisms (Bann, 2008).

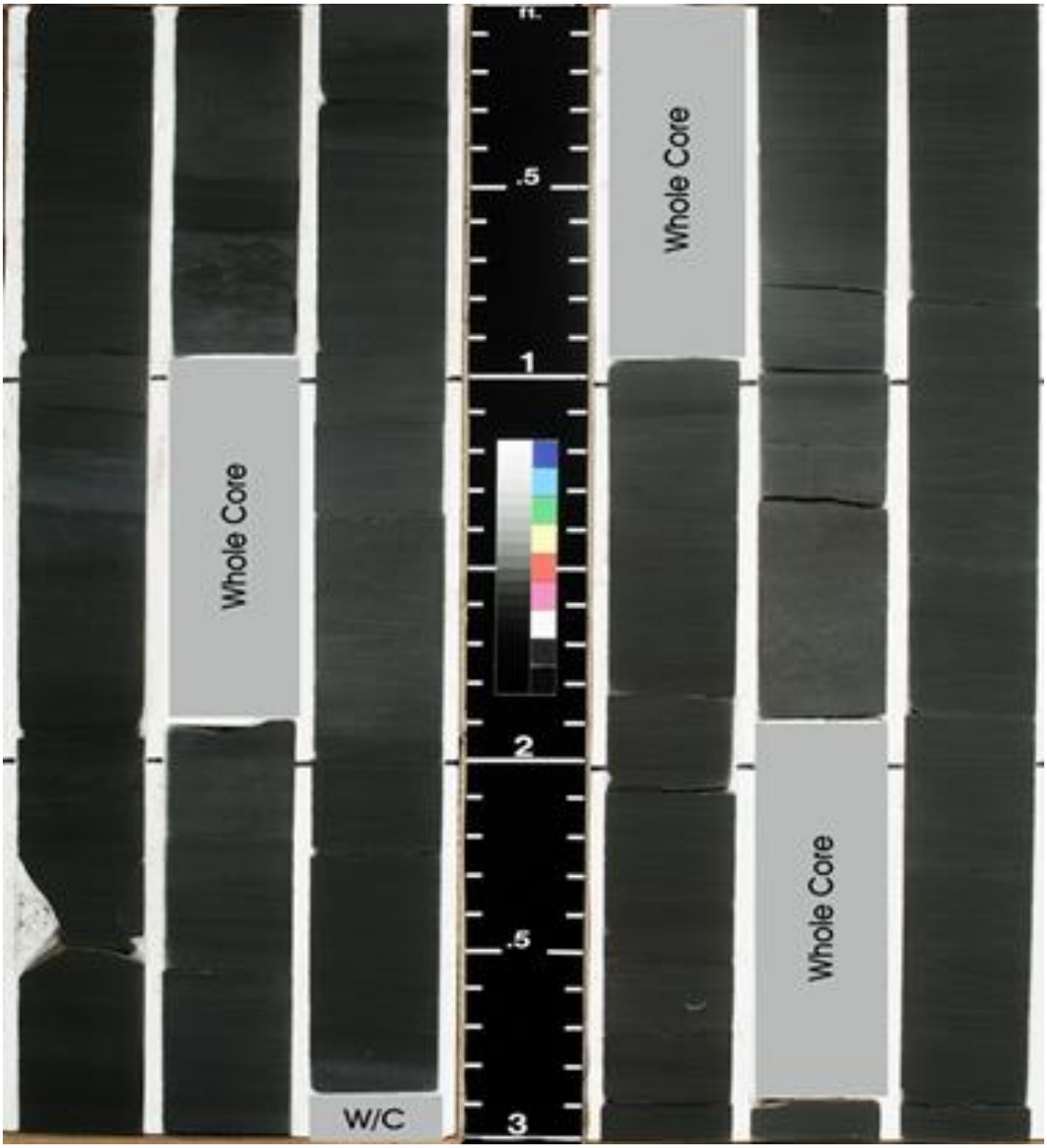

Figure 45. Core photograph of mudstone facies that are laminated, cross-ripple laminated and thin bedded. Bioturbation indices are low indicating stressed benthic conditions.

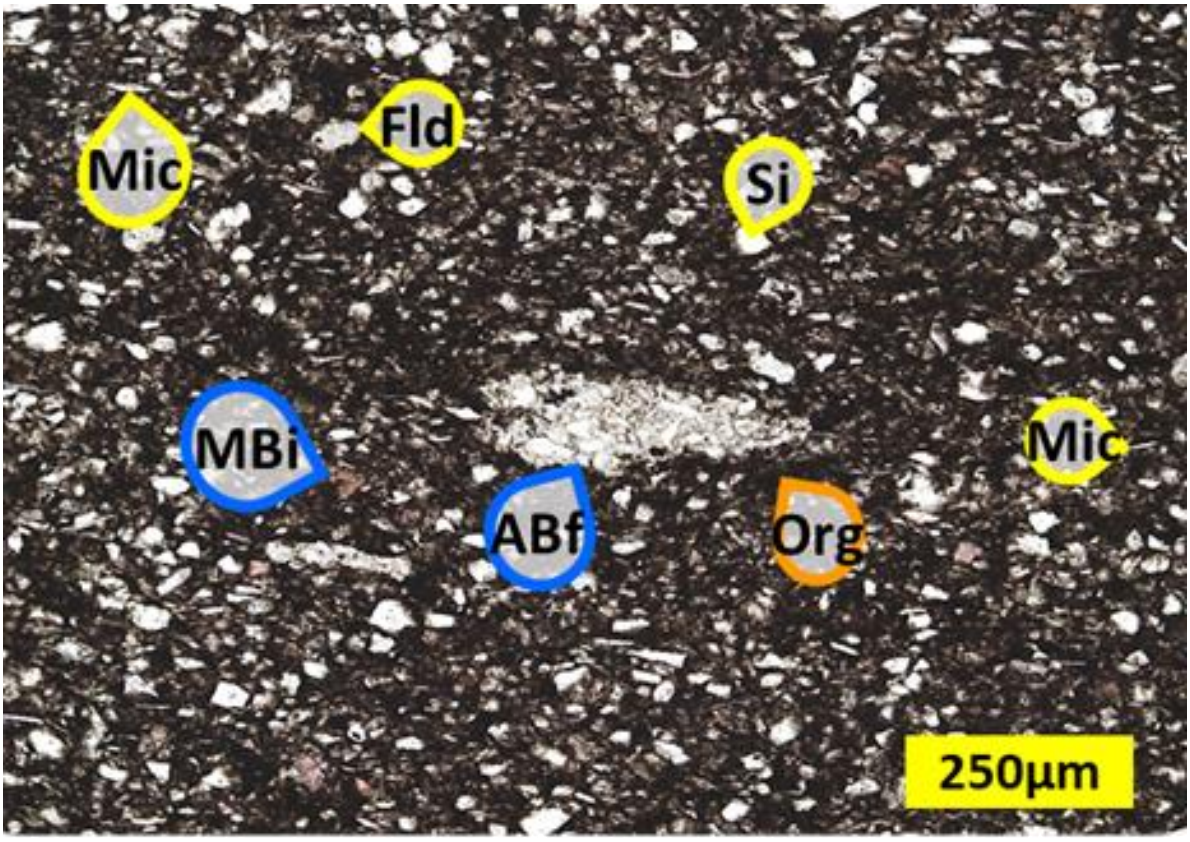

Figure 46. Thin section photomicrograph containing quartz and feldspar, mica, clay, agglutinated benthic foraminifera, organic matter, and minor carbonate microbioclastic debris.

Depositional Architecture: Integrated facies and gamma-ray logs were utilized for regional correlations across the project area (Fig. 47). The lowest gamma ray signatures ranging from 0-25 API units represent carbonate grainstone, packstone, and sponge-bearing chert facies due to their low concentration of radioactive minerals. The subarkosic sandstone, calcareous sandstone and siltstone facies are represented by higher gamma-ray values ranging from 25-75 API units in response to an increase in the radioactive material in the form of clay and feldspar. The wackestone, mudstone, and glauconitic-phosphatic sandstone facies have gamma counts above 75 API units in response to the abundance of radioactive material in the form of organic matter, clay, feldspar, phosphate, and glauconite.

Thick carbonate successions are developed in the northern part of the study area, and siliciclastic sediment is more common in the southern part. The shoal and proximal storm deposits comprised of the carbonate grainstone and packstone facies are observed only in the northern project area, indicating a relatively high position on the carbonate ramp. The distal storm and outer ramp deposits comprising calcareous sandstone, siltstone, and mudstone facies dominate in the south, indicating a progression to more distal environments over a distance of ~100 km (60 mi). Vertical facies distributions demonstrate an overall shoaling upward through time, with initial deposition characterized by distal storm and outer ramp deposits across the project area. Biostromal sponge deposits formed at the toe of slope along the distal fringes of the ramp crest shoals and proximal storm deposits. The carbonate depositional system was succeeded by a siliciclastic dominated system, with proximal storm deposits composed of subarkosic sandstone in the north transitioning to distal storm and outer ramp deposits containing of calcareous sandstone, siltstone, and mudstone in the south.

The depositional architecture of lower Carboniferous (Mississippian) strata in the Midcontinent of Oklahoma is characterized by a clinoformal mixed carbonate-siliciclastic ramp system (Fig. 48). Initial deposition was characterized by a carbonate system that abruptly transitioned to a siliciclastic system. Facies stacking patterns demonstrate net progradation of the depositional system, with proximal carbonate facies building out from the Burlington shelf in Kansas and Missouri to establish the Boardman ramp in north-central Oklahoma. Final deposition is characterized by longshore transport of sediment parallel to the carbonate banks off the Burlington and Boardman margins, which deposited thick successions of siliciclastic strata in the Anadarko Basin derived from the Wedington and Batesville deltaic systems to the northeast. These observations are consistent with other regional studies of time equivalent strata, and provide insight into the depositional architecture of lower Carboniferous (Mississippian) strata

within the Anadarko Basin (Boardman 2013; Franseen 2006; Godwin 2020; Grammer 2020; Hanford 1986, 1988, 1995; Hunt, 2015; Mazzulo 2011, 2013; Stuckey, 2020).

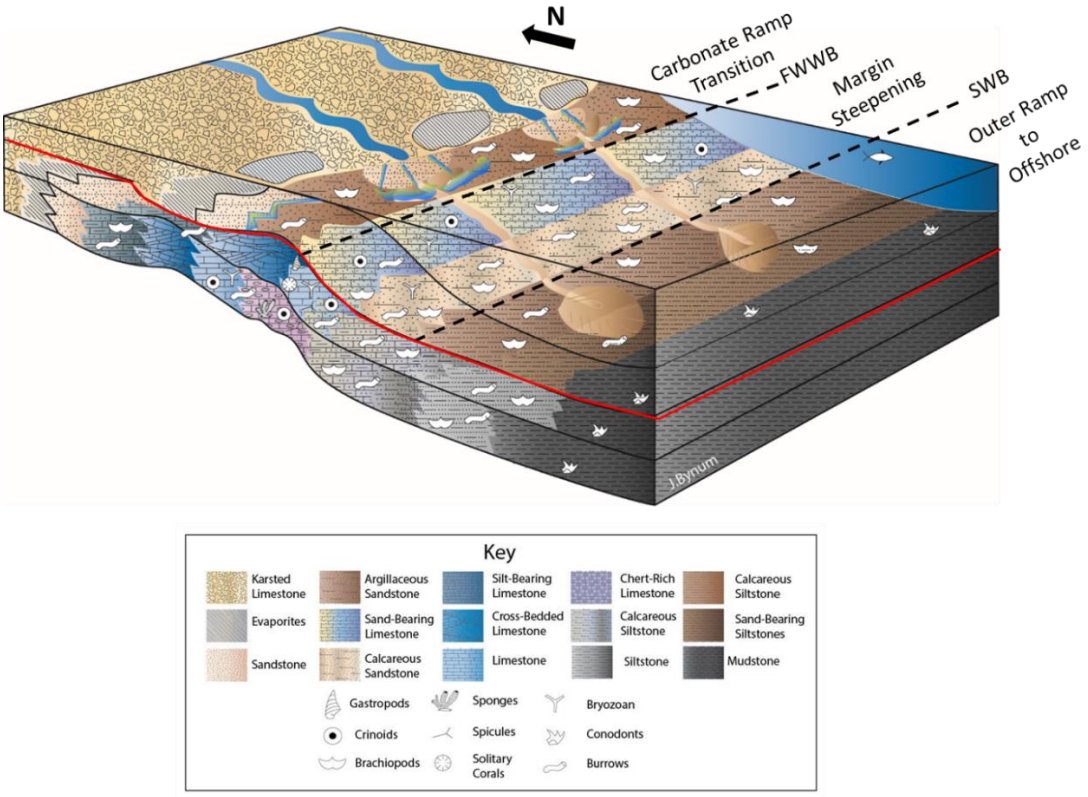

Figure 47. Block diagram demonstrating the stratigraphic transition from a carbonate-dominated system in the lower Mississippian to a siliciclastic-dominated system in the upper Mississippian (Bynum, 2022). Stabilization and aggradation of the carbonate ramp system is characteristic of early Mississippian deposition across the North American craton, and is recognized as the Burlington shelf. Progradation of the carbonate system followed extending the shallow carbonate margin to its furthest basinward location in northern Oklahoma. The carbonate system is abruptly inundated by siliciclastics in the late Mississippian with clastic sedimentation prograding and depositing thick successions of sandstone and siltstone off the Boardman ramp crest margin.

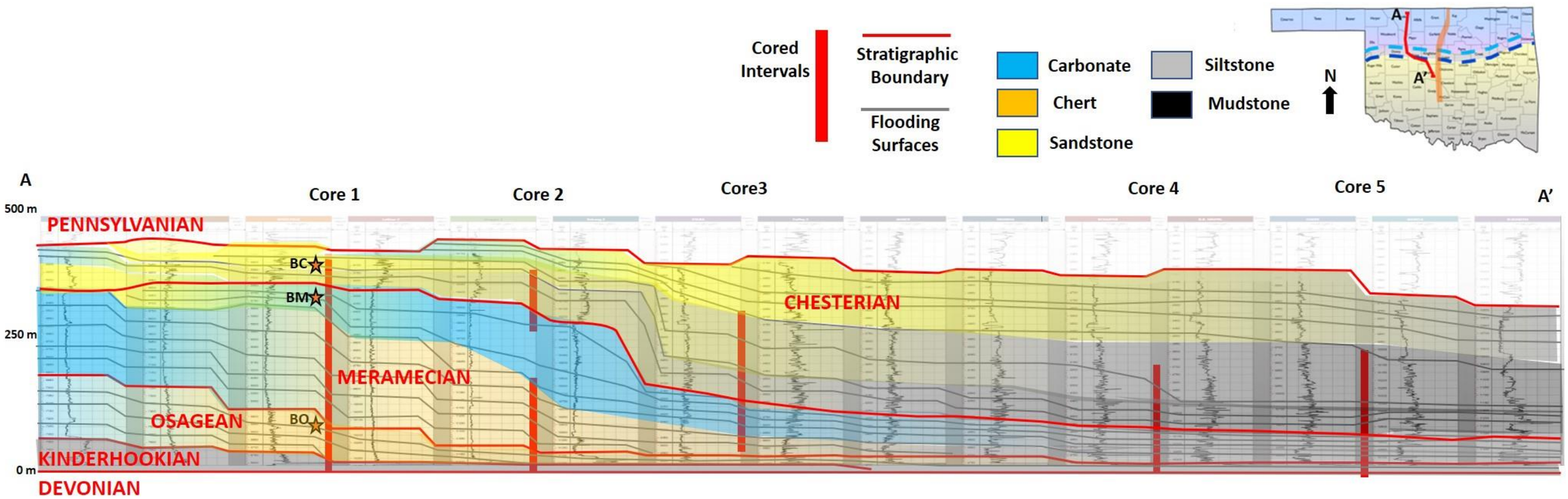

Figure 48. Cross section showing facies relationships and stratal geometry in the Mississippian section. Depositional packages to the north are dominated by carbonate shoals on the Boardman ramp crest and are composed of grainstone and packstone facies represented by the distribution of blue (modified from Bynum, 2022). While transitioning down dip to the biostromal sponge facies at the ramp crest toe of slope represented by the distribution of purple. Depositional packages to the south are dominated by the distal storm and outer ramp deposits composed of calcareous sandstone, siltstone, and mudstone facies represented by the distribution of yellow and gray. Biostratigraphic age constraints were analyzed in Core 1 (Stukey, 2020), and conodont zonations are represented by the orange stars. BO represents the top of the Osagean, BM represents the top of the Meramecian, and BC represents Chesterian deposition. These zonations are marked by significant stratigraphic surfaces identified in core, and they are correlated regionally to define the Meramecian Boardman ramp crest margin. Chesterian clastic units thicken off the Boardman margin and comprise the majority of the Mississippian succession in the Anadarko Basin.

Stratigraphic Architecture: Lower Mississippian sedimentation is characterized by the formation of a widespread prograding carbonate bank across the US Midcontinent. This event established the Kinderhookian-Osagean (Tournaisian-Visean) Burlington shelf, which is north of the project area (Boardman 2013; Franseen 2006; Mazzulo 2011, 2013). The age-equivalent strata in this study were designated using the biostratigraphic zonation of Stukey and Godwin (2020). Facies analysis indicates the project area is the outer ramp of the Burlington shelf, which is dominated by inner ramp carbonates north of the study area. This stratigraphic interval is the thinnest package analyzed in the project area, and continues to thin to the south where it is condensed atop the Devonian Woodford Shale.

Osagean-Meramecian (Visean) strata are characterized by progradation of the carbonate system beyond the Burlington shelf, and carbonate rocks represent the bulk of sedimentation in the northern project area. This depositional episode establishes a new ramp margin in north-central Oklahoma, which is called the Boardman ramp margin, which can be considered as an extension of the Burlington Shelf. Biostratigraphic zonation of Core 1 indicates these strata are Meramecian (Visean), and are represented by formation of carbonate shoals, proximal storm deposits, and biostromal sponge gardens to the north, and distal storm deposits of the mid ramp and finer grained deposits of the outer ramp to the south. The interval thins to the south from the ramp margin and sits on top of Tournaisian condensed section in the Anadarko Basin.

Upper Mississippian strata are characterized by an abrupt transition to a siliciclastic dominated system, and includes the bulk of the section in the southern part of the study area. With the red demarcation representing the Meramecian-Chesterian boundary. This depositional episode is marked by thick siliciclastic packages that accumulated principally basinward of the Boardman ramp margin. Biostratigraphy in Core 1 indicates these strata are Chesterian (Visean-Serphukovian), and are represented by proximal storm deposits on the Boardman ramp margin that pass southward into distal storm deposits and muddy outer ramp deposits. This stratigraphic

interval is the thickest package analyzed in the southern project area and is truncated by the sub-Pennsylvanian unconformity.

Mississippian stratigraphic architecture in the project area is represented by three distinct depositional episodes (Fig. 49). Initial Kinderhookian-Osagean (Tournaisian-Visean) deposition is distinguished by widespread clinoform outer ramp facies in the project area, which are time equivalent to the shallow-water carbonates that accumulated on the Burlington shelf. The second episode is marked by the progradation of the carbonate system basinward from the Burlington shelf, thereby establishing high-amplitude clinoforms basinward of the Boardman ramp margin in north-central Oklahoma during Meramecian (Visean) time. The last episode is marked by an abrupt change from a carbonate-dominated system to a siliciclastic-dominated system near the start of the Chesterian (Visean-Serpukhovian). The Chesterian silicicastic sediment is preserved mainly basinward of the Boardman ramp margin in the Anadarko Basin.

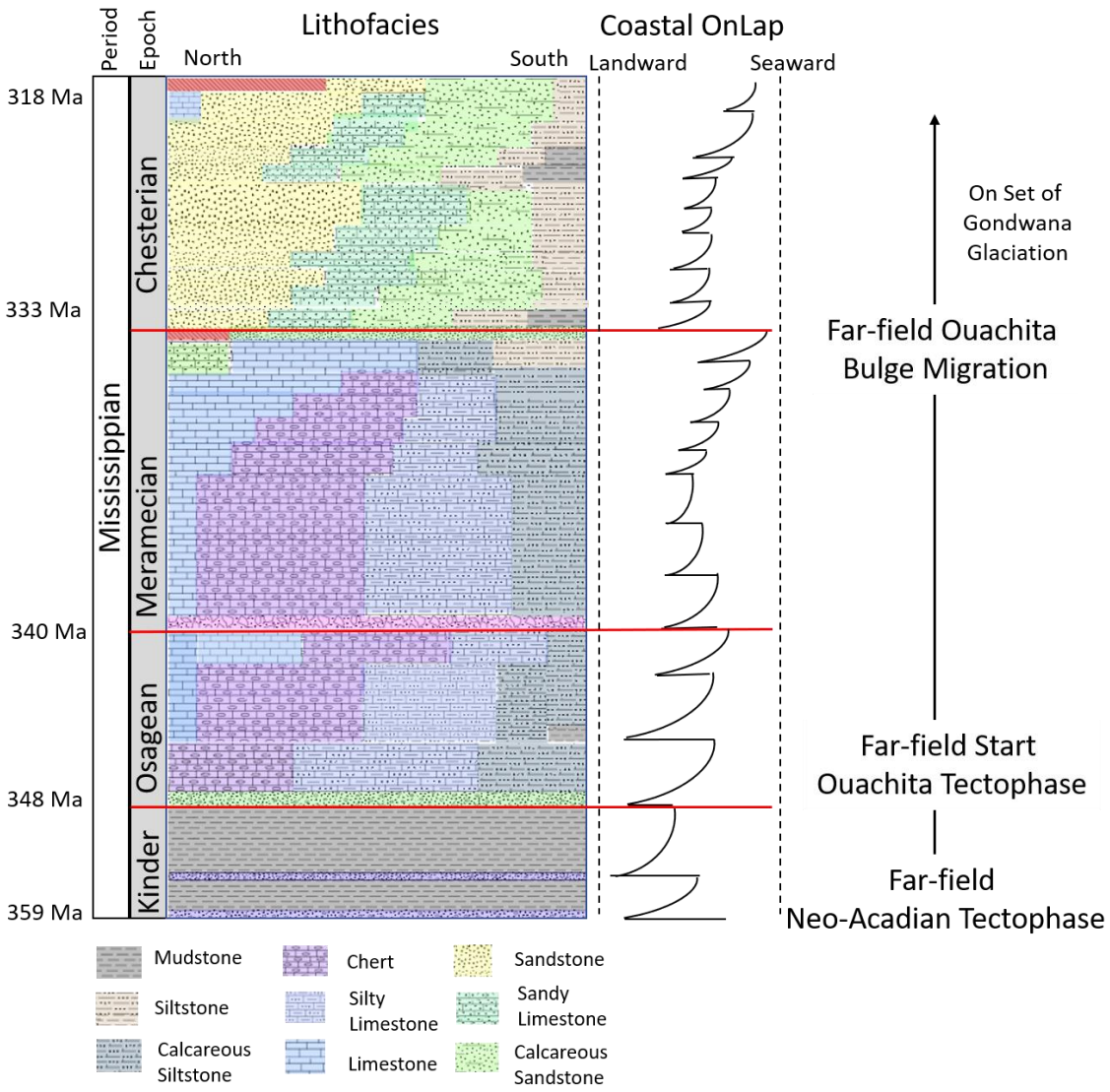

Figure 49. Wheeler diagram of the study area showing lithofacies, sea-level cycles, and tectonic onset for Mississippian rocks of the Anadarko basin and shelf.

Depositional Controls:

The Mississippian (Lower Carboniferous) section is part of the tectonic controlled 2nd-order Kaskaskia supersequence. Tectonic effects related to the Neo-Acadian and particularly the early Ouachita orogenies, during the Kinderhookian and Osagean, are observed within the study area and are expressed as regional disconformities. East of the study area, a major disconformity is present in the Ouachita foreland of the Arkoma Basin, Cherokee Platform, and Ozark Plateau in which Chesterian strata of the Fayetteville Shale and Caney Shale overlie the Upper Devonian (Famennian) Woodford Shale. This disconformity has been interpreted as a result of forebulge migration from the Ouachita Orogen (Al Atwah, 2019). A similar disconformity at the Meramecian-Chesterian boundary has been identified as far east as the Black Warrior Basin in Alabama and has been attributed to inception of the Ouachita Orogeny along the southwestern margin of the Alabama Promontory (Pashin, 1993, 1994; Pashin and Rindsberg, 1993, 1994). The magnitude of the Meramecian-Chesterian disconformity in the Anadarko basin and shelf is substantially smaller than in the Ouachita foreland, and points toward limited far-field effects of Ouachita forebulge development in the Anadarko Basin.

The Kinderhookian-Osagean boundary is marked by a sharp-based glauconitic sandstone exhibiting vertical burrows extending into the underlying substrate as a *Glossifungites* surface, with burrows filled by the overlying glauconitic sandstone (Fig. 50). These types of features are consistent with deposition of a transgressive sandstone associated with shoreface erosion (MacEachern, 2007). The Osagean-Meramecian boundary is marked by diagenetically altered chert exhibiting sharp basal and upper contacts (Fig 51). The unit contains deformed bedding and angular chert clasts within a dolomitic matrix. The regional correlation of this transition is potential response to far-field effects related to the early stages of Neo-Acadian flexural relaxation. The next regional disconformity observed within biostratigraphic studies of the outcrop belt is within the Meramecian, and related to bulge migration within the Ouachita

tectophase as a response to an unloading relaxation phase producing cratonward prograding clastic wedges from the Appalachian basin (Ettensohn, 2004; Godwin, 2020; Mazzullo, 2020) (Fig. 52). This also marks the transition from a carbonate dominated system to a siliciclastic dominated system within the Anadarko basin. The youngest major regional unconformity is in response to the onset of Alleghenian Orogeny near the Chesterian-Morrowan boundary in the Appalachian region (Ettensohn, Pashin, 2019; Pashin, 2009, in press) (Fig. 53). This unconformity represents major regional erosion and paleovalley incision.

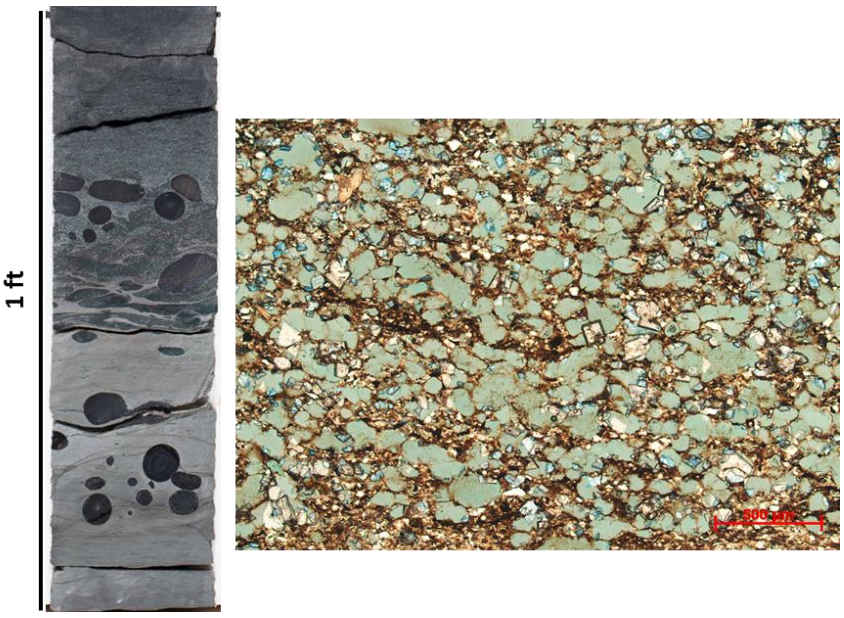

Figure 50. Major stratigraphic boundaries in core. Left image is a core photograph of a glauconitic sandstone and represents a disconformity at the Kinderhookian-Osagean boundary. Commonly observed as a Glossifungites surface with burrows penetrating the underlying substrate. Burrows are filled with overlying glauconite sand grains and phosphate nodules concentrated at the base of the bed. Right image is a thin section photomicrograph containing sand- sized glauconite grains, sand- to silt- sized quartz, ferroan dolomite, conodont and bone fragments.

Figure 51. Major stratigraphic boundary in core. Left image is a core photograph of a diagenetically altered chert bed sharply overlain by mudstone and represents a disconformity at the Osagean-Meramecian boundary. Chert clasts are highly fractured, and the matrix between clasts is composed of dolomite and clay. Right image is a thin section photomicrograph containing spicules, and other microbioclastic debris and microbioclastic ghosts. Multiple episodes of cementation include calcite, chert, and dolomite.

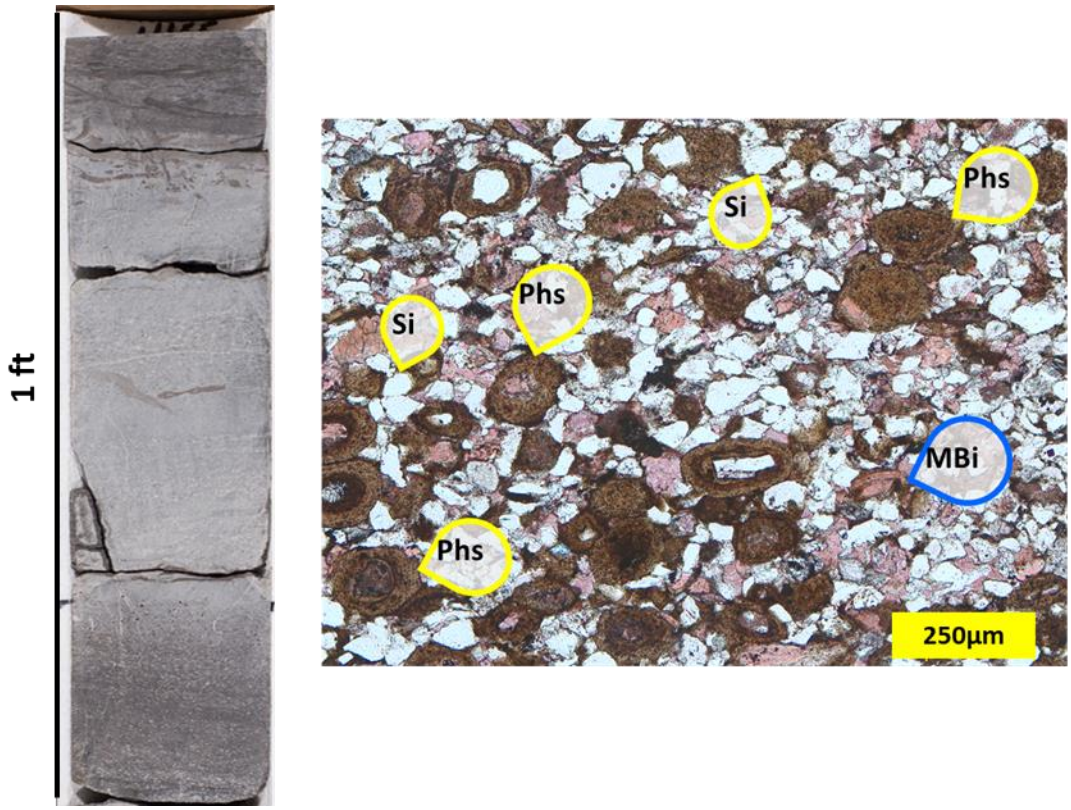

Figure 52. Major stratigraphic boundary in core. Left image is a core photograph of a phosphatic sandstone and a disconformity at the Meramecian-Chesterian boundary. Phosphatic grains and carbonate skeletal debris are concentrated at the base of the bed that fines upward with vertical burrows penetrating from the upper unit. Right image is a thin section photomicrograph containing abundant sand- sized quartz, feldspar, microbioclastic debris, phosphatic ooids, and calcite cement.

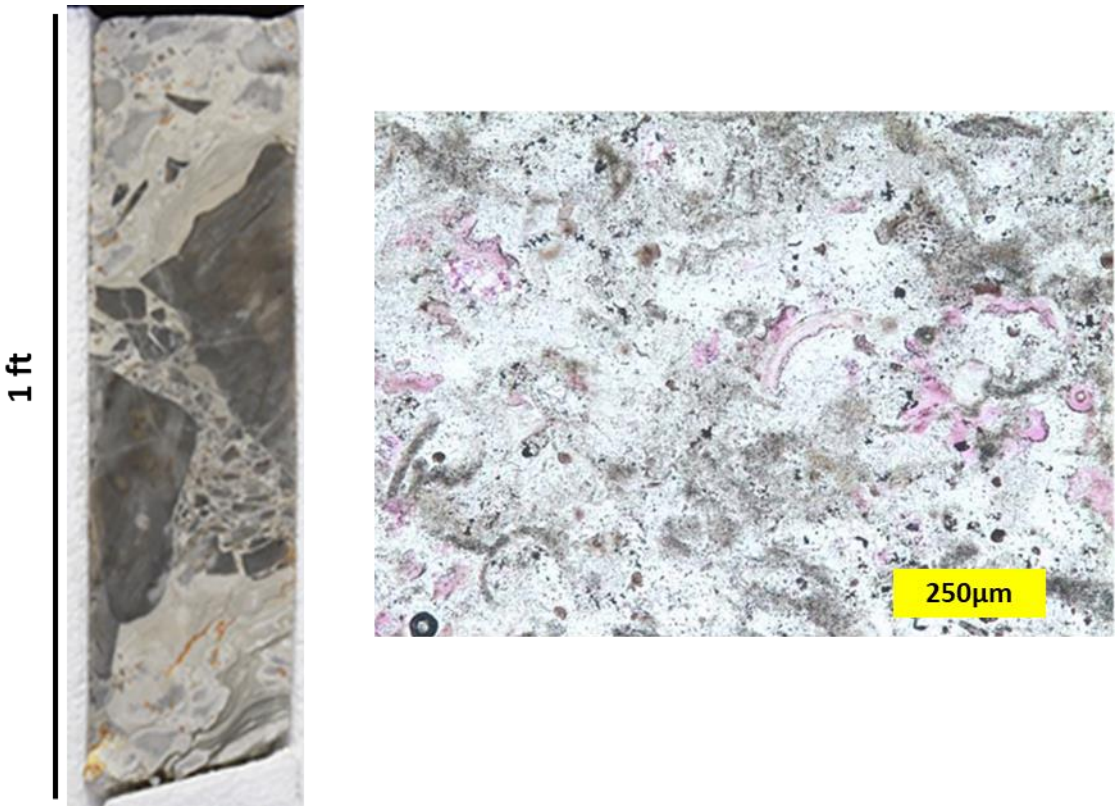

Figure 53. Major stratigraphic boundary in core. Left image is a core photograph of brecciated chert and represents an unconformity at the Chesterian-Pennsylvanian boundary. Clasts are angular to sub-angular with fine chert and clay rich matrix that contains root traces. Right image is a thin section photomicrograph of a chert clast containing ghosts of spicules and microbioclastic debris that has been altered to chert while pink epi-fluorescent dyed epoxy indicate microporosity.

The parasequences observed in core subdivide the Meramecian and Chesterian strata into two distinct parasquence sets spanning 359-328 Ma, and are correlatable across the study area using integrated facies and geophysical logs. The parasequences are shoaling-upward successions punctuated by glauconitic-phosphatic sandstone layers marking ravinement surfaces and dark mudstone layers marking marine flooding surfaces. The complete succession in the study area

appears to be subaqueous, and it is arguable that any evidence for exposure has been obscured by reworking of sediment below the ravinement surfaces. The average parasequence duration is around 1.5 Ma. The lower parasequence set defined from Kinderhook to Meramecian contains 13 major parasequences, with an average duration of 2 Ma. The Chesterian parasequence set contains 8 major parasequences, however, the upper Chesterian strata are not represented within the cored intervals. The parasquence stacking pattern defines a clinoform, net shoaling-upward succession that prograded southward with offshore shaly strata most common at the bottom of the section and shelf-ramp carbonate and sandstone most common at the top. Wells in the northwest contain strata enriched in calcareous fossil debris and bioturbation, as well as coarser grained siliciclastic deposits. Wells to the southeast, by contrast, contain deeper water depositional facies enriched in organic matter, clay, and silt. Indeed, proximal depositional environments of the Anadarko Shelf are recorded in the northwestern part of the cross section, and distal shelf environments are recorded in the Anadarko Basin. The clinoform strata can be subdivided into two distinct parasequence sets separated by a disconformity (sequence boundary) that marks the Meramecian-Chesterian boundary and is coeval with inception of the Ouachita Orogeny. The first parasequence set constitutes the carbonate-rich Tournaisian-Visean (Kinderhookian-Meramecian) section, and the second constitutes the sicliciclastic-dominated Visean-Serpukhovian (Chesterian) section. A pronounced disconformity separates Mississippian and Pennsylvanian strata in the study area, with only a few Chesterian parasequences preserved in the northern part of the study area and numerous parasequences preserved in the southern part.

Conclusions: Two distinctly different depositional systems occur in Lower Carboniferous (Mississippian) strata of the Anadarko Shelf and Anadarko Basin. A carbonate-dominated system of Tournaisian-Visean (Kinderhookian-Meramecian) age is characterized by 4 main lithofacies: grainstone, packstone, wackestone, and sponge boundstone-spiculitic chert. A siliciclastic-dominated system of Visean-Serpukhovian (Chesterian) age is characterized by 4 main

lithofacies: sandstone, calcareous sandstone, siltstone, and dark mudstone. The depositional environments observed in the carbonate system range from grainstone-rich inner ramp deposits to outer-ramp deposits rich in calcareous siltstone. By contrast, the siliciclastic strata are dominated by storm deposits and range from arkosic sandstone in the inner- and mid-ramp siltstone and dark shale in the outer ramp.

The Mississippian section in the study area can be characterized as containing two progradational parasequence sets separated by a disconformity associated with inception of the Ouachita Orogeny. Parasequences within these sets have an average duration of 1.5 Ma. While individual cores record facies variations relative to one another, they all exhibit three common patterns: 1) stacked coarsening-upward packages define parasequences within the parasequence sets, 2) carbonate system passes basinward into a siliciclastic system that is 3) succeeded by a siliciclastic system in the Chesterian. These patterns are consistent with other regional studies of the Lower Carboniferous in Laurussia, where a carbonate ramp system gives way to widespread siliciclastic sedimentation. While the transition from an icehouse to greenhouse system was underway in the Lower Carboniferous, subsidence associated with the early stages of the Ouachita Orogeny enabled transport of siliciclastics to the outer ramp via the Mississippi Valley Graben beginning in the Tournaisian. Marine circulation changes associated with reduced upwelling as oceanic currents were impeded by the uplifting Ouachita Orogen began to affect the distribution of biohermal sponges and the health of the carbonate fauna in the Meramecian. Ultimately, carbonate sedimentation was succeeded by the regional influx of cratonic clastics in the Chesterian.

CHAPTER V

CONCLUSIONS

The depositional and stratigraphic architecture of Mississippian strata in the southern Midcontinent of North America is characterized by a mixed carbonate-siliciclastic ramp system. The depositional architecture is characterized by a period of stabilization and aggradation of a widespread carbonate bank across the Midcontinent, established as the Kinderhookian-Osagean (Tournaisian-Viséan) Burlington shelf, and is represented by distal storm deposit and outer ramp facies within the project area. This is followed by an episode of carbonate deposition and progradation beyond the Burlington shelf, establishing the Meramecian (Viséan) Boardman ramp margin in north-central Oklahoma, where thick successions of proximal carbonate shoal and storm-generated carbonate sheet sand facies accumulated. The closing depositional episode is characterized by a thick siliciclastic succession of Chesterian (Viséan-Serpukhovian) sediment that prograded beyond the Boardman ramp margin, filling the southwestern part of the Anadarko Basin.

Statistical analysis indicates that the Mississippian System in the STACK play of the Anadarko Basin is fundamentally a highly layered rhythmic succession in which a variety of carbonate rock types, siliciclastic rock types, and chert tend to form couplets with siltstone. Thickness-frequency distributions and Markov chain analysis indicate that sediment thickness and lithologic transitions were stochastically regulated and that lithologic cyclicity is not apparent. Overall lithologic trends indicate a transition from carbonate to sandstone in the mid ramp and from carbonate to mudstone

and siltstone in the outer ramp. Stratal geometry defines a series of south-prograding clinoforms, and detailed analysis of vertical trends in the distribution of mudstone, siltstone, sandstone, chert, and carbonate facilitates identification of shoaling-upward parasequences that can be correlated regionally.

The Mississippian section in the study area can be characterized as containing two progradational parasequence sets separated by a disconformity associated with inception of the Ouachita Orogeny. Within the parasequence sets, individual parasequences represent a mean duration of 1.5 Ma, indicating that sedimentation was modulated by 3rd-order sea-level changes. While individual cores record a broad range of facies variation, three basic patterns were identified: 1) stacked coarsening-upward packages define parasequences, 2) Meramecian carbonates pass basinward into a siliciclastic-rich system, and 3) the carbonate system is succeeded regionally by a siliciclastic-rich system at the start of the Chesterian, which overlapped the Meramecian ramp. These patterns are consistent with other regional studies across the Lower Carboniferous Laurentia continent where the stable carbonate ramp system gives way to widespread siliciclastic sedimentation. While the transition from an icehouse to greenhouse system was underway in the Lower Carboniferous, deposition within the midcontinent is represented by a prograding carbonate ramp that was succeeded by a siliciclastic ramp as the subsidence related to the Ouachita Orogeny began feeding cratonic siliciclastics to the outer ramp through the Mississippi Valley Graben in the Tournaisian. Marine circulation changes associated with reduced upwelling during the early stages of the Ouachita Orogeny began to affect the distribution of biohermal sponges and the viability of the calcareous fauna in the Meramecian. Ultimately, the carbonate system was succeeded by regionally extensive deposition of cratonic clastics at the start of the Chesterian.

REFERENCES

Abdel-Fattah Z., Mahmoud K., Raafat, S. (2018) Depositional environments and sequence stratigraphy of a mixed siliciclastic-carbonate ramp: An example from the Cenomanian to Turonian Galala Formation in northern Eastern Desert, Egypt. Journal of African Earth Sciences 147: 352–373.

2019 Al Atwah*, I., J. Puckette, J. Pantano, K. Arouri, J. M. Moldowan, Organic Geochemistry and Crude Oil Source Rock Correlation of Devonian-Mississippian Petroleum Systems in Northern Oklahoma: AAPG Memoir 122: 301-322..

Algeo T., Rowe H., Hower J.C., Schwark L., Hermann A., Heckel P. (2008) Changes in ocean denitrification during Late Carboniferous glacial-interglacial cycles. Nature Geoscience 1: 709–714.

Aurell M., Ipas J., Badenas B., Ramajo J. (2010) Sedimentary evolution of an Upper Jurassic carbonate ramp (Iberian Basin, NE Spain). Geological Society of London Special Publications 329: 89–111.

Badenas B., Aurell M. (2000) Proximal-distal facies relationships and sedimentary processes in a storm dominated carbonate ramp (Kimmeridgian, northwest of the Iberian Ranges, Spain). Sedimentary Geology 139: 319–340.

Ball M., Henry M., and Frezon S. (1991) Petroleum geology of the Anadarko Basin region, province (115), Kansas, Oklahoma, and Texas. U.S. Geological Survey Open-File Report 88-450W: 1-38.

Boardman D., Godwin C., Mazzullo S., Wilhite B., Morris B. (2013) High resolution conodont zonation for Kinderhookian (Middle Tournaisian) and Osagean (Upper Tournaisian-Lower Visean) strata of the western edge of the Ozark Plateau, North America. Oklahoma City Geological Society Shale Shaker 64: 98–151.

Bracket, R., Bush D. (1986) Sedimentary characteristics of modern storm-generated sequences: North Insular Shelf, Puerto Rico: in Moslow T, Rhodes E (ed) Modern and ancient shelf clastics: A core workshop. SEPM Society for Sedimentary Geology 9: 125-148.

Buatois L., Mangano G. (2011) Ichnology organism-substrate interactions in space and time. Cambridge, Cambridge University Press: 358.

Burchette T., Wright V. (1992) Carbonate ramp depositional systems. Sedimentary Geology 71: 3–57.

Bynum J., Pashin J., Wethington, C. (2022) Depositional and Stratigraphic Architecture of a mixed carbonate-siliciclastic depositional system in the Mississippian (Lower Carboniferous) of the Southern Midcontinent, Oklahoma, USA. Facies 68: 1-20.

Choquette P., Pray L. (1970) Geologic Nomenclature and Classification of Porosity in Sedimentary Carbonates. American Association of Petroleum Geologists Bulletin 54: 207–250.

Cluff R. (1984) Carbonate sand shoals in the Middle Mississippian (Valmeyeran) Salem-St. Louis-Ste. Genevieve Limestones, Illinois Basin. in Harris P (ed) Carbonate Sands - A core workshop. SEPM Core workshop notes 5: 94.

Cotter E. (1990) Storm effects on siliciclastic and carbonate shelf sediments in the medial Silurian succession of Pennsylvania. Sedimentary Geology 69: 245–258.

Craddock J., Konstantinou A., Vervoort J., Wirth K., Davidson C., Blasi L., Juda N., Walker E. (2013) Detrital zircon prvenance of the Mesoproterozoic Midcontinent Rift, Lake Superior Region, USA. Journal of Geology 121: 57–73.

Crowley T., Yip K., Baum S. (1993) Milankovitch cycles and carboniferous climate. Geophysical Research Letters 20: 1175–1178.

Dunham R. (1962) Classification of carbonate rocks according to depositional texture. In Ham W. (ed) Classification of Carbonate Rocks. American Association of Petroleum Geologists, Tulsa, 108–121.

Ettensohn F. (2004) Modeling the nature and development of major Paleozoic clastic wedges in the Appalachian Basin, USA. Journal of Geodynamics 37: 657-681.

Ettensohn F., Pashin J., Gilliam W. (2019) The Appalachian and Black Warrior foreland basins in the eastern United States. In Miall A (ed) Sedimentary Basins of United States and Canada, 2nd edition. Elsevier, Amsterdam: 129-237.

Fielding C., Frank T., Isbell J. (2007) Resolving the Late Paleozoic Ice Age in Time and Space. Geological Society of America Special Publication 441: 355.

Frakes L., Francis J., Sykuts J. (1992) Climate modes of the Phanerozoic. Cambridge University Press, Cambridge: 288.

Frank T., Koch J. (2020) Controls on diagenetic pathways in Mississippian Carbonates of the Anadarko Shelf, Oklahoma. In Grammer G., Gregg J., Puckette J., Jaiswal P., Mazzullo S., Pranter., M, Goldstein R. (ed) Mississippian Reservoirs of the Midcontinent, American Association of Petroleum Geologists Memoir 122, Tulsa: 379-398.

Franseen E. (2006) Mississippian (Osagean) shallow-water, mid-latitude siliceous sponge spicule and heterozoan carbonate facies: An example from Kansas with implications for regional controls and distribution of potential reservoir facies. Earth Sciences Bulletin 252: 1-23.

Folk R. (1980) Petrology of Sedimentary Rocks. Austin, Hemphill Publication Company: 184.

Friedman G. (1988) The Catskill tectonic fan-delta complex: Northern Appalachian basin. Northern Geology 10: 254-257.

Gingras M., Dashtgard S., MacEachern J., Pemberton S. (2008) Biology of shallow marine ichnology: a modern perspective. Aquatic Biology 2: 255-268.

Godwin C., Boardman D., Puckette J. (2020) Meramecian-Chesterian (Upper Visean) Conodont Biostratigraphy and Revised Lithostratigraphy along the Southwestern Flank of the Ozark Uplift, Southern Midcontinent USA. In Grammer G, Gregg J, Puckette J, Jaiswal P, Mazzullo S, Pranter M, Goldstein R (ed) Mississippian Reservoirs of the Midcontinent, American Association of Petroleum Geologists Memoir 122, Tulsa, 59-88.

Godwin C., Puckette J. (2020) Depositional Cyclicity Within the Mayes Group (Meramecian-Chesterian) Along the Western Edge of the Mississippian Outcrop Belt in Northeastern Oklahoma. In Grammer G., Gregg J., Puckette J., Jaiswal P., Mazzullo S., Pranter M., Goldstein R. (eds.) Mississippian Reservoirs of the Midcontinent, American Association of Petroleum Geologists Memoir 122, Tulsa, 107-130.

Grammer M., Harrison W., Barnes D., Voice P. (2018) Paleozoic Stratigraphy and Resources of the Michigan Basin: Geological Society of America Special Papers 531, Boulder: 531.

Grammer G., Gregg J., Puckette J., Jaiswal P., Mazzullo S., Pranter M., Goldstein R., eds., (2020) Mississippian Reservoirs of the Midcontinent: American Association of Petroleum Geologists Memoir 122: 560.

Gutschick R., Sandberg C. (1983) Mississippian Continental Margins of the Conterminous United States, SEPM Special Publication 33: 79-96.

Handford C. (1995) Baselap patterns and the recognition of lowstand exposure and drowning, a Mississippian-ramp example and its seismic signature. Journal of Sedimentary Research B65-3: 323-337.

Handford C. (1988) Review of carbonate sand-belt deposition of ooid grainstones and application to Mississippian Reservoir, Damme Field, Southwestern Kansas. AAPG Bulletin 2: 1184-1199.

Handford C. (1986) Facies and bedding in shelf-storm-deposited carbonates – Fayetteville Shale and Pitkin Limestone (Mississippian), Arkansas. Journal of Sedimentary Petrology 56: 123-137.

Hasiotis S. (2012) A brief overview of the diversity and patterns in bioturbation preserved in the Cambrian-Ordovician carbonate and siliciclastic deposits of Laurentia; In Derby J., Fritz R., Longacre S., Morgan W., and Sternbach C. (ed) The Great American Carbonate Bank: The Geology and Economic Resources of the Cambrian-Ordovician Sauk Megasequence of Laurentia. AAPG Memoir 98: 113-127.

Higley D. (2014) Thermal maturation of petroleum source rocks in the Anadarko Basin province, Colorado, Kansas, Oklahoma, and Texas. U.S. Geological Survey Digital Data Series DDS-69-EE: 1-52.

Johnson K. (1988) Geologic evolution of the Anadarko Basin, In Kenneth S., Johnson K. (eds) Anadarko Basin Symposium: Oklahoma Geological Survey and the U.S. Geological Survey: 7-16.

Lazar O., Bohacs K., Schieber J., Macquaker J., Demko T. (2015) Mudstone Primer: Lithofacies variations, diagnostic criteria, and sedimentologic-stratigraphic implications at lamina to bedset scale. SEPM Concepts in Sedimentology and Paleontology 12: 204.

Leinfelder R., Nose M., Krautter M. (1993) Siliceous sponge facies from the Upper Jurassic of Portugal. Neues Jahrbuch fur Geologie und Palaontologie 189: 199-254.

Lindzey K., Pranter M., Marfurt K. (2020) Lithological and petrophysical controls on production of the Mississippian Limestone, Northeastern Woods County, Oklahoma. In Grammer G., Gregg J., Puckette J., Jaiswal P., Mazzullo S., Pranter M., Goldstein R. (ed) Mississippian Reservoirs of the Midcontinent. American Association of Petroleum Geologists Memoir 122, 541-560.

Liu, Y., and Gastalda, R. A., 1992, Characteristics of a Pennsylvanian ravinement surface:

Sedimentary Geology 77: 197-213.

Lubeseder S., Redfern J., Boutib L. (2009) Mixed siliciclastic-carbonate shelf sedimentation - Lower Devonian sequences of the SW Snti-Atlas, Morocco. Sedimentary Geology 215: 13-32.

MacEachern J., Bann K. (2008) The role of ichnology in refining shallow marine facies models. In: Hampson G, Steel R, Burgess P, Dalrymple R (ed), Recent Advances in Models of Siliciclastic Shallow-Marine Stratigraphy. SEPM Special Publication 9, 73–116.

Mazzullo S., Wilhite B., Boardman D. (2011) Lithostratigraphic architecture of the Mississippian Reeds Spring Formation (Middle Osagean) in southwest Missouri, northwest Arkansas, and northeast Oklahoma: Outcrop analog of subsurface petroleum Reservoirs. Oklahoma City Geological Society Shale Shaker 61: 254-269.

Mazzullo S., Boardman D., Wilhite B., Godwin C., Morris B., (2013) Revisions of Outcrop lithostratigraphic nomenclature in the Lower to Middle Mississippian subsystem (Kinderhookian to Basal Meramecian Series) along the shelf-edge in Southwest Missouri, Northwest Arkansas, and Northeast Oklahoma. Oklahoma City Geological Society Shale Shaker 63: 414-454.

Mazzullo S., Boardman D., Wilhite B., Godwin C., and Morris B. (2020) Lithostratigraphy, Biostratigraphy, Stratigraphic Architecture, and Depositional Systems in Lower to Middle Mississippian Strata on the Western Flank of the Ozark Dome, Midcontinent USA. In Grammer, G., Gregg J., Puckette J., Jaiswal P., Mazzullo S., Pranter, M., Goldstein R. (ed) Mississippian Reservoirs of the Midcontinent. American Association of Petroleum Geologists Memoir 122, Tulsa, 25-57.

Meckel L (1970) Paleozoic alluvial deposition in the central Appalachians: In Fisher, G., (ed) Studies of Appalachian Geology: Central and Southern. New York, Wiley-Interscience: 49-67.

Miller K, and West R., (1998) Identification of sequence boundaries within cyclic strata of the Lower Permian of Kansas, USA: Problems and alternatives: Journal of Geology 106:119-132.

Miller J., Puckette J., Godwin C. (2020) Conodont Biostratigraphy-Constrained Diachronous Lithofacies, Boone Group (Upper Osagean to Lower Meramecian), Western Ozarks: Breakdown of Lithostratigraphic Correlations at a Regional Scale. In Grammer, G., Gregg J., Puckette J., Jaiswal P., Mazzullo S., Pranter, M., Goldstein R. (ed) Mississippian Reservoirs of the Midcontinent. American Association of Petroleum Geologists Memoir 122, Tulsa: 89-105.

Moore S., Birgenheier L., Greb M., Minisini D., Tunik M., Omarini J. (2020) Facies heterogeneity and source potential of carbonate-mudstone-dominated distal ramp deposits, Agrio Formation, Neuquen Basin, Argentina. Journal of Sedimentary Research 90: 533-570.

Noel J., Dalrymple R. (2010) Facies Models 4. Geological Association of Canada, Kingston: 586.

Pashin J. (1994) Cycles and stacking patterns in Carboniferous rocks of the Black Warrior Foreland Basin. Gulf Coast Association of Geological Societies Transactions 44: 555-563.

Pashin J., Cecil K. (2017) Origin, source-rock, and reservoir characteristics of novaculitic chert in the southern Midcontinent: Geological Society of America Abstracts with Programs 49-6. doi: 10.1130/abs/2017AM-302432.

Pashin J., Gastaldo R., Greb S., Chesnut D. (2009) Carboniferous of the Black Warrior basin: Carboniferous of the Appalachian and Black Warrior Basins. Kentucky Geological Survey Special Publication 10: 10-21.

Pashin, J. C., in press, Stratigraphic and thermal maturity evidence for a break-back thrust sequence in the southern Appalachian thrust belt, Alabama, USA, in Catlos, L., ed., Compressional Tectonics: Plate Convergence to Mountain Building: New York, Wiley, American Geophysical Union.

Pemberton G., MacEachern J., Dashtgard S., Bann K., Gingras M., Zonneveld J. (2012) Shorefaces: Developments in Sedimentology. In Knaust D., and Bromley R., (ed) Trace Fossils as Indicators of Sedimentary Environment, Elsevier, Amsterdam: 563-603.

Perry W. (1989) Tectonic evolution of the Anadarko Basin region, Oklahoma. U.S. Geological Survey Bulletin 1866: 1-28.

Posamentier H., Allen G. (1999) Siliciclastic Sequence Stratigraphy: Concepts and Applications. SEPM Concepts in Sedimentology and Paleontology 7: 210.

Sandberg C., Gutschick R., Johnson J., Poole F., Sando W. (1982) Middle Devonian to Late Mississippian geologic history of the overthrust belt region, western United States. Rocky Mountain Association of Geologists, Geologic studies of the Cordilleran Thrust Belt 2: 691-719.

Saunders W., Ramsbottom W. (1986) The mid-Carboniferous eustatic event: Geology 14-3, 208-212.

Schieber J., Southard J. (2009) Bedload transport of mud by floccule ripples – Direct observation of ripple migration process and their implications. Geology 37-6: 483-486.

Scholle P., Spearing D. (1982) Sandstone Depositional Environments. American Association of Petroleum Geologists Memoir 31: 210.

Scholle P., Bebout D., Moore C. (1983) Carbonate depositional environments. American Association of Petroleum Geologists Memoir 33: 708.

Seilacher, A., 2007, Trace Fossil Analysis: Amsterdam, Springer: 290.

Silberling N., Nichols K., Mack D., Trappe J. (1995) Upper Devonian-Mississippian stratigraphic sequences in the distal Antler Foreland of western Utah and adjoining Nevada. U.S. Geological Survey Bulletin 1988-H: 41.

Smith L., Read J. (2000) Rapid onset of late Paleozoic glaciation on Gondwana: Evidence from Upper Mississippian strata of the Midcontinent, US. Geology 28: 279-282.

Tucker M., Wright P. (1990) Carbonate Sedimentology. Blackwell Publishing Company, Oxford: 252.

Wang, Y., Thompson, T., and Grammer, M., 2019, Fracture characterization of the

"Mississippian Limestone," north-central Oklahoma, United States: American Association of

Petroleum Geologists Memoir 122, 271-299.

Wentworth C. (1922) A scale of grade and class terms for clastic sediments. Journal of Geology 30: 377-392.

Wilkinson B., Merrill G., and Kivett (2003) Stratal order in Pennsylvanian cyclothems. GSA Bulletin 115: 1068-1087.

Wright V., Faulkner T (1990) Sediment dynamics of Early Carboniferous ramps. Geological Journal 25: 139-144.

Xie X., O'Connor P., Alsleben H. (2016) Carboniferous sediment dispersal in the Appalachian-Ouachita juncture: Provenance of selected late Mississippian sandstones in the Black Warrior Basin, Mississippi, United States. Sedimentary Geology 342: 191-201.

Yang K., Dorobek S. (1995) The Permian Basin of West Texas and New Mexico: Tectonic history of a "composite" foreland basin and its effects on stratigraphic development. SEPM Special Publication 52, Tulsa, 149-174.

Yawar Z., Schieber J. (2017) On the origin of silt laminae in laminated shales. Sedimentary Geology 360: 22-34.

VITA

Jamar Carlie Marie Bynum

Candidate for the Degree of

Doctor of Philosophy

Dissertation: DEPOSITIONAL CONTROLS AND STRATIGRAPHIC ARCHETICTURE OF A MIXED CARBONATE-SILICICLASTIC DEPOSITIONAL SYSTEM IN THE MISSISSIPPIAN (LOWER CARBONIFEROUS) OF THE SOUTHERN MIDCONTINENT, OKLAHOMA, USA.

Major Field: Geology

Biographical:

Education:

Completed the requirements for the Doctor of Philosophy in Geology at Oklahoma State University, Stillwater, Oklahoma in December, 2022.

Completed the requirements for the Master of Science in Geology at Oklahoma State University, Stillwater, Oklahoma in 2010.

Completed the requirements for the Bachelor of Science in Earth and Planetary Sciences at University of New Mexico, Albuquerque, New Mexico in 2007.

Experience: Jamar is a geologist with over 12 years of experience in the energy industry analyzing carbonate, siliciclastic, and mixed depositional systems. Her industry experience ranges from basin scale modeling of petroleum systems, to play scale facies analysis using seismic, petrophysics, and core, to micro scale pore typing and distributions analysis for evaluating seal and reservoir quality. Her current research efforts are focused on the energy transition applications within the CCUS/EOR, CCS, and geothermal sectors.

Professional Memberships: AAPG, SEPM, GSA, SPE, AWG